# IOWA STATE UNIVERSITY
**Digital Repository**

2017

# Modeling of filament deposition rapid prototyping process with a closed form solution

Steven Leon Devlin
*Iowa State University*

**Modeling of filament deposition rapid prototyping process with a closed form solution**

by

**Steven Leon Devlin**

A dissertation submitted to the graduate faculty

in partial fulfillment of the requirements for the degree of

DOCTOR OF PHILOSOPHY

Major: Industrial and Agricultural Technology

Program of Study Committee:
David Grewell, Major Professor
Matthew Charles Frank
Steven A. Freeman
Gretchen Ann Mosher
W. Robert Stephenson

The student author, whose presentation of the scholarship herein was approved by the program of study committee, is solely responsible for the content of this dissertation. The Graduate College will ensure this dissertation is globally accessible and will not permit alterations after a degree is conferred.

Iowa State University

Ames, Iowa

2017

DEDICATION

This dissertation is dedicated to

my parents, the late Judith L. Devlin and Leon G. Devlin, who taught me to push beyond life's expectations

and

my family, Colleen E. Devlin, Rebecca E. Devlin, and Connor S. Devlin, who give my life purpose

# TABLE OF CONTENTS

# LIST OF FIGURES

Page

LIST OF TABLES

NOMENCLATURE

| | |
|---|---|
| 3D Printing | 3 Dimensional Printing |
| ABS | Acrylonitrile Butadiene Styrene |
| AM | Additive Manufacturing |
| Anisotropic Properties | Directionally dependent properties |
| ASTM | ASTM International |
| Boltzmann Constant | $1.3807 * 10^{-23}$ J/K |
| CAD | Computer Aided Design |
| CIRP | International Academy of Production Engineers |
| CNC | Computer numeric control |
| Coalescence | The process by which two or more particles merge to form a single mass |
| Conduction | Heat transfer through matter |
| Convection | Heat transfer due to bulk movement of molecules |
| DFAM | Design for Additive Manufacturing |
| DFM | Design for Manufacturing |
| DMLS | Direct metal laser sintering |
| EBM | Electron beam melting |
| Euclidean Space | Encompassing 2D planes and 3D space of Euclidean geometry |
| Extrusion | Pushing material through a die to create a desired cross-section |
| FDM | Fused Deposition Modeling |
| FFF | Fused Filament Fabrication |
| FFM | Fused filament manufacturing |
| ISO | International Standards Organization |
| k | Thermal conductivity |
| Laplace Transform | Integral transform |
| LOM | Laminated Object Manufacturing |
| Micrograph | Digital image taken through a microscope to show a magnified item |
| Microtome | Instrument used to cut extremely thin slices of material |
| NSF | National Science Foundation |
| PC | Polycarbonate |
| PLA | Polylactic acid |
| PPSU | Polyphenylenesulfone |
| Profilometer | Instrument used to measure a surfaces' profile |
| RepRap | Replicating rapid-prototyper |
| RM | Rapid Manufacturing |
| RP | Rapid prototyping |
| SAE | Society of Automotive Engineers |
| Sintering | Forming a solid through heat or pressure below liquefaction |

| SLA | Sterolithography |
|---|---|
| SLS | Selective Laser Sintering |
| Taylor Series Expansion | Representation of a function as an infinite sum of terms calculated from the functions derivatives at a single point |
| Tg | Polymer glass transition temperature |
| Tribological Properties | Science & Engineering of interacting surfaces in relative motion |
| Viscoelastic | Having both viscous and elastic properties when undergoing deformation |
| Weld Strength | Degree of polymer chain diffusion and entanglement |

ACKNOWLEDGMENTS

As I come to this milestone in my academic career, I recognize the many contributions others have made to help me on this journey. My graduate education and completion of my doctoral degree has been a collaborative effort.

First, I thank my major professor, David Grewell, for offering me the chance to earn my doctorate, helping me understand the path of experimental research, and sticking with me long after this journey began. In addition, I appreciate the opportunity to work with other members of your research team, contribute to a wide array of topics, and influence research projects. I also thank each of my committee members for their contributions and support of my program of study and research. Bob Stephenson – your courses on applied statistics for industry helped me connect to data and build an understanding and appreciation of measurement I would not have learned otherwise. Matt Frank – your understanding of manufacturing methods and material processing has provided an engineering framework for my study of additive manufacturing methods. Gretchen Mosher – your example as an ISU researcher, working through graduate school, earning your doctorate, and becoming a faculty member has provided a continuing light at the end of my journey. Steve Freeman – you gave me the advice, support, and encouragement I needed to keep this effort going. You helped me negotiate the many complexities of finishing my degree many years after I should have been finished. Thank you all for your assistance, guidance, and encouragement.

In addition to the committee, I had the opportunity to work with many other faculty and staff at Iowa State University and other institutions. I would like to thank Roger Smith and Ron Meier, who introduced me to graduate school, research, and rapid prototyping. Thank you to my former colleagues in the Center for Industrial Research and Service, particularly Ron Cox and

ABSTRACT

Fused Deposition Modeling (FDM™) or fused filament fabrication (FFF) systems are extrusion-based technologies used to produce functional or near functional parts from a wide variety of plastic materials. First patented by S. Scott Crump and commercialized by Stratasys, Ltd in the early 1990s, this technology, like many additive manufacturing systems, offers significant opportunities for the design and production of complex part structures that are difficult if not impossible to produce using traditional manufacturing methods. Standing on the shoulders of a twenty-five year old invention, a rapidly growing open-source development community has exponentially driven interest in FFF technology. However, part quality often limits use in final product commercial markets. Development of accurate and repeatable methods for determining material strength in FFF produced parts is essential for wide adoption into mainstream manufacturing.

This study builds on the empirical, squeeze flow and intermolecular diffusion model research conducted by David Grewell and Avraham Benatar, applying a combined model to predict auto adhesion or healing to FFF part samples. In this research, an experimental study and numerical modeling were performed in order to drive and validate a closed form heat transfer solution for extrusion processes to develop temperature field models. An extrusion-based 3D printing system, with the capacity to vary deposition speeds and temperatures, was used to fabricate the samples. Standardized specimens of Polylactic Acid (PLA) and Acrylonitrile Butadiene Styrene (ABS) filament were used to fabricate the samples with different speeds and temperatures. Micro-scanning of cut and lapped specimens, using an optical microscope, was performed to find the effect of the speed and the temperature on the geometry of the cross-sections.

It was found that by increasing the speed of the extrusion printing, the area of the cross-section and the maximum thickness decrease, while the weld/bead geometry minimum thickness increases at higher speeds, although actual part strength appeared to plateau for speeds above 15mm/sec. Temperature effect was found to increase the geometry minimum thickness. In most cases, test results show that by increasing the speed and the temperature, the geometry strength increases. Non-Linear finite element based numerical modeling was performed to predict the strength of the samples. The geometry produced from the optical microscope scanning and typical PLA material properties were used to create the model. The finite element model was able to predict the strength of the tested samples at different speeds and temperatures. Analysis of resulting data and examination of tested samples offer favorable insights and opportunities for additional and continuing investigation.

## CHAPTER 1.  INTRODUCTION TO RESEARCH

This study attempts to identify and quantify the critical factors associated with thermoplastic extrusion based methods of additive manufacturing, and their influence on final part strength. In essence, all additive manufacturing methods are based on the concept of creating physical parts using numerous smaller building blocks, which are bonded in some manner. In fused deposition modeling or fused filament fabrication the building blocks are extruded beads of thermoplastic material and the bonds between each bead represent a basic unit that can be used to evaluate final part strength. This research presents three primary areas of investigation. Development and documentation of a sample fabrication and testing method for weld strength, documented in chapters three and four. Investigation and numerical modeling of the extruded bead geometry documented in chapter five.  Finally, development and analysis of a predictive model for part strength based on squeeze flow and intermolecular healing presented in chapter six.

Over thirty years ago the U.S. Patent and Trademark office issued to Charles Hull a patent (number 4575330) for an Apparatus for Production of Three-Dimensional Objects by StereoLithography (Hull, 1986). This development launched the Rapid Prototyping /Rapid Manufacturing industry. Rapid Prototyping (RP) or Rapid Manufacturing (RM), sometimes referred to as solid freeform fabrication or Additive Manufacturing (AM), is a method of fabricating parts through additive manufacturing processes. These processes typically allow parts to be developed at relatively low volumes because of their slow production speeds. It is ideal for prototyping, fit and function modeling, patterns for metal casting, technological pieces for functional purposes and other situations where parts are needed in small quantities (i.e. production-quality parts needed for small runs).  More and more AM systems are being used to

create end-use parts, with over a third of the 3D printing market in 2013 (Wohlers, 2014). Companies like General Electric, Boeing, and Johnson & Johnson making significant investments in additive manufacturing capabilities. Because of this, it has significant potential to affect product development and manufacturing.

In 1987 the SLA®-1 system was released by 3D Systems, representing the first commercially available system using additive manufacturing technology. While StereoLithography is recognized as the first, many other competitive systems/technologies were developed over the next decade. Today there are seven technologies offered through numerous manufacturers worldwide: Selective Laser Sintering (SLS), Fused Deposition Modeling (FDM), Laminated Object Manufacturing (LOM), Electron Beam Melting (EBM), 3D Printing (3DP), Direct Metal Laser Sintering (DMLS) and StereoLithography (SLA).

Fused Deposition Modeling (FDM™) or fused filament fabrication (FFF) systems are extrusion-based technologies used to produce functional or near functional parts from a wide variety of plastic materials. First patented by S. Scott Crump and commercialized by Stratasys, Ltd in the early 1990s, this technology, like many additive manufacturing systems, offers significant opportunities for the design and production of complex part structures that are difficult if not impossible to produce using traditional manufacturing methods. Standing on the shoulders of a twenty-five year old invention, a rapidly growing open-source development community has exponentially driven interest in FFF technology. However, part quality often limits use in final product commercial markets. Development of accurate and repeatable methods for determining material strength in FFF produced parts is essential for adoption into mainstream manufacturing.

Additive Manufacturing can use a wide variety of base materials: metals, plastics, corn starch, ceramics, and recently bio-materials. Currently thermoplastics and thermosets dominate the industry with metals being the third most popular choice. Some of the major advantages of plastics as a base material compared to metals include:

1. Performance and ease of manufacturing

2. Cost-effectiveness because of:

   a. Low energy consumption

   b. Low weight

   c. Low cost of tooling, especially for complex shapes and styling

   d. Fast tooling time

3. Corrosion resistance

4. Styling latitude allowing creation of parts that might not be possible using traditional fabrication methods

These advantages underscore why plastics lead the industry, particularly in the automotive industry (Bickrest, 1986).

As stated previously, parts formed by the method of layer-by-layer synthesis, Rapid Prototyping (RP) or additive manufacturing, are most frequently use for three applications: for model-prototypes, models for production of metal casts, or as technological pieces for functional purposes. In the latter case, the properties of the construction material used in the RP process (the physico-mechanical, chemical and corrosion resistance factors) are of significant importance. Over all, the properties determine the functional-operational characteristics of the finished products. When selecting a material, not only is the purpose of the part important but also the type of RP technology that will be used to manufacture it. Any material selected will

have restrictions both in the chemical composition and in the physical state of the initial material (Sevidova, 2008).

For almost two decades Stratasys fused deposition modeling has been one of the most important rapid prototyping technologies (Kruth, 1998). For this process both building material as well as a support material is needed. The building and support material are molten in a liquefier unit and extruded through a die onto a platform to create a two-dimensional cross section of the model. Subsequently the platform is translated and the next layer is extruded and fused onto the previous layer (Crump, 1992). This process continues until the part is completed; afterwards the part's sacrificial support structures, used to support overhanging features, are removed. Parts with 0.1 mm high layers and a minimum wall thickness of 0.5 mm can be obtained by FDM. The commercially available materials for this process include a number of thermoplastics such as: ABS, PC, polyphenylenesulfone (PPSU) and a PC/ABS-blends, with ABS dominating use in most industrial applications. It has been reported that ABS plastic prototype models have relatively high strength and durability used across many industries (Hadas, (2008). Such materials are provided as filaments (diameter of $1.75 \pm 0.05$ mm) in several standard colors (Wendel, 2008).

Many professional service providers claim FDM carries an indisputable advantage over other additive manufacturing technologies because of the potential for final machining and cutting of rapid prototyped parts. Parts made from ABS can be milled, turned, and grinded or have threads cut in formed holes. Machining requires specific cutting speeds and tooling because of the low melt temperature and layered structure, but can produce "near-functional" features (Hadas, 2008).

Additive manufacturing has the potential to disrupt traditional manufacturing practices because it allows fabrication of objects directly from 3D model data, layer by layer, as opposed to traditional manufacturing technologies, such as subtractive and formative manufacturing (Laverne, et al., 2015). With the capability of using commercial grade thermoplastic materials, Fused Deposition Modeling (FDM) or Fused Filament Manufacturing (FFM) offers some distinct advantages for production part fabrication. One aerospace supplier uses FDM to make thermoform molds for air ducts, engine cowlings, and antenna covers. Fused Deposition Modeling tooling reportedly costs less and has shorter lead-time than composite molds made by hand lay-up of pre-impregnated carbon-fiber fabrics (Grande, 2008).

**Interfacial Healing**

Joining materials to create functional components and finished products is a central concept of manufacturing. Mechanical methods of joining material are extensively used in assemblies but have little application in the development of complex geometries and small components. In these situations, more permanent methods of joining, such as welding, brazing, and adhesive bonding, are utilized to produce parts out of a number of different materials. The FDM process has been described as being analogous to welding, where two pieces of a similar material are joined using a pool of molten material to heat and diffuse into the base material creating a permanent bond as strong as or stronger than the base material (Amberg & Do-Quang, 2007). Therefore understanding the thermoplastic bonding process is critical to understanding final part strength in additive manufacturing.

In thermoplastic materials, welding occurs when two polymer surfaces are brought together in a plasticized state allowing them to conform to each other and begin the intermolecular diffusion and polymer chain entanglement necessary for fusion bonding (Grewell

& Benatar, 2008). The degree of healing or welding being dependent on a number of factors including temperature, base material properties, time and interfacial pressure (Wool, 1995). As in casting and molding processes, with material temperatures above the polymer glass transition ($T_g$), the multi-stage healing process can occur, including surface rearrangement, surface approach, wetting, diffusion, and randomization (Vogel, et al., 2012).

**Squeeze flow**

To understand the process of interfacial healing it is useful to separate the complex process into two fundamental mechanisms, squeeze flow and molecular diffusion. When two polymer faying surfaces are joined, a number of peaks and valleys must be displaced to allow the surfaces to come in full contact. During the welding process these peaks soften and deform to fill the gaps between surfaces(Grewell & Benatar, 2008). As part of this research, the asperity deformation is initially modeled as an idealized squeeze flow of many small identical cylinders of molten material placed between two rigid plates separated by some distance 2h as described by Grewell and seen in Figure 1.
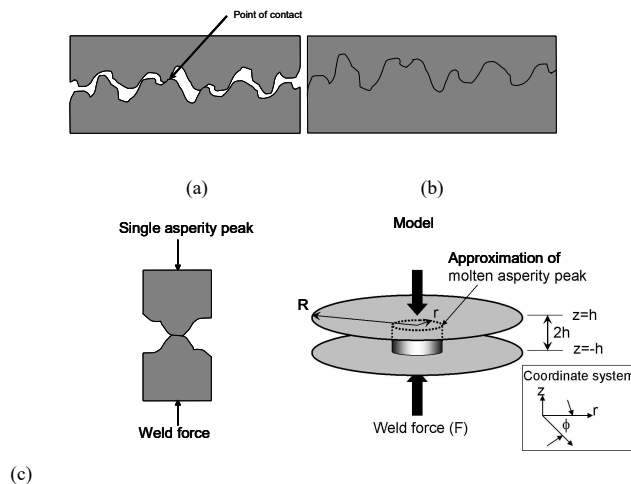
Figure 1. Cartoon of polymer interface with asperity peaks, (a) before welding (b) after welding and (c) idealized model

To further simplify the model, a single asperity peak is modeled, where the original height and radius are defined as $h_0$ and $r_0$, respectively and the final radius is defined as $r_{od}$. Assuming a Newtonian fluid with a viscosity ($\mu$) and other standard assumptions, Bird, et al. (1987), developed a similar model for a case where the volume between the gap is fully filled. Independent of the gap being fully filled, they showed that the pressure (p) is defined as a function of time (t). By integrating that function over the asperity peak model, and by conversion of mass it is possible to define the time varying radius as a square root of $r_0^2 h_0/h$ and be substituted into the integration of the pressure function. With further integration relative to time we find the nondimensional asperity height defined in equation 1, which can be used to predict the closing of two faying surfaces as a function of time.

$$\frac{h_0}{h(t)} = \left( \frac{16\pi F h_0^2}{3\mu r_0^4} t - 1 \right)^{1/4} \qquad \text{Eq. 1}$$

Interfacial healing occurs as the faying surfaces come into intimate contact. It is important to note, healing originates wherever connection occurs, even before the squeeze flow has deformed the asperity peaks and filled the surface gap. Therefore, squeeze flow and healing occur simultaneously (Grewell & Benatar, 2008). Healing of the interfaces occurs through diffusion of polymer chains across the interface and entanglement with other polymer chains. Figure 2. displays the chain diffusion at various times and degrees of healing. Ideally, at complete healing, polymer chains from each side migrate across the interface so that it essentially becomes indistinguishable from the bulk material, in this case the degree of healing or degree of welding (DW), is 1 when the interface is fully healed.
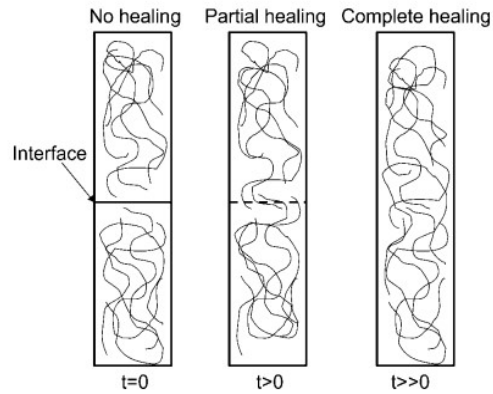
Figure 2. Molecular diffusion and interfacial healing (Grewell & Benatar, 2008)

Using reptation theory, the diffusion of polymer chains can be modeled as a function of molecular structure, molecular weight, chemical structure, and time and temperature (DeGennes, 1971). Other factors, such as pressure, can also affect this process.  In this model, each polymer chain is considered to be contained in an imaginary tube of length L.  The tube is constrained by neighboring polymer chains and thus, the ends of the polymer chains have more freedom of movement compared to the bulk of the chain. The distance that a polymer chain moves outside the original tube is referred to as the diffusion distance $<l>^2$, and can be related to time as shown in Figure 3.  In this case, the diffusion distance is noted as "$<l>$" is the mean square distance.
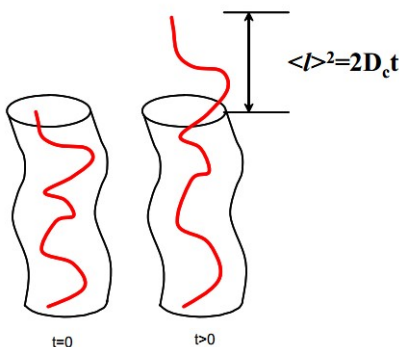


Figure 3. Single molecule motion (Grewell & Benatar, 2008)

It is possible to relate the mean diffusion distance squared ($<l>^2$) of any one chain near the interface to the distance that chain propagates across the interface (X) as shown in equation 2.

$$X \approx \sqrt{<l>^2}$$

By using Einstein's diffusion equation and Eq. 1, where D is the diffusion coefficient, it is possible to show that healing time is related to time by a power of ¼, as shown in equation 3.

$$<l>^2 = 2Dt \Rightarrow l = \sqrt{2Dt} \Rightarrow X = (2Dt)^{\frac{1}{4}}$$
$$\therefore$$
$$X \sim t^{\frac{1}{4}}$$

In addition, Jud, et al., proposed that the diffusion coefficient is an Arrhenius function of temperature (*T*) and it can be expressed as shown in equation 4 (Jud, et al., 1981).

$$D(T) = D_0 e^{\left[\frac{-E_a}{RT}\right]}$$

where $D_0$ is the diffusion constant, $E_a$ is the activation energy and k is the Boltzmann constant ($1.3807 \times 10-23$ J/K). While many investigators have assumed that activation energy is temperature-independent, there is data in the open literature that suggest differently. For example, Loos and Dara (1985), studied the healing of polysulphone and assumed an activation energy to be temperature-independent. Grewell and Benatar (2008), were able to estimate the activation energy by evaluating the relationship between plotted natural logs of the slopes of the various weld strength temperatures, as functions of the reciprocal of the temperatures, see Figure

4 (Grewell & Benatar, 2008). In this figure, the solid line is the slope assumed by Loos. While this estimate is reasonable, Grewell and Benatar proposed a better fit is one that has a slope that is temperature-dependent (dashed line).
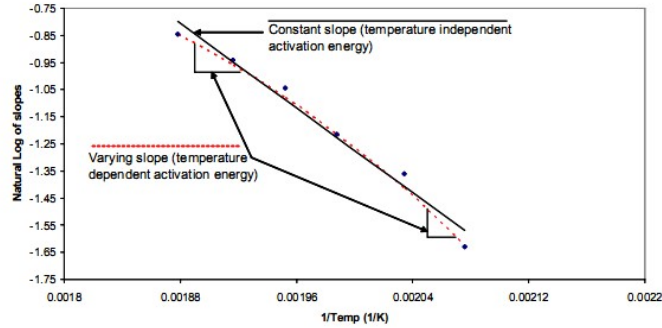


Figure 4. Natural log of slopes as a function of inverse temperature (Grewell & Benatar, 2008)

By using a temperature-dependent proposed by Grewell and Benatar (2008), provided more accurate predictions of interfacial healing. Such a deviation from the classical model of a temperature independent activation energy, may be justified because their model lumps diffusion and squeeze together.

"Because most industrial processes produce temperature histories that are time-dependent, then each duration at a given temperature contributes incrementally to healing until the interface is fully healed. For a continuously varying temperature it is possible to divide a given temperature history into finite time intervals ($\Delta t$)." Thus it is possible that the degree of welding (DW), which combines squeeze flow and healing, can be defined as:

$$DW(T,t)_h = \sum_{t=0}^{t=t'} K_0 \cdot e^{-\frac{E_a}{kT}} \cdot \Delta t^{1/4}$$

Eq. 5

Which is graphically depicted in Figure 5.
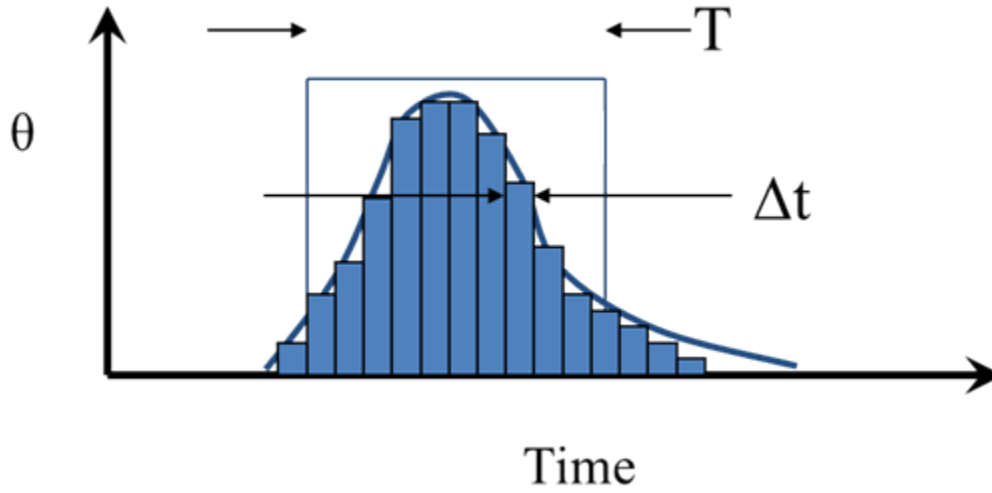


Figure 5. Graphical illustration of adhesion with varying temperature history

**Thermal model**

In order to predict the temperature in the extruded filament, a model based on 1st order principles was used. The variables include:

$\rho$  Material density of the filament

$\lambda$  Thermal conductivity of the filament material

C  Heat capacity of the filament material

H  Heat loss coefficient through convection between the filament and the surrounding air

$\theta_d$  Temperature of the die

$\theta_{air}$ Temperature of the air surrounding the filament

V  The speed of the filament extrusion

The assumption of the model were:

- Constant material properties
- Homogeneous material
- No phase change
- Constant velocity

- Heat loss only through convection

- Assume constant coefficient of heat loss

- Assume rod is uniform temperature in r-direction ($\frac{\partial \theta}{\partial r} = 0$)

- No internal heat loss/generation (Q=0)

- Steady state condition($\frac{\partial \theta}{\partial t} = 0$)

- Fully developed system

The model is seen in Figure 6, where $q_r^h$ is the heat flux for the convection heat transfer (to the air) in the r-direction, $q_x^{cv}$ is the heat flux of the convection heat transfer (material movement) in the x-direction. The origin of the two dimensional coordinate system (x, r) are at the opening of the die and in the center of the die. A small volume with a dimension in the x-direction of dx is considered. Thus the heat flux entering the are detonated as $q_x$ and the heat fluxes at the existing the element are at $d_{x+dx}$ .

In order to simplify the model by reducing the number of independent parameters, a coordinate system fixed at the opening is defined and the system is assumed to be fully developed. This allows the time derivates to be set to zero.
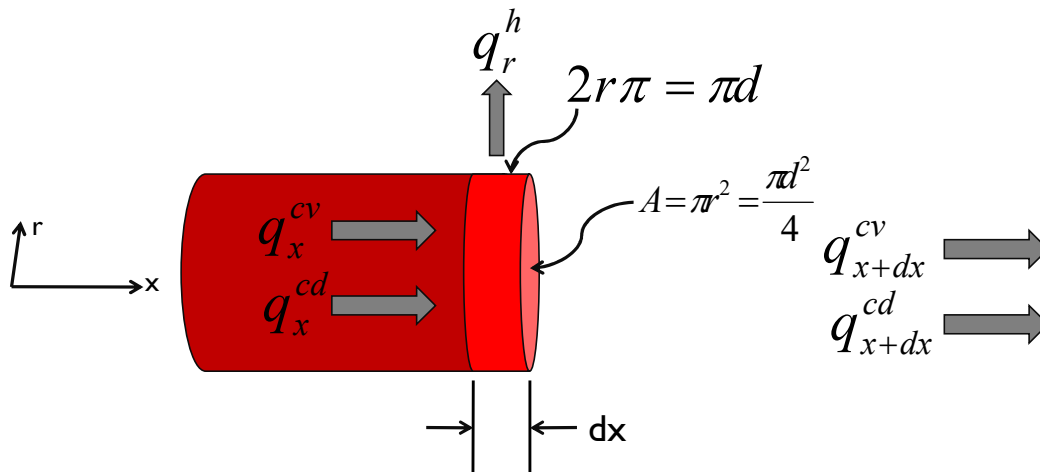


Figure 6. General model for filament extrusion

The circumferential surface area of the element (A) is $\pi d^2$ and the cross-sectional surface area of the element is $\frac{\pi d^2}{4}$. By summing the heat fluxes it is possible to obtain equation 6, defined the energy balance where t is time.

$$\underbrace{q_x^{cv} - q_{x+dx}^{cv} + q_x^{cd} - q_{x+dx}^{cd} - q_r^{h} + Q}_{\text{Energy in, out and generated}} = \underbrace{\rho C \frac{d\theta}{dt}}_{\text{Change of energy in element}}$$

Eq. 6.

In terms of the unit volume Eq. 6 can be expanded to include the defined geometry as seen in equation 7.

$$Aq_x^{cv} - Aq_{x+dx}^{cv} + Aq_x^{cd} - Aq_{x+dx}^{cd} - \pi d \cdot dxq_r^{h} + QAdx = \rho C \frac{d\theta}{dt} Adx$$

Eq. 7.

By use of Taylor series expansion it is possible to redefine the x+dx terms as x terms as detailed in equations 8 and 9.

$$q_{x+dx}^{cv} = q_x^{cv} + \frac{\partial q_x^{cv}}{\partial x} dx$$

Eq. 8

$$q_{x+dx}^{cd} = q_x^{cd} + \frac{\partial q_x^{cd}}{\partial x} dx$$

Eq. 9

Substituting equations 8 and 9 in for Eq. 7, equation 10 is derived.

$$Aq_x^{cv} - A\left( q_x^{cv} + \frac{\partial q_x^{cv}}{\partial x} dx \right) + Aq_x^{cd} - A\left( q_x^{cd} + \frac{\partial q_x^{cd}}{\partial x} dx \right) - \pi d \cdot dxq_r^{h} + QAdx = \rho C \frac{d\theta}{dt} Adx$$

Eq. 10.

By expanding the terms in equation 10 it can be seen that many of the terms negate each other (noted as arrows) and assuming no internal heat generation (Q=0).

$$Aq_x^{cv} - Aq_x^{cv} - A\frac{\partial q_x^{cv}}{\partial x}dx + Aq_x^{cd} - Aq_x^{cd} - A\frac{\partial q_x^{cd}}{\partial x}dx - \pi d \cdot dxq_r^{h} + QAdx = \rho C\frac{d\theta}{dt}Adx$$

Eq. 11.

Thus equation 11 reduces to equation 12.

$$-A\frac{\partial q_x^{cv}}{\partial x}dx - A\frac{\partial q_x^{cd}}{\partial x}dx - \pi d \cdot dxq_r^{h} = \rho C\frac{d\theta}{dt}Adx$$

Eq. 12.

By dividing the entire equation by A, equation 13 derived.

$$-\frac{\partial q_x^{cv}}{\partial x} - \frac{\partial q_x^{cd}}{\partial x} - \frac{\pi d \cdot q_r^{h}}{A} = \rho C\frac{d\theta}{dt}$$

Eq. 13.

By substituting constitutive relations seen in equation 14.

Eq. 14.

$$q_x^{cd} = -\lambda\frac{\partial\theta}{\partial x} \qquad q_x^{cv} = -\rho CV\theta \qquad q_r^{h} = h(\theta-\theta_d)$$

It is possible to derive a general differential equation governing the model as seen in equation 15.

$$-\rho CV\frac{\partial\theta}{\partial x} + \lambda\frac{\partial^2\theta}{\partial x^2} - \frac{4h(\theta-\theta_d)}{d} = \rho C\frac{d\theta}{dt}$$

Eq. 15.

By defining thermal diffusivity ($\kappa$) as seen in equation 16, it is possible to define the material properties in relationships that can used to simplify Eq. 16.

$$\kappa = \frac{\lambda}{\rho C} \Rightarrow \lambda = \kappa \rho C \Rightarrow \rho C = \frac{\lambda}{\kappa}$$

Eq. 16.

Thus a simplified governing differential equation can be derived as seen in Eq. 17.

$$\frac{\partial^2 \theta}{\partial x^2} - \frac{V}{\kappa} \frac{\partial \theta}{\partial x} - \frac{4h}{d\lambda} (\theta - \theta_d) = \frac{1}{\kappa} \frac{d\theta}{dt}$$

Eq. 17.

To find a solution to the general governing differential equation (Eq. 17), it is possible to use a Laplace transform and assuming a general solution for A as seen in equation 18.

$$\theta(x) = Ce^{Dx}$$

Eq. 18

Thus the 1st and 2nd derivative relative to x are seen in equation 19.

$$\frac{\partial \theta(x)}{\partial x} = CDe^{DX}$$
$$\frac{\partial^2 \theta(x)}{\partial x^2} = CD^2 e^{DX}$$

Eq. 19.

Substituting equations 18 and 19 in the general differential equation (Eq.17), a form as seen in equation 20 is derived.

$$CD^2 e^{Dx} - \frac{V}{\kappa} CDe^{Dx} - \frac{4h}{d\lambda} (Ce^{Dx} - \theta_d) = \frac{1}{\kappa} \frac{d\theta}{dt}$$

Eq. 20.

The differential equation can then be further reduced by applying the predefined assumption of steady state allowing the time derivative to be set to zero as seen in equation 21.

$$CD^2 e^{Dx} - \frac{V}{\kappa} CDe^{Dx} - \frac{4h}{d\lambda}(Ce^{Dx} - \theta_d) = 0$$

Eq. 21.

By using a temporary (dummy) variable relating the difference in the die temperature to any location in the x-direction as (Eq. 22),

$$\theta' = \theta - \theta_d$$

Eq. 22.

It is possible to further reduce the governing differential equation as seen in equation 23.

$$CD^2 e^{Dx} - \frac{V}{\kappa} CDe^{Dx} - \frac{4h}{d\lambda} Ce^{Dx} = 0$$

Eq. 23

Dividing equation 23 by the common terms ($Ce^{Dx}$), it is further reduced as seen in equation 24,

$$D^2 - \frac{V}{\kappa} D - \frac{4h}{d\lambda} = 0$$

Eq. 24.

The constant D in equation 24 can be defined using the general solution to a second order quadrate equation as seen in equation 25.

$$D = \frac{-b \pm \sqrt{b^2 - 4ac}}{2a} = \frac{\frac{V}{\kappa} \pm \sqrt{\left(\frac{V}{\kappa}\right)^2 - 4\left(\frac{-4h}{d\lambda}\right)}}{2}$$

Eq. 25.

Substituting the solution for D back into the assumed solution, equation 18, the general solution

is seen in equation 26.

$$\theta'(x) = Ce^{Dx}$$

$$= C_1 \exp\left(\frac{\frac{V}{\kappa} + \sqrt{\left(\frac{V}{\kappa}\right)^2 + 4\left(\frac{4h}{d\lambda}\right)}}{2}\right)x + C_2 \exp\left(\frac{\frac{V}{\kappa} - \sqrt{\left(\frac{V}{\kappa}\right)^2 + 4\left(\frac{4h}{d\lambda}\right)}}{2}\right)x$$

Eq. 26.

Knowing that the boundary condition at the die (x=0) and at infinity (x=), as seen in equation 27,

$$\text{at } x \to \infty \quad \theta = 0 \therefore C_2 = 0$$
$$\text{at } x \to 0 \quad \theta = \theta_d \therefore C_1 = \theta_d$$

Eq. 27

…it is possible to reduce the general equation as seen in equation 28.

$$\theta'(x) = \theta_d \exp\left(\frac{\frac{V}{\kappa} - \sqrt{\left(\frac{V}{\kappa}\right)^2 + 4\left(\frac{4h}{d\lambda}\right)}}{2}\right)x$$

Eq. 28

This solution can then be simplified into a time domain or absolute temperature by further

substituting in the constitutive relations.

**Purpose of Research**

In the 21st Century, manufacturers are facing significant challenges, market disruption,

innovation, business accelerators, and workforce skills are just a few of the factors making it

difficult to be competitive in an increasingly unknown market. In previous years, large companies possessed significant knowledge about, product requirements, material availability, and customer expectations, and would use this information to help them develop budgets, create proprietary infrastructure, manage intellectual property, and strategically position themselves in respect to the competition. However, in today's global market that just is not possible. In the world market of today, companies need new ways to analyze, design, manufacture, and distribute their products and services. Additive manufacturing is an innovative and agile group of technology processes that have the potential to help companies address the increasingly narrow niche market needs with products designed and customized to meet specific customer requirements.  With growing interest, and a significant level of public hype, AM is still in the adolescent stage of its development. After thirty years of research there continues to be a significant need for study in materials, processes, and methods that will facilitate wide spread adoption into the manufacturing industry.

This study builds on the empirical, squeeze flow and intermolecular diffusion model research conducted by David Grewell and Avraham Benatar, applying a combined model to predict auto adhesion or healing to FFF part samples.  In this research, an experimental study and numerical modeling were developed and utilized to drive and validate a closed form heat transfer solution for extrusion processes to develop temperature field models.  An extrusion-based 3D printing system, with the capacity to vary deposition speeds and temperatures, was used to fabricate the samples. Standardized specimens of Polylactic Acid (PLA) and Acrylonitrile Butadiene Styrene (ABS) filament were used to fabricate the samples with different speeds and temperatures. Cross sectioning and microscopic observation was performed to find the effect of the speed and the temperature on the geometry of the cross-sections.

It was found that by increasing the speed of the extrusion printing, the area of the cross-section and the maximum thickness decrease, while the filament geometry minimum thickness increases at higher speeds, although actual weld strength appeared to plateau for speeds above 15mm/sec. Temperature effect was found to increase the weld/bead geometry minimum thickness. In most cases, test results show that by increasing the speed and the temperature, the part strength increases. Non-Linear finite element based numerical model was performed to predict the strength of the samples. The geometry produced from the micro-scanning and typical PLA material properties were used to create the model. The finite element model was able to predict the strength of the tested samples at different speeds and temperatures. Analysis of resulting data and examination of tested samples offer favorable insights and opportunities for additional and continuing investigation.

## Research Questions

The study has been guided by the following research questions:

1.  What is the acceptable range of extrusion head temperatures available for producing parts in ABS and PLA using fused deposition modeling?

2.  What are the acceptable limits of extrusion head velocity available for producing parts in ABS and PLA using fused deposition modeling?

3.  What combinations of speed and temperature can be used to increase final part strength?

4.  What is the effect on part strength of extruded road geometry?

5.  Is it possible to predict FDM part strength using a closed form mathematical formula for different additive manufacturing materials?

## Measurement and Methodology

To gather information needed to answer the research questions, the methodology was completed in five phases. In the first two phases, exploratory experimentation was conducted to help determine research feasibility, including extrusion temperature ranges, head speed options, strength test methodologies, sample part build parameters, and material properties. The third phase of this research included pre-experimental tests to help identify appropriate fabrication and testing methods. Phase four included an experimental test to validate the experimental design and to set processing limits for the ABS and PLA experiments. Phase five consisted of fabrication of one experimental set of ABS samples and three runs of PLA samples. Tensile testing and microtome analysis of the fabricated samples was then completed. These phases are detailed in the following sections.

Phase I – Exploratory experimentation was conducted at Iowa State University to determine the preferred strand orientation and material strength test method for the final experiment. Test samples were fabricated from ABS filament on a Stratasys 1650 Fused Deposition Modeling system. Evaluations were made of samples with strands oriented at 90˚ to the axis of the sample part and tested in tension using ASTM D638-03 standard test method for tensile properties of plastics. Evaluations were also made on samples with strands oriented parallel to the sample part axis and tested in three point shear using ASTM D 2344/D 2344M-00 Standard Test Method for Short-Beam Strength of Polymer Matrix Composite Materials and Their Laminates. Based on previous experience there was some concern about significant scatter in the data for parts tested in tension as there is relatively little healed material present in the axis of load (tension). Initial findings suggested samples should be tested in short beam bend test in order to determine weld strength between the fibers.

Phase II - Exploratory experimentation was also conducted on PLA films to assess the accuracy of the proposed intermolecular healing model as well as estimating the fitting parameters of the models. Films were produced at Iowa State University from PLA and ABS filaments/pellets provided by Erlangen University. The films were cut utilizing an ultrasonic cutting die or knife with a die to provide consistent sample geometry. The film was welded utilizing an impulse welder with water chilled head and fixture. The process parameters that were studied included time (5x) and temperature (5) using a full factorial design of experiments. All experiments were repeated five times. Weld strengths were evaluated using ASTM D 882-02 Standard Test Method for Tensile Properties of Thin Plastic Sheeting. This strength of weld analysis provides estimates of fitting parameters for the healing models.

Phase III - Pre-experimental sample fabrication was conducted by the researcher and Erlangen staff on the Stratasys FDM 2000 and 8000 to validate deposition system and test sample model. Samples were fabricated from PLA filament and ABS filament. Samples were evaluated for material strength utilizing the selected test method determined in Phase I experimentation.

Results from pre-experimental sample fabrication and testing revealed difficulties inherent to the direct fabrication of test samples using FDM and an inability to vary deposition speed because of the restricted controls available on Stratasys machines. A revised experimental method was then developed where sample blanks (of 10, 25, and 50 mm) would be fabricated using the FDM process and the resulting blanks would then be CNC machined by Erlangen technical staff for testing using the ASTM D638-03 Standard Test Method for Tensile Properties of Plastics using a Zwick / Roell Zmart.Pro tensile testing instrument.

In addition, samples produced using PLA filament provided by Erlangen staff proved insufficient to provide consistent experimental data. Variation associated with material formulation and filament diameter limited evaluation of weld strength. Initial attempts to produce PLA material for AM extrusion from bulk resin resulted in filaments with highly variable cross-sectional diameters and limited durability. Pre-extruded PLA filaments would often break, slip, and clog prior to entering the material liquefier, suggesting further research was needed to identify and acquire a PLA formulation applicable to the extrusion process.

Phase IV – Experimental pilot test of sample fabrication of ABS and PLA parts, working with an undergraduate research assistant and using a Mendel 190 3D printer, at Iowa State University, using 3MM filament material purchased from MakerBot Industries. Combinations of extrusion speed and head temperature were tested to determine printable ranges for both materials. Acceptable sample blanks were obtained for ABS ranging from 10 to 25 millimeters per second with temperatures from 230 to 250 degrees Celsius. Acceptable sample blanks were obtained for PLA ranging from 10 to 25 millimeters per second with temperatures from 195 to 220 degrees Celsius.

Phase V – Sample ASTM equivalent specimen (dog bones) were produced by printing rectangular tensile testing coupons and machining to remove the outer shell and shape them in accordance with ASTM D638-03 standards. Samples were machined on a standard vertical mill using a circular milling cutter tool and secured using a proprietary jig fixture. Finished specimens were subsequently tested by the researcher to the ASTM D638-03 Standard Test Method for Tensile Properties of Plastics using a tensile testing instrument. Data was logged for break strength.

Upon completion of the tensile properties testing, the researcher conducted a microtome analysis of selected specimen based on PLA material specimens, extrusion temperature (high and low), and deposition speeds (fast and slow). Microtome sampling were completed to produce across profiles of the filament sections to identify extruded filament shape and voids between filaments. Untested samples were also analyzed for comparison.

## Statistical Analysis

In this study extrusion temperature and printer head-speed are being considered as factors of the healing function associated with thermoplastic materials deposited on a translational build platform to create three dimensional parts using a layering method. Ideally, it would be beneficial to develop a comprehensive index of all possible temperature-speed combinations using empirical methods. Multiple replication of such an investigation would require significant time and investment to accurately define the index values. However, given the limitation of this study it was determined a semi-empirical study would be utilized to develop guide points for temperature and velocity settings that would enable increased part strength.

Based on pre-experimental tests and an abbreviated pilot test, possible parameter ranges were identified for both extrusion temperature (PLA @ 195◦ - 225◦ C, ABS @ 230◦ – 250◦ C) and printer head-speed (10 – 25 MM/Sec). Full factorial experimental designs were then developed for each material with 20 treatment combinations for ABS and 28 treatment combinations in PLA. The experimental fabrication runs were then randomized utilizing Table 1 and Table 2 as seen below. Experiments were replicated five times for each velocity-temperature combination. Four PLA experimental runs have been completed, two fabricated on a MakerBot

2000 printer (2016 Exp. 1&2), and two on a Prusa i3 printer (2017 Exp. 1&2). One ABS

experimental run was completed using the Mendel 190 3D printer.

Frequency histograms were then created for each experimental run to assess whether the

tested sample data sets were approximately normally distributed, seen in Figure 7, the tested

sample data display an approximately normal distribution, although the 2017 E2 run, with a

0.20mm layer, may be of concern. Descriptive statistics were calculated for each treatment

combination within experimental runs for both PLA and ABS and can be found in appendix B.,

summary statistics are provided in Table 3. PLA 2017 experiment 1 demonstrated the highest

average strength 56.4 MPa with a standard deviation of 3.48 MPa. The descriptive statistics

indicate that strength is proportional to temperature as expected considering diffusion in

polymers is a function of thermal energy, with PLA average breaking strength ranging from 26.4

to 60.3 MPa over the three comparative experiments. Least-Squares Regressions were developed

for both changes in speed within individual temperatures, as well as for changes in temperature

within head speeds to determine if the data would accurately represent the predicted values.

Summary values listed in Table 4 and Table 5 where we see the linear regressions have a

relatively poor fit to the experimental data with $r^2$ values ranging from 0.0002 to 0.5046.

Table 1. ABS Randomized

| Run Order | Speed | Temp | Sample 1 | Sample 2 | Sample 3 | Sample 4 | Sample 5 |
|-----------|-------|------|----------|----------|----------|----------|----------|
| 1 | 25 | 235 | ## | ## | ## | ## | ## |
| 2 | 25 | 245 | ## | ## | ## | ## | ## |
| 3 | 25 | 250 | ## | ## | ## | ## | ## |

| Table 1. (continued) | | | | | | | |
|---|---|---|---|---|---|---|---|
| 4 | 10 | 245 | ## | ## | ## | ## | ## |
| 5 | 15 | 235 | ## | ## | ## | ## | ## |
| 6 | 20 | 230 | ## | ## | ## | ## | ## |
| 7 | 20 | 240 | ## | ## | ## | ## | ## |
| 8 | 15 | 230 | ## | ## | ## | ## | ## |
| 9 | 10 | 250 | ## | ## | ## | ## | ## |
| 10 | 10 | 230 | ## | ## | ## | ## | ## |
| 11 | 15 | 250 | ## | ## | ## | ## | ## |
| 12 | 25 | 240 | ## | ## | ## | ## | ## |
| 13 | 25 | 230 | ## | ## | ## | ## | ## |
| 14 | 20 | 250 | ## | ## | ## | ## | ## |
| 15 | 15 | 245 | ## | ## | ## | ## | ## |
| 16 | 20 | 245 | ## | ## | ## | ## | ## |
| 17 | 15 | 240 | ## | ## | ## | ## | ## |
| 18 | 20 | 235 | ## | ## | ## | ## | ## |
| 19 | 10 | 240 | ## | ## | ## | ## | ## |

Table 2. PLA Randomized

| Run Order | Speed | Temp | Sample 1 | Sample 2 | Sample 3 | Sample 4 | Sample 5 |
|---|---|---|---|---|---|---|---|
| 1 | 25 | 220 | ## | ## | ## | ## | ## |

| Table 2. (continued) | | | | | | | |
|---|---|---|---|---|---|---|---|
| 2 | 15 | 205 | ## | ## | ## | ## | ## |
| 3 | 25 | 225 | ## | ## | ## | ## | ## |
| 4 | 15 | 200 | ## | ## | ## | ## | ## |
| 5 | 20 | 220 | ## | ## | ## | ## | ## |
| 6 | 25 | 210 | ## | ## | ## | ## | ## |
| 7 | 25 | 205 | ## | ## | ## | ## | ## |
| 8 | 10 | 225 | ## | ## | ## | ## | ## |
| 9 | 10 | 210 | ## | ## | ## | ## | ## |
| 10 | 10 | 215 | ## | ## | ## | ## | ## |
| 11 | 20 | 210 | ## | ## | ## | ## | ## |
| 12 | 20 | 195 | ## | ## | ## | ## | ## |
| 13 | 10 | 205 | ## | ## | ## | ## | ## |
| 14 | 10 | 195 | ## | ## | ## | ## | ## |
| 15 | 10 | 200 | ## | ## | ## | ## | ## |
| 16 | 20 | 225 | ## | ## | ## | ## | ## |
| 17 | 15 | 215 | ## | ## | ## | ## | ## |
| 18 | 15 | 225 | ## | ## | ## | ## | ## |
| 19 | 15 | 195 | ## | ## | ## | ## | ## |
| 20 | 20 | 215 | ## | ## | ## | ## | ## |
| 21 | 25 | 195 | ## | ## | ## | ## | ## |
| 22 | 25 | 200 | ## | ## | ## | ## | ## |

| Table 2. (continued) | | | | | | | |
|---|---|---|---|---|---|---|---|
| 23 | 10 | 220 | ## | ## | ## | ## | ## |
| 24 | 15 | 220 | ## | ## | ## | ## | ## |
| 25 | 20 | 205 | ## | ## | ## | ## | ## |
| 26 | 20 | 200 | ## | ## | ## | ## | ## |
| 27 | 25 | 215 | ## | ## | ## | ## | ## |
| 28 | 15 | 210 | ## | ## | ## | ## | ## |
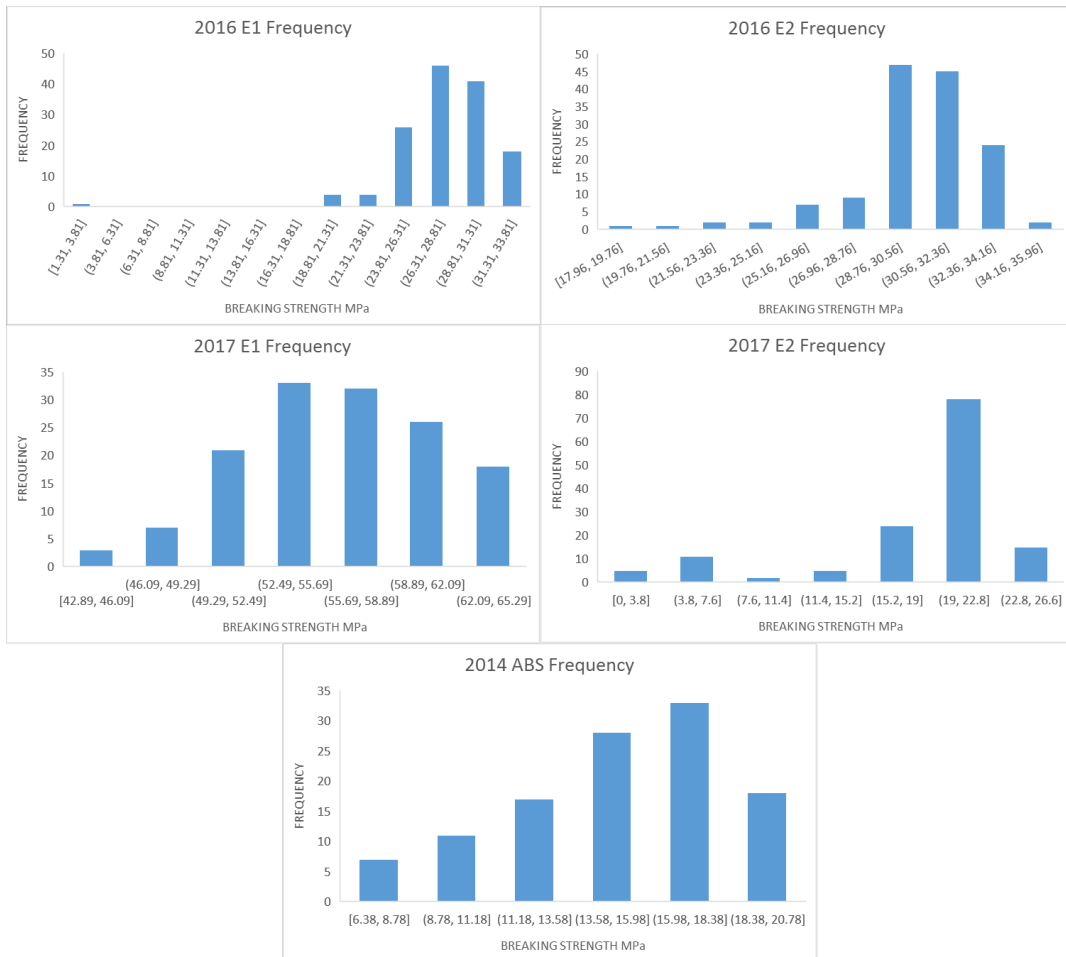


Figure 7. Experimental Frequency Histograms

Table 3. Summary Statistics

| | PLA 2016 Exp 1 | | | | | | PLA 2016 Exp 2 | | | | |
|---|---|---|---|---|---|---|---|---|---|---|---|
| Temp. C | Average Strength | Std Dev S | MM/Sec | Average Strength | Std Dev S | Temp. C | Average Strength | Std Dev S | MM/Sec | Average Strength | Std Dev S |
| 195 | 27.83 | 3.40 | 10 | 28.09 | 2.756 | 195 | 28.88 | 3.47 | 10 | 29.68 | 2.329 |
| 200 | 26.47 | 1.72 | 15 | 28.71 | 1.780 | 200 | 29.39 | 1.48 | 15 | 31.19 | 1.162 |
| 205 | 27.16 | 2.09 | 20 | 26.74 | 3.753 | 205 | 29.85 | 1.78 | 20 | 30.29 | 1.828 |
| 210 | 27.43 | 4.81 | 25 | 28.25 | 2.530 | 210 | 30.81 | 1.76 | 25 | 30.36 | 2.461 |
| 215 | 29.91 | 1.56 | | | | 215 | 31.89 | 1.19 | | | |
| 220 | 28.93 | 2.32 | | | | 220 | 30.94 | 1.94 | | | |
| 225 | 27.90 | 3.03 | | | | 225 | 30.91 | 2.00 | | | |

| | PLA 2017 Exp 1 | | | | | | PLA 2017 Exp 2 | | | | |
|---|---|---|---|---|---|---|---|---|---|---|---|
| Temp. C | Average Strength | Std Dev S | MM/Sec | Average Strength | Std Dev S | Temp. C | Average Strength | Std Dev S | MM/Sec | Average Strength | Std Dev S |
| 195 | 52.56 | 3.26 | 10 | 55.29 | 4.583 | 195 | 15.82 | 7.75 | 10 | 16.08 | 4.737 |
| 200 | 53.47 | 3.07 | 15 | 56.52 | 3.728 | 200 | 14.39 | 6.19 | 15 | 19.41 | 4.009 |
| 205 | 55.37 | 3.34 | 20 | 57.05 | 2.821 | 205 | 17.83 | 4.59 | 20 | 19.12 | 4.421 |
| 210 | 55.37 | 3.79 | 25 | 56.84 | 2.798 | 210 | 19.43 | 2.87 | 25 | 19.47 | 3.418 |
| 215 | 58.81 | 3.64 | | | | 215 | 20.48 | 2.49 | | | |
| 220 | 59.11 | 3.75 | | | | 220 | 21.14 | 2.67 | | | |
| 225 | 60.27 | 3.51 | | | | 225 | 20.55 | 2.48 | | | |

| ABS 2015 Exp 1 | | | | | |
|---|---|---|---|---|---|
| Temp. C | Average Strength | Std Dev S | MM/Sec | Average Strength | Std Dev S |
| 230 | 13.38 | 2.66 | 10 | 16.01 | 1.706 |
| 235 | 15.12 | 2.57 | 15 | 15.41 | 1.858 |
| 240 | 15.77 | 1.79 | 20 | 15.85 | 1.938 |
| 245 | 16.13 | 2.33 | 25 | 13.02 | 4.076 |
| 250 | 14.96 | 2.62 | | | |

Table 4. PLA Least-Squares Regression Summary

| Least-Squares Regression for Changes in Speed within Temperature | | | | | | | | | |
|---|---|---|---|---|---|---|---|---|---|
| **PLA 2016 E1** | | | | | **PLA 2016 E2** | | | | |
| **R Square** | **Slope** | **Intercept** | **Residual SS** | **P-value** | **R Square** | **Slope** | **Intercept** | **Residual SS** | **P-value** |
| 0.0002 | 0.0078 | 27.6930 | 232.1336 | 4.2312E-09 | 0.0021 | -0.0308 | 29.4192 | 286.9930 | 8.5789E-09 |
| 0.4102 | 0.2455 | 22.1742 | 54.1497 | 1.0529E-12 | 0.3843 | 0.2194 | 25.5522 | 48.1841 | 3.3661E-14 |
| 0.0416 | -0.0915 | 28.7636 | 120.4822 | 1.1164E-11 | 0.0483 | 0.0742 | 0.0742 | 67.6928 | 9.3390E-14 |
| 0.0049 | -0.0809 | 28.8459 | 829.1841 | 1.7608E-05 | 0.0926 | 0.1154 | 28.7901 | 81.5620 | 4.0231E-13 |
| 0.3940 | -0.2352 | 34.0247 | 53.2014 | 5.3679E-16 | 0.3315 | -0.1900 | 35.2128 | 45.4825 | 7.3615E-17 |
| 0.0007 | -0.0138 | 29.1760 | 158.9697 | 8.7971E-11 | 0.0070 | 0.0380 | 30.2763 | 127.8692 | 7.7829E-12 |
| 0.0068 | -0.0416 | 28.6245 | 157.8265 | 1.1340E-10 | 0.0327 | -0.0680 | 32.0967 | 85.6159 | 9.4080E-14 |
| **PLA 2017 E1** | | | | | **PLA 2017 E2** | | | | |
| **R Square** | **Slope** | **Intercept** | **Residual SS** | **P-value** | **R Square** | **Slope** | **Intercept** | **Residual SS** | **P-value** |
| 0.0150 | 0.0724 | 51.2992 | 215.2288 | 8.1929E-14 | 0.1185 | 0.4766 | 6.7132 | 1056.1379 | 2.4850E-01 |
| 0.5046 | 0.6367 | 42.3324 | 248.7350 | 7.4629E-12 | 0.1843 | 0.5282 | 4.7037 | 771.9626 | 3.4131E-01 |
| 0.0870 | 0.1839 | 52.1543 | 221.7557 | 7.9704E-14 | 0.0865 | -0.2534 | 22.2662 | 423.7124 | 6.8468E-06 |
| 0.0016 | 0.0258 | 54.9154 | 267.2811 | 1.6384E-13 | 0.2163 | 0.2590 | 14.8992 | 151.9504 | 1.6194E-06 |
| 0.1114 | -0.2189 | 62.6434 | 238.9783 | 6.3260E-15 | 0.0887 | 0.1495 | 17.8614 | 143.4676 | 8.4811E-08 |
| 0.1459 | -0.2834 | 64.0740 | 293.8179 | 2.5790E-14 | 0.1171 | 0.2478 | 16.8024 | 289.3224 | 2.0813E-05 |
| 0.2049 | 0.3080 | 0.3080 | 230.1290 | 4.5539E-14 | 0.2035 | 0.2456 | 16.2538 | 147.4799 | 4.0016E-07 |
| Least-Squares Regression for Changes in Temperature within Speed | | | | | | | | | |
| **PLA 2016 E1** | | | | | **PLA 2016 E2** | | | | |
| **R Square** | **Slope** | **Intercept** | **Residual SS** | **P-value** | R Square | Slope | Intercept | Residual SS | P-value |
| 0.0756 | 0.0865 | 9.9222 | 320.4498 | 3.7674E-01 | 0.1679 | 0.1157 | 5.3880 | 232.0400 | 5.7135E-01 |
| 0.1248 | 0.0949 | 8.7769 | 221.0018 | 3.4683E-01 | 0.3611 | 0.1084 | 8.4244 | 72.7932 | 1.1999E-01 |
| 0.0041 | 0.0329 | 19.8296 | 929.5947 | 3.0074E-01 | 0.0373 | 0.0488 | 20.0394 | 215.6555 | 3.4465E-02 |
| 0.0017 | 0.0107 | 25.9994 | 238.8630 | 1.0348E-02 | 0.0278 | 0.0476 | 20.3518 | 277.9883 | 5.6898E-02 |
| **PLA 2017 E1** | | | | | **PLA 2017 E2** | | | | |
| **R Square** | **Slope** | **Intercept** | **Residual SS** | **P-value** | **R Square** | **Slope** | **Intercept** | **Residual SS** | **P-value** |
| 0.2090 | 0.3083 | -49.2862 | 1259.4209 | 3.1588E-02 | 0.3605 | 0.3757 | -23.6130 | 876.3104 | 2.0621E-01 |
| 0.2245 | 0.2367 | -30.3815 | 677.4404 | 6.7995E-02 | 0.3988 | 0.3097 | -8.5183 | 506.0385 | 5.4465E-01 |
| 0.1433 | 0.1901 | -20.7903 | 756.1364 | 2.3029E-01 | 0.1707 | 0.1488 | 25.8107 | 376.3914 | 3.8927E-02 |
| 0.2438 | 0.2226 | -27.2679 | 537.7042 | 6.6079E-02 | 0.4498 | 0.2465 | 5.0691 | 260.1306 | 6.1479E-01 |

Table 5. ABS Least-Squares Regression Summary

| Least-Squares Regression for Changes in Speed within Temperature | | | | | | |
|---|---|---|---|---|---|---|
| | **2015 ABS** | | | | | |
| | | **R Square** | **Slope** | **Intercept** | **Residual SS** | **P-value** |
| **230** | | 0.0167 | 0.0638 | 12.2296 | 165.1992 | 2.6402E-06 |
| **235** | | 0.1694 | -0.2210 | 18.9920 | 179.6256 | 1.4276E-09 |
| **240** | | 0.5700 | -0.4651 | 23.9797 | 102.9643 | 1.7894E-11 |
| **245** | | 0.4071 | -0.3840 | 22.8600 | 148.4437 | 6.0452E-11 |
| **250** | | 0.0381 | 0.1258 | 12.8700 | 276.3262 | 5.9679E-05 |
| Least-Squares Regression for Changes in Temperature within Speed | | | | | | |
| | **2015 ABS** | | | | | |
| | | **R Square** | **Slope** | **Intercept** | **Residual SS** | **P-value** |
| **10** | | 0.0066 | -0.0373 | 24.8909 | 286.5674 | 2.6732E-01 |
| **15** | | 0.3904 | 0.2462 | -43.7161 | 141.9254 | 4.7695E-03 |
| **20** | | 0.2824 | 0.1712 | -25.2452 | 111.7601 | 5.1069E-02 |
| **25** | | 0.0013 | -0.0201 | 17.8558 | 426.3026 | 4.9923E-01 |

Based on evaluation of the summary statistics, least-squares regressions, and preliminary results of the predictive thermal model it is postulated, changes in extrusion head velocity play a minimal role in the healing process. However, further investigation will be needed to accurately answer this question, recent literature indicates head speeds of up to 150 mm/sec are possible with some machines.

Single factor ANOVA were created to further understand the influence of extrusion temperature on the healing process for both ABS and PLA experimental data. Analysis of the ABS results indicated significant difference between temperature groups for head speeds of 10, 15, and 20 mm/sec with P-values below the 0.05 limit (Table 6). ANOVA for the four PLA experimental runs were also developed for changes in temperature within each of the velocity levels with significant values being returned for the following: 2016 E1 – 15 mm/sec, 2016 E2 – 15 & 20 mm/sec, 2017 E1 – 10 mm/sec, and for 2017 E2 – all four speeds demonstrated significant variance as temperature was changed (Appendix C).

Table 6. ABS Single Factor ANOVA

ANOVA Single Factor 2015 ABS 10MM/S

| Source of Variation | SS | df | MS | F | P-value | F crit |
|---|---|---|---|---|---|---|
| Between Groups | 210.1008 | 4 | 52.525 | 14.745 | 5.3609E-06 | 2.817 |
| Within Groups | 78.3679 | 22 | 3.562 | | | |
| | | | | | | |
| Total | 288.4687 | 26 | | | | |

ANOVA Single Factor 2015 ABS 15MM/S

| Source of Variation | SS | df | MS | F | P-value | F crit |
|---|---|---|---|---|---|---|
| Between Groups | 114.2204 | 4 | 28.555 | 5.778 | 2.1030E-03 | 2.776 |
| Within Groups | 118.6015 | 24 | 4.942 | | | |
| | | | | | | |
| Total | 232.8219 | 28 | | | | |

ANOVA Single Factor 2015 ABS 20MM/S

| Source of Variation | SS | df | MS | F | P-value | F crit |
|---|---|---|---|---|---|---|

Table 6. (continued)

| | SS | df | MS | F | P-value | F crit |
|---|---|---|---|---|---|---|
| Between Groups | 60.2322 | 4 | 15.058 | 3.941 | 1.2930E-02 | 2.759 |
| Within Groups | 95.5140 | 25 | 3.821 | | | |
| Total | 155.7463 | 29 | | | | |

ANOVA Single Factor 2015 ABS 20MM/S

| Source of Variation | SS | df | MS | F | P-value | F crit |
|---|---|---|---|---|---|---|
| Between Groups | 38.5405 | 4 | 9.635 | 0.571 | 6.8654E-01 | 2.796 |
| Within Groups | 388.3253 | 23 | 16.884 | | | |
| Total | 426.8657 | 27 | | | | |

## Organization of Dissertation

This dissertation is written in the alternative manuscript format as defined by Iowa State University's Graduate College. Chapter one is the general introduction which outlines the basic ideas behind the research and summarizes the goals and objectives. Chapter two serves as the literature review of research used as a basis for and justification of the dissertation research. Chapters three, four, five, and six are four manuscripts formatted for submission to specified journals. Chapter seven is a general summary and interpretation of findings, recommendations for further research, and conclusions. Appendices include raw data charts for one experimental run in ABS material, four experimental runs of PLA material at a layer thickness of 0.4 mm, and one run of PLA material with a layer thickness of 0.2 mm. In addition, general descriptive statistics and single factor ANOVA are included.

## References

Amberg, G., & M. Do-Quang, (2007). Thermocapillary convection and phase change in welding. International Journal of Numerical Methods for Heat & Fluid Flow, Vol. 18 No. 3/4, pp. 378-386, DOI: 10:1108/09615530810853637.

Bickrest, E.J., et al., (1996). "Material Selection" Chapter 2. Tool and Manufacturing Engineers Handbook, Vol. 8 Plastic Part Manufacturing, Society of Manufacturing Engineers, Dearborn, Michigan, ISBN-10: 0872634566.

Bird R., R. Armstrong, & O. Hassager, (1987). Dynamics of polymer liquids. 2nd ed., Wiley, New York, Vol. 1, 20.

Crump, S., (1992). Apparatus and method for creating three-dimensional objects. U.S. Patent 5,121,329 A, Filed Oct 30, 1989.

DeGennes P.G., (1971). Reptation of a polymer chain in the presence of fixed obstacles. Journal of Chemical Physics, Vol. 55, Issue 2, pp. 572. DOI: http://dx.doi.org/10.1063/1.1675789.

DeGennes P.G., (1983). Entangled polymers. Physics Today, Vol. 36, Issue 6, DOI: http://dx.doi.org/10.1063/1.2915700.

Grande J.A., (2008). Blow molders & thermoformers try plastic rapid tooling. Plastics Technology, July.

Grewell D., & A. Benatar, (2008). "Semi-empirical, squeeze flow and intermolecular diffusion model. I. Determination of model parameters. Polymer Engineering and Science, Vol. 48, Issue 5, pp 860-867.

Grimm T., (2004). User's guide to rapid prototyping. Society of Manufacturing Engineers, Dearborn, Michigan, ISBN-10: 0872636976.

Hadas Z., J. Zouhar, V. Singule, & C. Ondrusek, (2008). Design of energy harvesting generator base on rapid prototype parts. 13th International Power Electronics and Motion Control Conference (EPE-PEMC 2008).

Hull, C. W., (1986). Apparatus for production of three-dimensional objects by stereolithography. U.S. Patent # 4575330 A, Filed Aug 8, 1984.

Jud, K., H.H. Kausch, & J.G. Williams, (1981). Fracture mechanics studies of crack healing and welding of polymers. Journal of Materials Science, Vol. 16, Issue 1, pp. 204-210.

Kruth, J. P., M. C. Leu, T. Nakagawa, (1998). Progress in additive manufacturing and rapid prototyping. Annals of the CIRP, Vol. 47, Issue 2, pp. 525-540, DOI: https://doi.org/10.1016/S0007-8506(07)63240-5

Laverne, F., F. Segonds, N. Anwer & M. Le Coq, (2015). Assembly Based Methods to Support Product Innovation in Design for Additive Manufacturing: An Exploratory Case Study. Journal of Mechanical Design, December 2015, Vol. 137 / 121701-1.

Loos, A.C. & P.H. Dara, (1985). Thermoplastic matrix composites processing model. Interim Report 57, NASE Cooperative Agreement NAG-1-343, Document ID 19860012148.

Sevidova E.K., L.I. Pupan, & V.N. Tsyuryupa, (2008). Influence of coatings on the surface strength of rapid prototyping products. Surface Engineering and Applied Electrochemistry, Vol. 44 No. 5.

Vogel, J., M. Kessler, S. Sundararajan, & D. Grewell, (2012). Activation energy for diffusion and welding of PLA films. Polymer Engineering and Science, Vol. 52 (8), pp. 1693-1700, DOI: http://dx.doi.org/10.1002/pen.23120.

Wendel, B., D. Rietzel, F. Kühnlein, R. Feulner, G. Hülder, & E. Schmachtenberg, (2008). Additive processing of polymers. Macromolecular Materials and Engineering, Vol. 293, Issue 10, pp. 799-809, DOI: 10.1002/mame.200800121.

Wohlers T., (2009). A low volume production site: coming to a garage near you. Time Compression, July/August.

Wool, R.P., (1995). Polymer interfaces: structure and strength. Hanser, Munich, Germany, ISBN 1569901333.

## CHAPTER 2. LITERATURE REVIEW

This literature review addresses five broad areas of additive manufacturing developments. The review is not intended to be exhaustive. Topics addressed provide a theoretical basis for topics included in the subsequent research articles and the overall dissertation research. Topics reviewed include: (1) the growing interest and historic rise of additive manufacturing technology as it has been described by researchers, business analysts, and electronic press, (2) the current status, challenges, and opportunities for industrial adoption of additive manufacturing for production applications, (3) the development of additive manufacturing technologies, material, and processes associated with fused deposition modeling (FDM), (4) the experimental methodologies associated with additive manufacturing research as presented in academic literature, and (5) activity associated with the development and implementation of standardized industry practice associated with additive manufacturing.

### Growing Interest

The ASTM International Committee F42 on Additive Manufacturing (AM) Technologies defines AM as the "process of joining materials to make objects from three-dimensional (3D) model data, usually layer by layer, as opposed to subtractive manufacturing methodologies" (ASTM, 2017). Compared to conventional production, such as machining, foundary and injection molding, AM offers unprecedented possibilities in shape complexity and custom geometry. Geometries can be generated that are optimized for strength and material volume. While the modern era of additive manufacturing is rooted in technologies such as stereolithography, fused deposition modeling, and selective laser sintering, the original concepts reach back to cut and stack approaches such as topography and photosculpture techniques where

multiple photograph silhouettes were used to produce sculpture sections (Huang & Leu, 2014). Research on additive manufacturing can be broadly covered in the fields of materials, software and new processes.

For most of the twentieth century, manufacturing was dominated by two primary methods, "subtractive/cutting," using mills, lathes, drills, or grinding tools, or "formative," also known as net-shape forming, including bending, casting, or molding (Beyer, 2014). While the introduction of stereolithography is generally considered the starting point for additive manufacturing, the first modern demonstration of an AM process, was proposed by Ciraud in 1972, a powder deposition method using localized heat source (laser, electron beam, or plasma) (Bourell, Beaman, & Rosen, 2009). A number of additive manufacturing processes, techniques and systems have been developed over the last 30 years. With advances in this technology enabling a shift from rapid prototyping to rapid manufacturing of tooling and end-use parts for aerospace, automotive, biomedical and many other applications.

Pioneers in additive manufacturing research, professors Dr. Joseph Beaman and Dr. David Bourell, from the University of Texas at Austin, have acknowledged "a renaissance of interest and activity worldwide" in the field (Beaman et al., 2014). However, this is not without reason, noting that the Annual International Solid Freeform Fabrication Symposium is now in the 28th year of existence. As interest and development in additive manufacturing grows, the number of technology manufacturers, material suppliers, users, and applications are rapidly outpacing the knowledge base. Massachusetts Institute of Technology (MIT) professor, Neil Gershenfeld, has claimed there is "a new digital revolution" sweeping the globe "in fabrication" (2012). Additive manufacturing, is at the heart of that revolution, beginning with the development of

stereolithography just over thirty years ago, this technology is opening new opportunities for designers and manufactures looking to serve the world market. A world market that is increasingly focused on individualized or personalized products.

Additive manufacturing has the potential to disrupt traditional manufacturing practices because it allows fabrication of objects from 3D model data, layer by layer, as opposed to traditional manufacturing technologies, such as subtractive and formative manufacturing (Laverne, et al., 2015). With the capability of using commercial grade thermoplastic materials, Fused Deposition Modeling (FDM) or Fused Filament Manufacturing (FFM) offers some distinct advantages for production part fabrication. Bagsik, et al. (2014), note that it is "one of the most used additive manufacturing processes" serving both commercial applications as well as the burgeoning private user markets. High-end motorsport applications have been especially suitable for additive manufacturing methods. "Unlike passenger cars, vehicles for motorsports usually use light-weight alloys (e.g. titanium) and have highly complex structures and low production volumes" (Guo & Leu, 2013).

Beyer (2014), notes "even though we are advanced, the current accomplishments are still far from the level which can be expected in the future". Stories in the popular press and industry newsletters recount numerous examples of mainstream industrial manufacturers, such as Airbus, taking steps to prepare for full integration of additive manufacturing processes (Sher, 2015). The McKinsey Institute says: "…senior executives must prepare for five disruptions that are being or will be caused by AM," 1) Accelerated product development cycles; 2) New manufacturing strategies and footprints; 3) Shifting sources of profit, mass customization; 4) New capabilities; 5) Disruptive competitors (Cohen, et al., 2014). All of these factors are leading to further

implementation of the "Long Tail" theory, where companies move away from focusing a few large market products and produce a large number of niche market products customized to specific customers (Anderson, 2004).

As Dr. Gershenfeld points out, digital fabrication methods such as additive manufacturing have the potential to make significant changes in the market, allowing "individuals to design and produce tangible objects on demand, wherever and whenever they need them (Gershenfeld, 2012). A growing number of researchers, companies, and end-users have recognized the advantages of additive manufacturing. Recent innovations in materials and processes are transforming 3D printing from rapid prototyping to rapid manufacturing, allowing manufacturing near the point of use, enabling "on-demand" manufacturing and drastically reducing inventories and wait times. Digital fabrication enables manufacturing on demand of small volumes of products that are produced locally, with little or no stock. The roadmap for AM indicates a rise of personalized products and/or (spare) parts that can economically and functionally meet the traditional production techniques such as injection molding (Doubrovski, et al., 2011). Additive manufacturing technologies offer especially great benefits for medical implant products such as hip and knee replacements that require customization (Weeden, et al., 1996).

## Technology Adoption

Comparing additive manufacturing to the plastics industry, it could be postulated, there are a number of factors holding back widespread adoption of this technology. Musso, et al. (2006), noted that it can take up to 15 years for a new plastic material to reach commercial level production levels, with an industry average of nearly 11 years. Similar to the commercial plastics

industry, the additive manufacturing technologies have compounding obstacles to industry

adoption. In addition, while nearly all of the successful plastic materials benefited from the

demand of a specific industry application, all new plastics are faced what might be called

"adoption obstacles" that we also see in additive manufacturing.

Table 7. Adoption Obstacles

| Obstacle | Driving Force | AM Evidence |
|---|---|---|
| Identify Application Markets | Tunnel Vision – focused development | Early focus on rapid prototyping, investment casting, … |
| Value Chain Barriers | Challenges between technology producers and end users | AM Technology controlled by commercial machine manufacturers, 3D Systems, Stratasys, DTM, … |
| Technical Deficiency | Problems inherent in the materials and technology making them unfit for applications | Limited materials, accuracy issues, unknown design constraints, variable physical properties, … |

Educational curriculums are also seeing the effects of additive manufacturing technology.

MIT's Center for Bits and Atoms (CBA), initiated an outreach effort in 2003 that spawned what

have become known as "fab labs" (Gershenfeld, 2012). Supported by funding from the National

Science Foundation, these centers allow easy access to modern fabrication technologies, "with

the purpose to develop new uses and new users for the machines" (Gershenfeld, 2012).

Educational curricula, incorporating additive manufacturing, are being developed and used at

colleges and universities around the world (Williams & Seepersad, 2012).

Design for Manufacturing (DFM) methodologies are also being modified to account for

AM technologies. One area of Design for Additive Manufacturing (DFAM) research takes into

consideration part build orientation, "the Manufacturing Direction (MD) and the Manufacturing

Trajectories (MT)" (Ponche, et al., 2012), have significant implications on final part characteristics and performance.

Another indication that additive manufacturing is making its way into mainstream production part applications is the Lloyd's Register – TWI (The Welding Institute-Cambridge, UK) framework for certification of metallic parts built using AM (Clarke, 2017). Vice President of Stratasys Expert Services, Dr. Phil Reeves (2017), describes a business planning guide for companies considering additive manufacturing and poses three questions that need to be asked before investing: 1) Will AM enable the creation of parts that otherwise would be impossible or not economically feasible? 2) Will a geometrically complex part provide any advantage and improve the company's competitive position? and 3) Will added functionality, which otherwise would be impossible to manufacture, improve the current state of the art?

In 2013, Guo and Leu (2013), described additive manufacturing as "still is not widely accepted by most industries" and called for 5-10 year improvements to bring about a broader industry acceptance. Integration of additive manufacturing methods facilitate a product-development process that is more responsive to changing markets and can result in a product of far higher quality (Beyer, 2014). Parts and assemblies can be built with lighter weight and retain adequate stability and performance.

**Equipment Research**

Building on the field of numerically controlled machining, first developed at MIT in 1952 (Gershenfeld, 2012), rapid prototyping technologies from companies such as 3D systems, LOM, Stratasys, and DTM made it possible to build up parts layer by layer using 3D computer aided design (CAD) data.

According to Kruth, Leu and Nakagawa (1998), many manufacturing experts were skeptical about the possibility of slow and inaccurate rapid prototyping processes being good for any other purpose than producing look-at prototypes. "Today, a great deal of the challenge has been won to turn additive manufacturing into a production technique with a wide scope of application that may further revolutionize the manufacturing world beyond the year 2000" (Kruth, et al., 1998). Much of the research conducted in the first decade following stereolithograpy, and even into the 2000s, was centered on the development and perfection of original rapid prototyping nature. Similar to traditional prototyping, investment casting played a significant role in this process and therefore many papers were published looking at the accuracy and applicability of replacing the time and professional skills needed to create the sacrificial patterns used to make ceramic molds (Atwood, et al., 1996; Lynch, 1995; Mueller, 1992 &1995). After ten years of research and development, the materials available for rapid prototyping/additive manufacturing were starting to improve. Kruth, Leu and Nakagawa reported in 1998, "better mechanical, thermal and dimensional properties" with a pallet of nearly all materials.

Like many technology developments over time, additive manufacturing has had its growing pains. As Gershenfeld notes, "just as with the old mainframes" and "early bulky and expensive computer-controlled milling devices" the first AM systems were limited to institutional organizations because of the large investment costs (Gershenfeld, 2012). Recent years have seen dramatic changes in the costs of additive manufacturing technology, "developments from companies such as 3D Systems, Stratasys, Epilog Laser, and Universal brought the price" … "down from hundreds of thousands of dollars to tens of thousands, making them attractive to research groups" (Gershenfeld, 2012). The RepRap development initiative and

numerous open-source additive manufacturing projects have pushed the boundaries even further, driving prices to a level in the hundreds of dollars that allows individual user participation (Jerez-Mesa, et al., 2016).

Early rapid prototyping technologies suffered from poor quality issues such as: dimensional accuracy, stair-stepping curves, limited part strength, and long build times. Many developments in the 1990s were focused on addressing these issues, introducing geometric and algorithmic methods to optimize additive manufacturing processes (Ziemian & Crawn, 2001). Additive manufactured part performance is highly dependent on part orientation and build strategy, and while expert users have the qualitative knowledge needed to adjust process variables to obtain desired results, this is a difficult process to quantitatively predict (Ziemian & Crawn, 2001). Many AM technology manufacturers limit operator modifications, utilizing so-called "expert-system" to control build plans, these methods improve performance on narrow applications of AM, but limit expansion and innovation.

While additive manufacturing technology has, the potential to facilitate part designs unattainable using traditional manufacturing methods, different AM technologies and materials have distinct limiting factors such as, bonded and non-bonded elements, material voids, and materials accumulations (Guido & Zimmer, 2014). Sood et al. (2012), found that "the FDM process is highly complex" using a Taguchi design of experiments to identify the optimum levels of several process parameters they noted that "the considered factors affect the responses in a nonlinear way". Many process variables associated with fused filament technology (FDM/FFM) have compounding and conflicting affects. Part build speeds can be significantly reduced by including longer tool paths, sharp changes in road direction require coordinate controlling

systems to slow head speeds prior to turning and then to accelerate back to set velocities.

Therefore, to create faster build speeds designers often incorporate the longest tool paths possible into their fill strategies. However, this has a negative effect on part build strength, as the adhesion of filament strands is typically better when the time between deposition is minimized and strand solidification is limited (Kulkarni & Dutta, 1999). Some research indicates adjustments in material liquefier settings may have little effect on the bond strength between filaments, Sun, et al. (2008), conducting experiments using ABS material and adjusting extrusion temperatures between 260 and 280˚C found no significant changes in the heat profiles of deposited roads.

Parts fabricated using FDM typically have two separate tool paths within a sliced layer: a parallel path along the boundary of the layer typically referred to as the contour, and a series of directionally parallel paths in the interior area of the layer called the fill. In standard build operations, the former can be altered to improve surface quality of the model and the latter is used to ensure a fast fabrication (Jin, et al., 2013). However, when attempting to build for part strength, operators adjust road widths in an attempt to maximize interior fill rates. In addition, the effect of build orientation and print path become increasingly important when FDM is used to create production parts (Bellini & Guceri, 2003).

Another area of additive manufacturing research has focused on surface quality, specifically as it results from the translation of curved surfaces and the stair-stepping effect of layer-by-layer fabrication. As with traditional manufacturing methods, greater detail and specialized approaches are needed to closely approximate complex curves. Adaptive slicing is a technique used in additive manufacturing to address this need, varying layer thickness in different sections to limit stair-step effects in critical areas (Ziemian & Crawn, 2001). This is

especially relevant to the current research, as layer bond strength has been shown to vary with layer thickness. Ziemian and Crawn (2001) identified a number of research efforts to develop "methods of filling the interior of each layer" … "in order to produce parts quickly, that are strong, or that have a good surface finish".

For many industrial applications, FDM technology adoption is limited by a restricted accuracy and poor surface roughness. Boschetto and Bottini (2014) classify these weaknesses as either computer and/or mechanical aspects of the fabrication process: with "the former related to approximation involved in surface tessellation and virtual model slicing; the latter regarding positioning error and filament solidification problems". Surface quality, which subsequently affects dimensional accuracy of FDM parts, is highly dependent upon the tool paths used to deposit extruded material. As a result, there has been significant research into alternative or adaptive methodologies to optimize FDM processes. Adaptive slicing is one such method used to modify layer thickness when attempting to approximate a curved surface. However, there is a proportional relationship between the height or thickness of a layer and the width of the roads forming that layer. "If the distance between tool paths is too large, a gap between two adjacent strips of forming material may appear. However, a too small distance may result in a ridge between strips" (Jin, et al., 2013). This is especially important in the current research where degree of weld between extruded roads is being used to predict part strength.

Acrylonitrile Butadiene Styrene (ABS) and Polylactic Acid (PLA, Polylactide) dominate the realm of additive manufacturing thermoplastics, because of their relative ease of use and commercial availability. However, a number of production grade thermoplastic materials have been studied for use in Fused Deposition Modeling, Boschetto and Bottini (2014), created parts

using ULTEM™9085 and polycarbonate as part of their research into superior methods for accuracy and surface finish.

> ULTEM 9085 is a flame retardant thermoplastic employed in transportation industry because of its high strength-to-weight ratio. Polycarbonate is an industrial thermoplastic widely used in automotive, aerospace, medical, and many other applications. It presents superior mechanical properties to ABS and a number of other materials employed in FDM (Boschetto & Bottini, 2014).

Tensile tests of raw filament and printed roads have been conducted on an extensive basis, typically utilizing disposable frame and epoxy fixtures, as seen in Figure 8. In these tests a rectangular frame of cardboard or compressed paper is constructed with partial channels on opposite sides to support the printed strands or raw filaments. After printing the channels are filled with an epoxy adhesive and secured with small covers. Once the disposable frame has been mounted in a tensile instrument with the grips at the cover locations, the disposable frame is cut to allow testing.
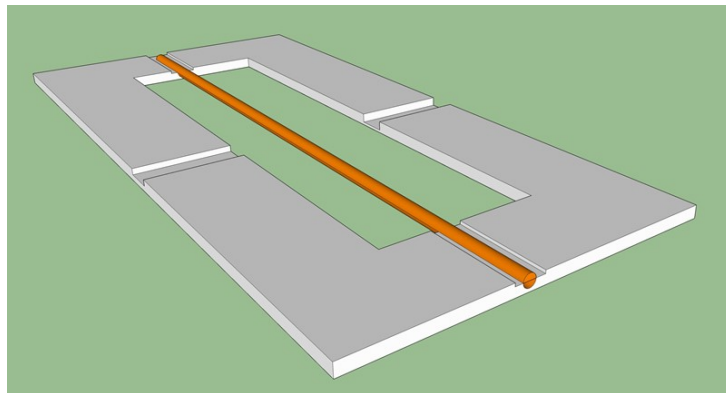


Figure 8. Disposable Filament Test Frame

In fused deposition modeling, parts are built up layer by layer from strands or roads of molten plastic material. The part strength is dependent upon the inter-road adhesion or weld strength. These roads and layers show anisotropic properties, within layers along the direction of the roads, and between layers where there is cross-road adhesion (Bellini & Guceri, 2003). A number of FDM related studies have described similar properties to composite material models, the fused extruded fibers mimicking traditional composite lay-up structures. This allows the use of some of analytical tools developed earlier for anisotropic products (Bellini & Guceri, 2003).

Anisotropic materials are materials whose properties are directionally dependent. Unlike isotropic materials that have uniform properties in all directions, anisotropic material's properties such as Young's Modulus, change with direction along the object. Common examples are wood and composites (Lovelady, 2013). Savvakis, et al. (2014), specifically studied the mechanical properties of parts manufactured using fused deposition modeling or fused filament manufacturing methods, noting an anisotropic behavior in their tested specimens. However, even within this single study, the researchers observed confounding information, finding both "that building direction does not significantly influence … tensile strength" and "the anisotropic behavior and tensile strength of the parts is different between the parts built in different directions".

Differing from other additive manufacturing technologies, FDM utilizes extruded strands of semi-molten polymer materials to build up part layers line by line and can be thought of as drawing with a glue-gun. Bonding between lines of material, and between layers, is driven by the combined heat energy present in previously deposited roads and the current extrusion (Sun, et al., 2008). A number of research projects have looked into methodologies for optimizing FDM part strength by varying material and build envelope temperatures, and while these settings are

generally assumed to be constant for the entire fabrication, many researchers have discovered variability in the process. Sun, et al. (2008), found that material deposited on the bottom layers of FDM parts, saw temporary increases in temperature, "above the glass transition temperature", as subsequent layers were added to the part indicating some level of heat conduction within and between layers.

FDM/FFM technologies, extrude a heated strand of material using a computer controlled X – Y coordinate system. Extruded fibers are deposited on a vertically adjusted build platform, either directly (RepRap style) or onto a disposable platform cover (foam or sheet, Stratasys). Molten fibers conform to the circular geometry of the extrusion tip and can be thought of as cylinders of semi-solid material. However, depending on head speed (X – Y motion) and layer thickness, deposited material roads may have elliptical or flattened profiles (Kulkarni & Dutta, 1999). Other research has begun to breakdown additive manufacturing processes, to better understand the conditions and process affecting final part production. Focusing their efforts on the thermal aspects of fused filament extrusion technology, specifically the liquefying components, in an attempt to improve material deposition (Jerez-Mesa, et al., 2016). This is especially important in the current environment of personalized production exploding because of "RepRap" style machines. In 2003, Bellini and Guceri (2003), found reducing the average road length, resulted in stronger interlayer bonds between adjacent roads postulating that previously deposited roads did not cool completely before being reheated by the next road.

Other FDM research indicates a correlation between extruded fiber size and part strength, larger diameter fibers exhibiting weaker bonds and smaller diameters showing stronger ones (Jin, et al., 2015). This may be a combination of longer fabrication runs required by the smaller print

nozzles as Sun, et al. (2008) found evidence to indicate bond strength was effected by conductive heat built up over the length of a build run.

Another element of the FDM process is the physical "build volume", were the extruded fibers or roads are deposited on the build platform. Temperature variations in the build volume can have significant impact on parts final characteristics, influencing actual volume flow rates, liquefier inlet velocity, and nozzle exit velocity (Ramanath, et al., 2007). Stratasys brand FDM machines utilize enclosed build volumes and temperature control to limit variation in the build envelop. Newer RepRap style fused filament technology often fabricate parts on a simple platen open to the room environment. As such, there is significant evidence that build parameters may not account for changes in the filament heat profiles. Sun, et al. (2008), found parts made in different locations in Stratasys build envelops exhibited different heat profiles when measured with industrial thermocouples.

Even as industry begins to accept additive manufacturing as a production part method, research continues into innovative process improvements. Breaking the additive process down even further to nano and atom level constructions, a number of researchers are even looking to biomimicry as a guide on how to build better performing structures using AM (Frolich, et al., 2017). New developments in additive manufacturing applications are even putting pressure on the 3D file formats used to build computer-aided-design (CAD) objects. The standard tessellation language (STL) file format, has become a standard in AM, but is not well suited for the representation of the complex design structures developed today. Lattice structures, complex compound curves, and multi-faceted features result in impractically large files (Doubrovski, et al. 2011). Guo and Leu (2013), identified three primary opportunities for additive manufacturing research that are still relevant today and of particular interest in this study:

1) Developing a better understanding of the basic physics and

chemistry of AM processes that capture complexities in the

multiple interacting physical phenomena inherent in most AM

processes. 2) Screening methodologies for advanced materials to

answer why some materials can be processed by AM and some

cannot. 3) Development of sustainable (green) materials, including

recyclable, reusable, and biodegradable materials, to reduce

environmental impact (Guo & Leu, 2013).

**Experimental Additive Manufacturing Methods**

While the number and variety of additive manufacturing materials has grown over the

last 30 years, many gaps still exist in the pallet of materials and understanding needed for AM to

take a significant position in mainstream production. Deep understanding is needed to facilitate

predictive mathematical models that can account for the complex physics (Ponche, et al., 2012).

As predictive models are typically sensitive to changes in temperature, material formulations,

and process variability it is important to "use with caution" (Sun, et al., 2008). Few studies have

provided enough consistent experimental data to validate with any degree of certainty such

models.

Sun, et al. (2008), described two separate phenomena influencing bond strength between

extruded FDM filaments, molecular diffusion of the polymer chains occurring at the interface of

two filaments as well as polymer sintering. Sintering in polymeric materials is mostly a result of

the viscous flow mechanism. While the term is normally used to describe coalescence occurring

below the plasticized range of the material, the expression has been carried on and accepted in the literature for the coalescence of polymers above their glass and plasticized ranges.

In this research study a constant extrusion temperature has been assumed and is used in the predictive models, however, it is important to note there has been research indicating that the extrusion process used in FFF is non-isothermic in nature, meaning that actual material temperatures vary over the course of being printed. Jerez-Mesa, et al. (2016), found that extrusion liquefier controls typically utilize limits to turn on and off heating elements, creating "a typical balancing feedback loop system". Final part strength in parts fabricated using FDM technology is highly dependent upon the quality of inter-filament bonding within each layer. Material temperatures are set and adjusted by operators in the build parameters and controlled by feedback sensors located in the material liquefier. Previous research has indicated that material temperature profiles may vary significantly throughout the process traveling from the liquefier, out of the extrusion nozzle, and as it is deposited on the build platform (Sun, et al., 2008).

Other research studies have investigated the tensile strength of FDM/FFM fabricated parts. Savvakis, et al. (2014), tested specimens built as solids using Stratasys build standards that produce parts with fill rates of about 97%. This 3% void is particularly significant when attempting to evaluate filament weld strength as it creates a number of unknown variables. Another tool path variable affecting FDM parts is related to the abrupt corners between line and tiny arc at the end of a road, necessitating a sharp fluctuation of speed of the nozzle/print head. This change in speed and direction may produce unfilled areas near the turning points and at the same time, excessive filled area exist in the other side of the corner (Jin, et al., 2013). This fluctuation of extrusion head speed also occurs at the beginning and termination of each layer, and cannot be mitigated through current tool path planning methods. Additional and more

precise control of liquefier extrusion speeds will be needed to optimize these build road transitions (Jin, et al., 2013).

## Standardization

In today's global market, industrial standards help ensure customers get the product solutions they need, companies understand the specifications needed to produce needed products, and design engineers have guidelines that help solve the customers problems. For a manufacturing process to be adopted widely by industry, the repeatability and consistency of manufactured parts are critical. This is especially true in a developing technology such as additive manufacturing. As one considers setting standards for the technology, material, and processes associated with AM, it may be useful to benchmark the plastics industry as a measure of additive manufacturing development and to look at efforts related to its industry standards.

Even though the first man-made plastic material was introduced over 150 years ago (Parkes, 1865), the plastics industry faced a challenge as global markets were opening up, to facilitate global standards. Shastri, et al. (1996), presented a paper to the SAE International Congress & Exposition, a technical paper reporting U.S. efforts to convert to a "Global Testing Standard for Plastics". In it, they pointed out a significant rule-of-thumb, "In any product development effort, access to reliable and comparable material data is crucial for selecting the right material (or technology) for the intended application." This is especially applicable to additive manufacturing technologies and materials, already competing in a global market place. Moreover, while efforts have already been started, significant research and collaboration will be needed to attain full commercial adoption.

One of the early efforts for standardization within additive manufacturing was fostered by the International Academy of Production Engineers (CIRP)(STC E, 2017), starting in 1991 with the first survey of what was then termed the rapid prototyping industry, the Scientific Technical Committee for Electro-Physical and Chemical Process has provided a forum for research focused on "material removal, additive, and hybrid processes of a physical, physico-chemical or chemical nature, such as electro-discharge machining (EDM), electrochemical machining (ECM), the use of high energy laser, electron and ion beams, 3D printing, and biomanufacturing." Recently the 2009 Roadmap for Additive Manufacturing Workshop, sponsored by the National Science Foundation and the U.S. Office of Naval Research helped formalize and accelerate commercial acceptance of these technologies by trying to focus research efforts within the field (Huang & Leu, 2014).

Huang and Leu (2014), reported "insufficient repeatability and consistency of parts" as a continuing obstacle facing additive manufacturing, "... products must be fabricated rapidly, efficiently, and inexpensively while meeting all stringent functional requirements." Participants of the National Science Foundation Additive Manufacturing Workshop identified numerous opportunities for further development in the "fundamental material science, physics, biology, lasers, electronics, optics, metrology, and controls" utilized in additive manufacturing (Huang & Leu, 2014). Boschetto and Bottini (2014), note a technology, in order to be employed in industrial environment, needs a set of theoretical and/or empirical formulations, which allow the prediction of attainable part quality in terms of both surface roughness and accuracy.

As discussed earlier, even as new materials and processes are being developed, some research has been focused on developing guides for additive manufactured part design. So-called Design for Additive Manufacturing (DFAM) methodologies would provide much of the detailed

design information engineers need to apply AM fabrication to production applications. Many engineers and designer continue to demonstrate resistance to AM on a number of levels including: poor performance to price perceptions, unfavorable risk expectations, tradition barriers ("how we always do it"), and image barriers (Antioco & Kleijnen, 2009). These efforts attempt to break down some of the psychological barriers, limiting adoption of AM; however, much of DFAM development is limited because of the comparatively adolescent technologies of additive manufacturing (Ponche, et al., 2012). Noting that Fused Deposition Modeling (FDM) is rapidly being adopted for both prototyping and production applications, Savvakis, et al. (2014), point out a need "for the design engineer to know the mechanical behavior of these parts, not in their bulk unprocessed state, but after manufacturing them with AM." Nominal properties of polymers such as Acrylonitrile Butadiene Styrene (ABS) and Polylactic Acid (PLA) may change significantly depending on the process parameters used in manufacturing. Doubrovski, et al. (2011), note that if "AM produced parts are to be used for end products, the properties of the materials need to be known under different conditions, such as ageing, humidity and temperature." Another Design for Additive Manufacturing study conducted by Laverne, et al. (2015), describe the three axioms of innovation postulated by Perrin and use them as guiding principles in the application of DFAM:

- "No innovation without market validation." Innovation is the first commercial use of a product, process, or service that has never been used before.
- "No innovation without design stages": the design process must be the backbone of the innovation process.
- "No innovation without innovative companies." Innovation is an essential boost for companies to survive or grow in a globalized and increasingly competitive economy.

The following table (Table 8.) provides a listing of current industry standards related to additive manufacturing as defined by the ASTM International subcommittee on test methods (ASTM, 2017).

Table 8. ASTM International Standards

| Active Standards | F2971-13 Standard Practice for Reporting Data for Test Specimens Prepared by Additive Manufacturing |
|---|---|
|  | F3122-14 Standard Guide for Evaluating Mechanical Properties of Metal Materials Made via Additive Manufacturing Processes |
|  | ISO/ASTM52921-13 Standard Terminology for Additive Manufacturing-Coordinate Systems and Test Methodologies |
| Proposed Standards | WK56649 Standard Practice/Guide for Intentionally Seeding Flaws in Additively Manufactured (AM) Parts |
|  | WK49229 Orientation and Location Dependence Mechanical Properties for Metal Additive Manufacturing |
|  | WK55297 Additive Manufacturing -- General Principles -- Standard Test Artefacts for Additive Manufacturing |
|  | WK55610 the Characterization of Powder Flow Properties for Additive Manufacturing Applications |

Furthermore, ASTM International and the International Standards Organization have agreed to work on development of a structure that will facilitate additional industrial adoption of additive manufacturing processes (2017).

The purpose, experimentation, and objectives of this research were guided and based on the research reviewed here. The understanding and knowledge derived from research reviewed in Chapter 2 was integral in the design of experiments, analysis of measured and predicted data, and interpretation of the intermediate as well as final results.

**References**

Anderson, C., (2004). The long tail. Wired Magazine, 10.01.04, Downloaded from:
https://www.wired.com/2004/10/tail/.

Antioco, M., & M. Kleijnen, (2009). Consumer adoption of technological innovations: effects of psychological and functional barriers in a lack of content versus a presence of content situation. European Journal of Marketing, Vol. 44 No. 11/12, pp. 1700-1724, DOI: 10.1108/03090561011079846.

ASTM International, (2017). Subcommittee F42.01 on Test Methods – Active & Proposed Standards, Downloaded from:
https://www.astm.org/COMMIT/SUBCOMMIT/F4201.htm.

ASTM and ISO unveil plans to create global AM standards. (2017). Metal Powder Report, 72(1), 63-64.

Atwood, C.L., M.C. Maguire, B.T. Pardo, & E.A. Bryce, (1996). Rapid prototyping applications for manufacturing. SAMPE Journal, Vol. 32, No. 1, January/February.

Bagsik, A., S. Josupeit, V. Schoeppner, & E. Klemp, (2014). Mechanical analysis of lightweight constructions manufactured with fused deposition modeling. AIP Conference Proceedings 1593, 696 (2014); DOI: 10.1063/1.4873874.

Beaman, J., D. Bourell & D. Wallace, (2014). Editorial Special Issue: Additive Manufacturing (AM) and 3D Printing. Journal of Manufacturing Science and Engineering, Downloaded From http://manufacturingscience.asmedigitalcollection.asme.org/.

Bellini, B.A., & S. Guceri, (2003). Mechanical characterization of parts fabricated using deposition modeling. Rapid Prototyping Journal, 9(4), 252-264. Retrieved from http://search.proquest.com/docview/214027090?accountid=14576.

Beyer, C., (2014). Strategic implications of current trends in additive manufacturing. Journal of Manufacturing Science and Engineering, Vol. 136 / 064701-1, Downloaded From: https://manufacturingscience.asmedigitalcollection.asme.org/.

Boschetto, A. & L. Bottini, (2014). Accuracy prediction in fused deposition modeling. International Journal of Advanced Manufacturing Technology, (2014) 73:913-928, DOI 10.1007/s00170-014-5886-4.

Bourell, D.L., J.J. Beaman, M.C. Leu, & D.W. Rosen, (2009). "A Brief History of Additive Manufacturing and the 2009 Roadmap for Additive Manufacturing: Looking Back and Looking Ahead." Proceedings of RapidTech 2009: US-TURKEY Workshop on Rapid Technologies, pp. 1-8.

Clarke, C., (2017). Lloyd's Register, TWI release updated framework for 3D printed metal certification. 3D Printing Industry, March 8, Downloaded from: https://3dprintingindustry.com/news/lloyds-register-twi-release-updated-framework-3d-printed-metal-certification-107579/.

Cohen, D., M. Sargeant and K. Somers, (2014). "3-D Printing takes shape. McKinsey Quarterly, http://www.mckinsey.com/insights/manufacturing/3-d_printing_takes_shape?cid=other-eml-nsl-mip-mck-oth-1402.

Doubrovski, Z., J.C. Verlinden & J. M.P. Geraedts, (2011). Optimal design for additive manufacturing: opportunities and challenges. Proceedings of the ASME 2011 International Design Engineering Technical Conference & Computers and Information in Engineering Conference, DETC2011-48131, Downloaded From: http://proceedings.asmedigitalcollection.asme.org/.

Frolich, S., J. C. Weaver, M.N. Dean, & J. Birkedal, (2017). Uncovering nature's design strategies through parametric modeling, multi-material 3D printing, and mechanical testing. Advanced Engineering Materials, DOI: 10.1002/adem.201600848.

Gershenfeld, N., (2012). How to Make Almost Anything: The Digital Fabrication Revolution. Foreign Affairs, November/December.

Guido, A.A., & D. Zimmer, (2014). Design for additive manufacturing – element transitions and aggregated structures. CIRP Journal of Manufacturing Science and Technology, Vol. 7(1), pp 20-28, Downloaded from: http://dx.doi.org/10.1016/j.cirpj.2013.10.001.

Guo, N., & M. Leu, (2013). Additive manufacturing: technology, applications and research needs. Frontiers of Mechanical Engineering, 8(3): 215-243, DOI 10.1007/s11465-013-0248-8.

Huang, Y., & M.C. Leu, (2014). Frontiers of Additive Manufacturing Research and Education. NSF Additive Manufacturing Workshop Report, University of Florida Center for Manufacturing Innovation. March.

International Academy for Production Engineering, (2017). STC E – Electro-Physical and Chemical Processes. Downloaded from: https://www.cirp.net/scientific-groups/stc-scientific-technical-commitees/stc-e-electro-physical-and-chemical-processes.html,

ISO/TC 261 and ASTM F42, (2013). Joint plan for additive manufacturing standards development. Joint Planning Session.

Jerez-Mesa, R., J.A. Travieso-Rodriguez, X. Corbella, R. Busque, & G. Gomez-Gras, (2016). Finite element analysis of the thermal behavior of a RepRap 3D printer liquefier. Mechatronics, http://dx.doi.org/10.1016/j.mechatronics.2016.04.007.

Jin, Y.A., Y. He, & J. Fu, (2013). An adaptive tool path generation for fused deposition modeling. Advanced Materials Research Vol. 819, pp 7-12, Trans Tech Publications, Switzerland, DOI 10.4028/www.scientific.net/AMR.819.7.

Jin, Y., Y. He, G. Xue & J. Fu, (2015). A parallel-based path generation method for fused deposition modeling. Int J Adv Manuf Technol 77:927. https://doi.org/10.1007/s00170-014-6530-z.

Kruth, J.P., M.C., Leu, & T. Nakagawa, (1998). Progress in Additive Manufacturing and Rapid Prototyping. CIRP Annals, Volume 47, Issue 2 pp 525-540.

Kulkarni, P., & D. Dutta, (1999). Deposition strategies and resulting part stiffnesses in fused deposition modeling. Journal of Manufacturing Science and Engineering, Vol. 121, pp 93-103. Downloaded from: http://manufacturingscience.asmedigitalcollection.asme.org/.

Laverne, F., F. Segonds, N. Anwer & M. Le Coq, (2015). Assembly Based Methods to Support Product Innovation in Design for Additive Manufacturing: An Exploratory Case Study. Journal of Mechanical Design, December 2015, Vol. 137 / 121701-1.

Lovelady, K., (2013). Anisotropic materials. Draft manuscript submitted to Dr. Harry Millwater as part of ME 4913-002, University of Texas at San Antonio. Downloaded from: http://sivirt.utsa.edu/Documents/Kayla%20Lovelady.pdf

Lynch, W. L., (1995). Stereolithography – A tool for rapid castings. Paper presented at the American Helicopter Society 51st Annual Forum, Fort Worth, Texas May 9-11, 1995. Copyright 1995 by the American Helicopter Society, Inc..

Mueller, T.J., (1992). Using rapid prototyping techniques to prototype metal castings. SAE Technical Paper Series #921639, SAE International.

Mueller, T.J., (1995). Stereolithography-based prototyping: case histories of applications in product development. Northcon 95, I EEE Technical Applications Conference and Workshops, INSPEC # 5237539.

Musso, C., J. Grapski, & B. Frei, (2006). Old answers to new questions: dodging the obstacles of plastics innovation. Modern Plastics Worldwide. p. 18-20, September.

Parkes, A., (1865). Improvements in the manufacture of parkesine or compound of of pyroxyline, and also solutions of pyroxyline known as collodion. U.K. Patent No. 1313.

Ponche, R., J.Y. Hascoet, O. Kerbrat & P. Mognol, (2012). A new global approach to design for additive manufacturing. Virtual and Physical Prototyping, 7:2, 93-105, DOI: 10.1080/17452759.2012.679499.

Ramanath, H.S., M. Chandrasekaran, C.K. Chua, K.F. Leong & K.D. Shah, (2007). Key Engineering Materials Vols. 334-335 pp 1241-1244, Trans Tech Publications, Switzerland DOI 10.4028/www.scientific.net/KEM.334-335.1241.

Reeves, P., (2017). 3D Printing: understanding the business drivers for technology adoption. Stratasys©e-book. Downloaded from: http://www.stratasys.com/campaign/ebook/business-drivers-for-3d-printing-adoption.

Savvakis, K., M. Petousis, A. Vairis, N. Vidakis & A.T. Bikmeyev, (2014). Experimental Determination of the tensile strength of fused deposition modeling parts. Proceedings of the ASME 2014 International Mechanical Engineering Congress and Exposition IMECE2014-37553.

Shastri, R.K., S.J. Watson, D.R. Wilson, J.A. Grates, & H.P. Toner, (1996). The Status of Conversion to Uniform Global Testing Standards for Plastics in the U.S.. Paper presented to the SAE International Congress & Exposition, February 26-29, SAE Technical Paper Series 960702.

Sher, D., (2015). Additive Industries' MetalFAB1 3D printer flies into Airbus factory. 3D Printing Industry, 18 December, Downloaded from: http://3dprintingindustry.com/2015/12/18/63690/.

Sood, A. K., R.K. Ohdar, & S.S. Mahapatra, (2012). Experimental investigation and empirical modelling of FDM process for compressive strength improvement. Journal of Advanced Research, Vol. 3(1), pp 81-90, https://doi.org/10.1016/j.jare.2011.05.001.

Sun, Q., G.M. Rizvi, C.T. Bellehumeur, & P. Gu, (2008). Effect of processing conditions on the bonding quality of FDM polymer filaments. Rapid Prototyping Journal, Vol. 14 Issue: 2, pp. 72-80, https://doi.org/10.1108/13552540810862028 .

Weeden, B.A., A.P. Sanders, D.L. LaSalle, & G.P. Trottier, (1996). Alternative methods for custom implant production utilizing a combination of rapid prototyping technology and conventional investment casting. IEEE 0-7803-3131-1/96.

Williams, C. B., & C. C. Seepersad, (2012). Design for additive manufacturing curriculum: a problem and project based approach. 23rd Annual International Solid Freeform Fabrication Symposium – An Additive Manufacturing Conference, SFF 2012, P 81-92.

Ziemian, C.W. & P.M. Crawn, (2001). Computer aided decision support for fused deposition modeling. Rapid Prototyping Journal, 7(3), 138-147. Retrieved from http://search.proquest.com/docview/214011430?accountid=14576.

# CHAPTER 3. PROCESS PARAMETERS AND PRODUCT STRENGTH FOR FUSED DEPOSITION MODELING

David Grewell[a], Steven Devlin[b]

[a]Department of Agricultural and Biosystems Engineering, Iowa State University, Ames, IA

[b]College of Engineering, University of Missouri, Columbia, MO

**Abstract**

Fused Deposition Modeling (FDM™) or fused filament fabrication (FFF) systems are extrusion based technologies used to produce functional or near functional parts from a wide variety of plastic materials.  First patented by S. Scott Crump and commercialized by Stratasys, Ltd in the early 1990s, this technology, like many additive manufacturing systems, offers significant opportunities for the design and production of complex part structures that are difficult if not impossible to produce using traditional manufacturing methods. Standing on the shoulders of a twenty-five year old invention, a rapidly growing open-source development community has exponentially driven interest in FFF technology. However, part quality often limits use in final product commercial markets. Development of accurate and repeatable methods for determining material strength in FFF produced parts is Fused Deposition Modeling (FDM™) or fused filament fabrication (FFF) systems are extrusion based technologies used to produce functional or near functional parts from a wide variety of plastic materials.  First patented by S. Scott Crump and commercialized by Stratasys, Ltd in the early 1990s, this technology, like many additive manufacturing systems, offers significant opportunities for the design and production of complex part structures that are difficult if not impossible to produce using traditional manufacturing methods. Standing on the shoulders of a twenty-five year old invention, a rapidly

growing open-source development community has exponentially driven interest in FFF technology. However, part quality often limits use in final product commercial markets. Development of accurate and repeatable methods for determining material strength in FFF produced parts is essential for mainstream manufacturing.

This study builds on the empirical, squeeze flow and intermolecular diffusion model research conducted by David Grewell and Avraham Benatar, applying a combined model to predict auto adhesion or healing to FFF part samples. Experimental samples were fabricated from ABS and PLA filaments using a Mendel190 rep-rap style 3D printer, running 3MM material purchased from MakerBot Industries. Combinations of extrusion speed and head temperature were tested to determine printable ranges for both materials. Samples were post-processed into ASTM equivalent specimens and tested for tensile strength according to ASTM D638-03. Analysis of resulting data and examination of tested samples offer favorable insights and opportunities for additional and continuing investigation.

## Introduction

### Developing Industry – Additive Manufacturing

Approximately thirty years ago, the U.S. Patent and Trademark office issued to Charles Hull a patent (number 4575330) for an Apparatus for Production of Three-Dimensional Objects by Stereo Lithography. This development launched the rapid prototyping /rapid manufacturing industry. Rapid Prototyping (RP) or Rapid Manufacturing (RM), often referred to as solid freeform fabrication or Additive Manufacturing (AM), is a method of fabricating parts through additive manufacturing processes. This allows parts to be developed at relatively low volumes. It is ideal for prototyping, fit and function modelling, patterns for metal casting, technological

pieces for functional purposes and other situations where parts are needed in small quantities (i.e. production-quality parts needed for small runs). Because of this, it has the potential to significantly impact product development and manufacturing.

In 1987 the SLA®-1 system was released by 3D Systems, representing the first commercially available system using additive manufacturing technology. While stereo lithography is recognized as the first, many other competitive systems were developed over the following decades. Today there are seven primary technologies offered through numerous manufacturers worldwide: material extrusion, material jetting, binder jetting, sheet lamination, vat photo polymerization, powder bed fusion, and directed energy deposition [1].

Additive manufacturing can use a wide variety of base materials: metals, plastics, corn starch, etc. thermoplastics dominate the industry with metals being the second most popular choice. The major advantages of plastics as a base material compared to metals including: performance, ease of manufacturing, cost-effectiveness, corrosion resistance and design freedom. These advantages underscore why plastics lead the industry, particularly in the automotive sector [2].

## Benefits of Fused Deposition Modelling for Functional Parts

As stated previously, parts formed by the method of layer-by-layer synthesis, Rapid Prototyping (RP) or additive manufacturing, are most frequently used for three applications: for model-prototypes, models for production of metal casts, or as technological pieces for functional purposes. In the latter case, the properties of the construction material used in the RP process (the physicomechanical, chemical and corrosion factors) are of significant importance. Over all, the properties determine the characteristics of the finished products. When selecting a material,

not only is the purpose of the part important but also the type of RP technology that will be used to manufacture it [3].

Commercialised by Stratasys in 1991, FDM has grown to one of the most important rapid prototyping technologies [4].  For this process it is comon to have building material as well as a support material is needed.  The building and support materials are molten in a plastifying unit and extruded through a die onto a platform to create a two-dimensional cross section of the model. Subsequently the platform is lowered and the next layer is extruded and fused onto the previous layer [5]. This process continues until the part is complete; afterwards the part support structures are removed. Parts with 0.1 mm high layers and a minimum wall thickness of 0.5 mm can be produced by FDM. The commercially available materials for this process include ABS, PC, polyphenylenesulfone (PPSU) and a PC/ABS-blend. Such materials are provided as filaments (diameter of $1.75 \pm 0.05$ mm) in several standard colors.

One aerospace supplier uses FDM to make thermoform molds for air ducts, engine cowlings, and antenna covers.  Fused deposition modelling tooling reportedly costs less and has shorter lead time than composite molds made by hand lay-up of carbon-fiber prepreg [6]. It has been reported that ABS plastic prototype models have relatively high strength and durability. ABS is a strong, durable production-grade thermoplastic used across many industries.

Many professional service providers claim FDM carries an indisputable advantage over other additive manufacturing technologies because of the potential for final machining and cutting of rapid prototyped parts.  Parts made from ABS can be milled, turned, and ground or have threads cut in formed holes.  Machining requires specific cutting speeds and tooling because of the low plasticizing temperature and layered structure, but can produce "near-functional" features [7].

Growing demand for FDM or FFF systems in the open-source development community has expanded material options to include a significant use of Polylactic acid (PLA) based filaments. Produced from a renewable raw material (lactic acid), PLA offers a variety of applications while helping to conserve fossil resources [8]. Unsuitable for many durable goods applications, PLA filaments hold a significant market with artistic users because of its smoother surfaces, shinier appearance, and ease-of use [9]. However, with additional understanding of the mechanical properties associated with FFF parts made from PLA, additional short-term applications may be developed.

## Experimental Investigation

Beginning in 2005 the principle investigators developed a multi-phase experimental research process to identify and characterize the numerous variables associated with development of a part strength model for additive manufacturing. Two primary technologies were selected for evaluation based on current utilization in the commercial market, Selective Laser Sintering (SLS) and Fused Deposition Modelling (FDM™). Both technologies offered parts made from industry accepted materials, nylon powder for SLS and ABS filament for FDM™. However, after consideration of the complexities introduced by the multi-particle nature of SLS parts for the experimental process were limited to the extruded filament technology.

In the FDM process the material is a wire or filament at the cartridge which is entered to the printing head where the ABS, PLA or other material is plasticized and is pressed through a nozzle to the build platform. The nozzle moves to produce a profile of the part model, then the platform translates down and the next layer is built on top of the previous layer until the entire model is fully built. Typically a support structure is constructed for overhanging features [7].

Phase I - Preliminary experimentation was conducted at Iowa State University to determine the preferred strand orientation and material strength test method for the final experiment. Test samples were fabricated from ABS filament on a Stratasys 1650 Fused Deposition Modelling system. Evaluations were made of samples with strands oriented at 90˚ to the axis of the sample part and tested in tension using ASTM D638-03 Standard Test Method for Tensile Properties of Plastics. Evaluations were also made on samples with strands oriented parallel to the sample part axis and tested in three point shear using ASTM D 2344/D 2344M-00 Standard Test Method for Short-Beam Strength of Polymer Matrix Composite Materials and Their Laminates. Based on previous experience there was some concern about significant scatter in the data for parts tested in tension as there is relatively little healed/welded material present in the axis of load (tension). Initial findings suggested samples should be tested in short beam bend test in order to determine weld strength between the fibers.

Phase II - Preliminary experimentation was also conducted on PLA films to assess the accuracy of the proposed intermolecular healing model as well as estimating the fitting parameters of the models. Films were produced at Iowa State University from PLA and ABS filaments/pellets provided by Erlangen LTK University. The films were cut utilizing an ultrasonic cutting die or knife with a die to provide consistent sample geometry. The film was welded utilizing an impulse welder with water chilled head and fixture. The process parameters that were studied included time (5x) and temperature (5) using a full factorial design of experiments. All experiments were repeated five times. Weld strengths were evaluated using ASTM D 882-02 Standard Test Method for Tensile Properties of Thin Plastic Sheeting. This strength of weld analysis provides estimates of fitting parameters for the healing models.

Phase III – In collaboration with Prof. Dr.-Ing. Dietmar Drummer, Lehrstuhl fur Kunststofftechnik, pre-experimental sample fabrication was conducted by the researcher and LTK staff on the Stratasys FDM 2000 and 8000 to validate the deposition system and the test sample model.  Samples were fabricated from PLA filament and ABS filament.  Samples were evaluated for material strength utilizing the selected test method determined in Phase I experimentation.

Results from pre-experimental sample fabrication and testing revealed difficulties inherent to the direct fabrication of test samples using FDM and an inability to vary deposition speed.  A revised experimental method was then agreed upon where sample blanks (of 10, 25, and 50 mm) [Figure 1] would be fabricated using the FDM process and the resulting blanks would then be CNC machined by Erlangen technical staff for testing using the ASTM D638-03 Standard Test Method for Tensile Properties of Plastics using a Zwick / Roell Zmart.Pro tensile testing instrument.

In addition, samples produced using PLA filament provided by Erlangen staff proved insufficient to provide accurate experimental data, suggesting further research was needed to identify and acquire a PLA formulation applicable to the extrusion process.  Upon evaluation of pre-experimental test data, a determination was agreed upon by Dr. Grewell and Prof. Drummer to proceed to Phase IV.

## Materials and Methods

Phase IV: Samples were fabricated from ABS and PLA parts, with a Mendel190 rep-rap style 3D printer [Figure 2], at Iowa State University, running 3MM diameter material purchased from MakerBot Industries. Combinations of extrusion speed and head temperature were tested to

determine printable ranges for both materials.  Acceptable sample blanks were obtained for ABS ranging from 10 to 25 millimetres per second with temperatures from 230 to 250 degrees Celsius.  Acceptable sample blanks [Figure 3] were obtained for PLA ranging from 10 to 25 millimetres per second with temperatures from 200 to 220 degrees Celsius. [Figure 4]

Based on the samples produced and in consultation with Professor Robert Stephenson, PhD Department of Statistics – Iowa State University,  two possible experimental models were considered; namely 20 speed/temperature combinations using 5 samples and100 speed/temperature combinations using 1 sample.

Phase V: PLA and ABS experimental samples were fabricated, using a randomized experimental design with each of 28/20 speed/temperature combinations producing five test blanks for a total of 100 ABS and 140 PLA specimens. [Figure 5] ASTM equivalent specimens (dog bones) were machined by the researcher using a rotary cutting tool.  Finished specimens were tested to the ASTM D638-03 Standard Test Method for Tensile Properties of Plastics using a tensile testing instrument and data logged for break strength as well as elongation / toughness.

**Results and Discussion**

As expected, the ABS samples performed with higher average strengths and less variability within speed and temperature ranges. [Table 1]  PLA end of range samples were especially troublesome with filaments failing to adhere to the platen and filaments not welding to previously deposited filaments.  Several sample blanks were rejected because of voids present in the samples. [Figure 6] Samples produced from PLA at higher temperatures had a very low viscosity during the extrusion process with extrusion profiles spreading into a semi-solid blank. In addition, the PLA samples were more difficult to post process for tensile testing, showing a

greater tendency to introduce residual machining stresses and often resulted in complete part failures during machining. As a result, PLA data points for the lower limit of the temperature range are excluded from the data set. [Table 2]

The tensile strengths, for both ABS and PLA, were significantly lower than MakerBot® published tensile strengths. [8] Recorded results for ABS were approximately one-third to one-half of the 34 MPa listed on their strength data sheet, with PLA samples testing at approximately one-fourth to one-third of the 47 MPa listed.

The strength of PLA samples were as expected relative to velocity, with less standard deviation in strength relatively low in the middle of the range (10 – 25 MM/S) where the extrusion process is relatively stable. The strength of the ABS was generally inversely proportional to the velocity (10-25 MM/S). [Table 3, Figures 7 & 9] However, the strength appears to have an optimized temperature of approximately 245 Celsius. [Table 4, Figures 8 & 10]

While the recorded ABS data appear to be suitable for modelling additional experiments need to be completed with PLA in order to reduce the experimental error. Investigators are currently working to produce, machine, and test additional parts using the previously described process. Once the experimental data sets are completed, predictive strengths will be calculated using the combined model for auto adhesion and analyzed to determine effectiveness.

This experimental investigation has also revealed a number of opportunities for improving the process. Investigators will continue to search for and develop better methods for test sample creation. For parts that require post processing, improved techniques for machining test samples (dog-bones) may include different types of cutting tools, revised clamping templates, and possible CNC processing for sample repeatability.

Different methods for printing the test samples will be considered, including vertical

orientation to eliminate filament spread induced by the platen.  It may also be advisable to

reconsider the possibility of a direct test sample build to eliminate post processing stresses.  A

sub-investigation to evaluate the impact of road-path loops verses machine cut edges may be

needed.

Upon completion of modelling and analysis opportunities for replication will be

evaluated.  Replication using commercial grade FDM equipment will be needed before a final

predictive model can be incorporated into commercial market design. Investigations of

alternative rapid prototyping technologies will also be needed for commercial market adoption.

Figure  1 FDM Blanks at 10, 25, and 50mm

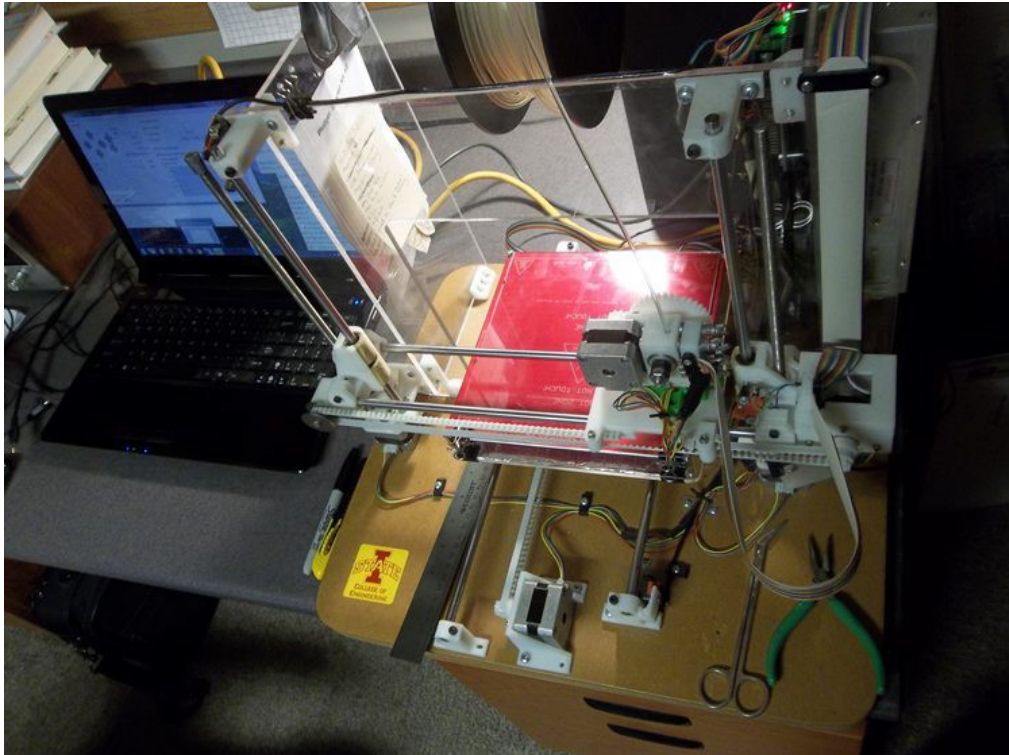Figure  2 Mendel190 Style 3D Printer



Figure 3 Single Layer Samples
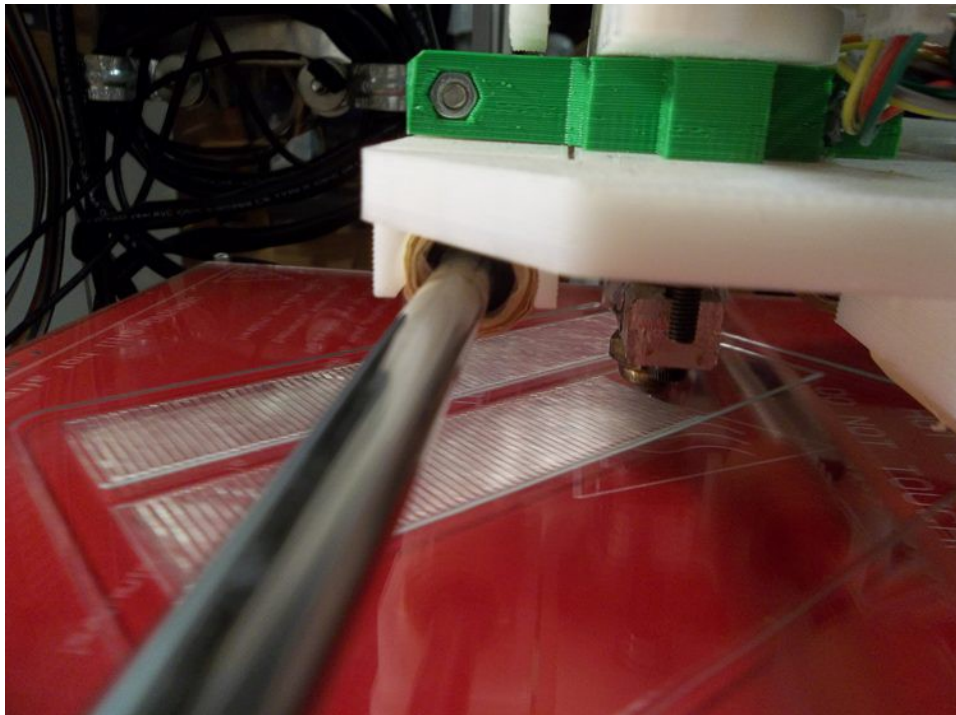
Figure 4 Experimental Samples
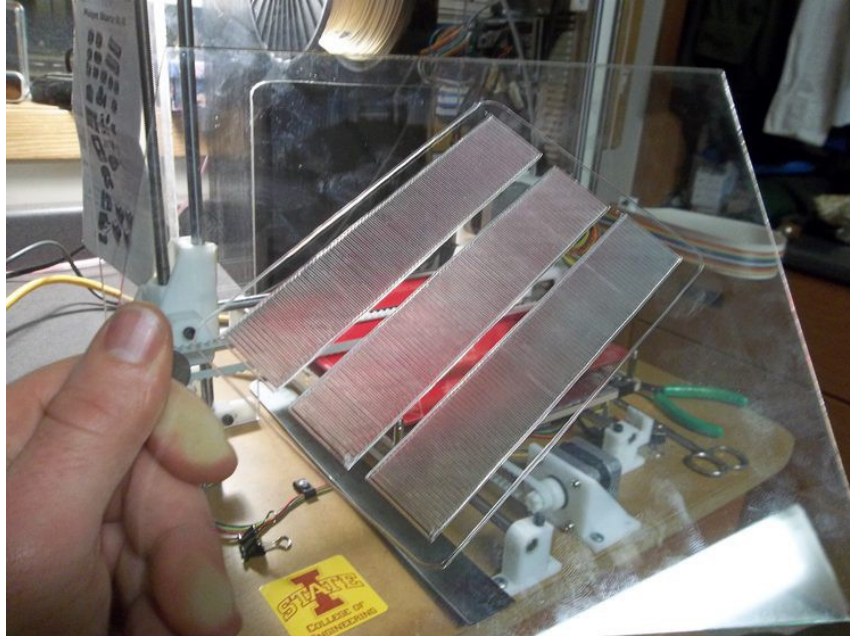


Figure 5 Test Blanks
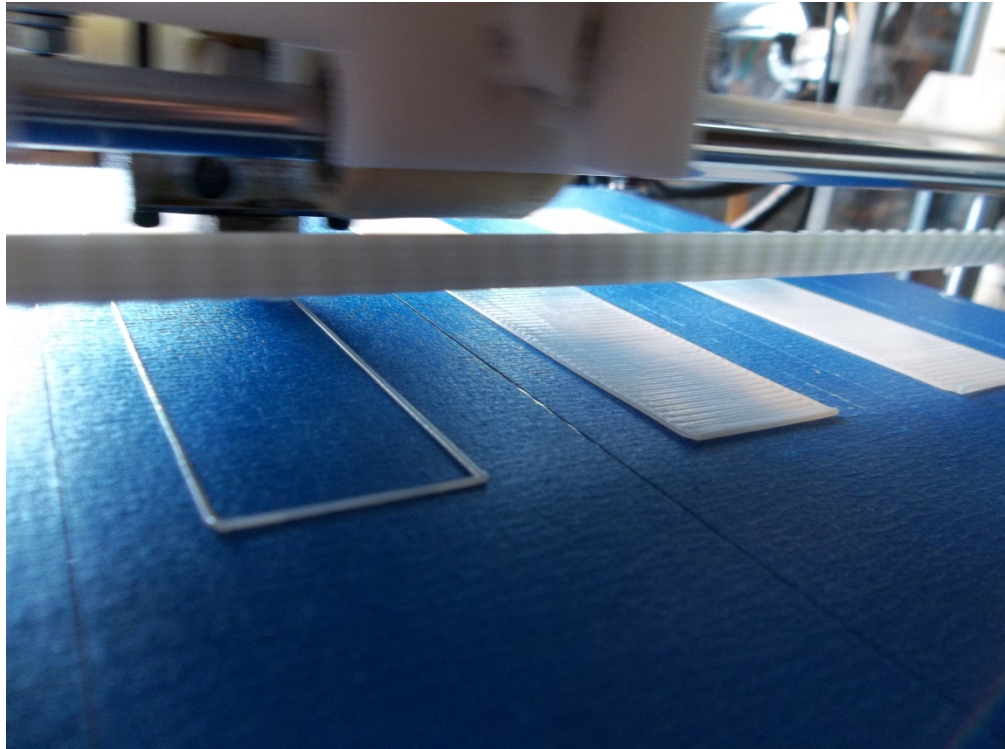
Figure 6 Rejected PLA Blank
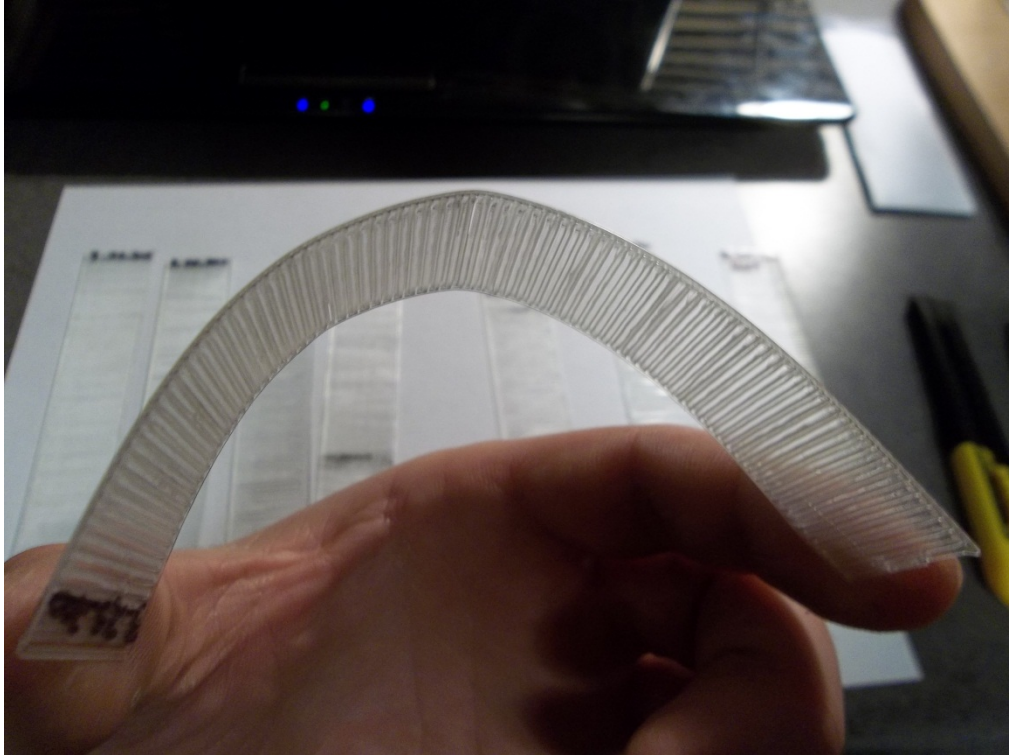


Figure 7 PLA Strength as a function of velocity
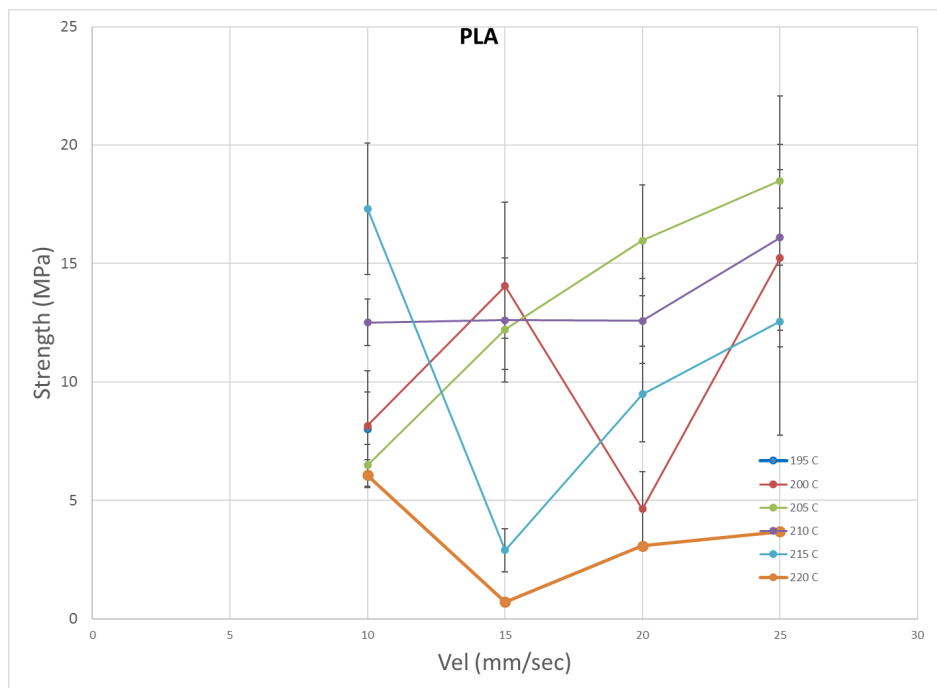
Figure 8 ABS Strength as a function of velocity
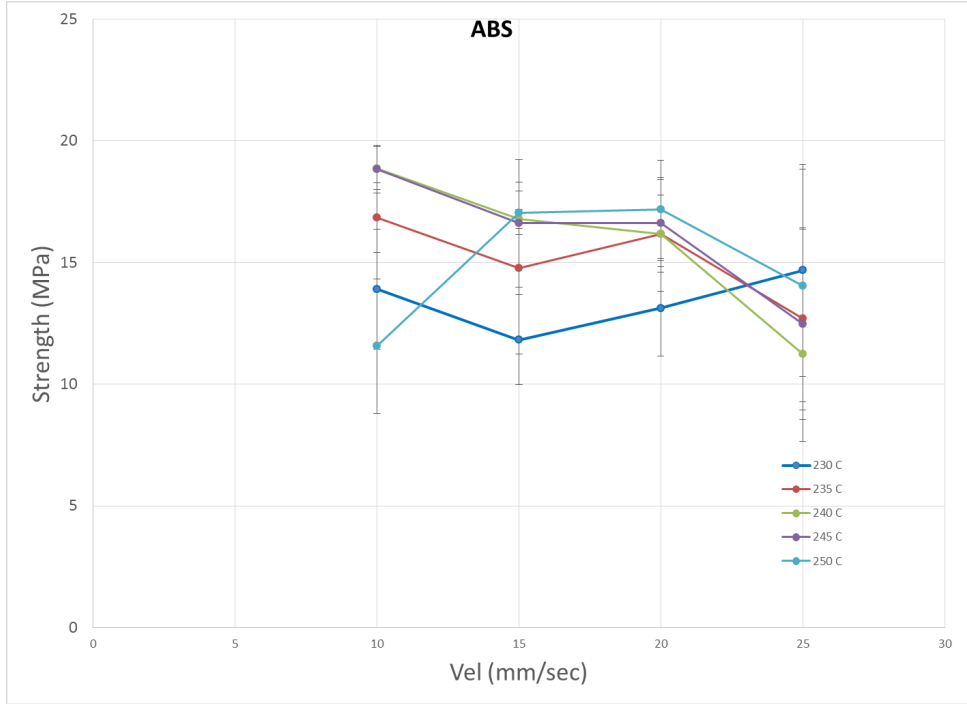


Figure 9 PLA Strength as a function of temperature
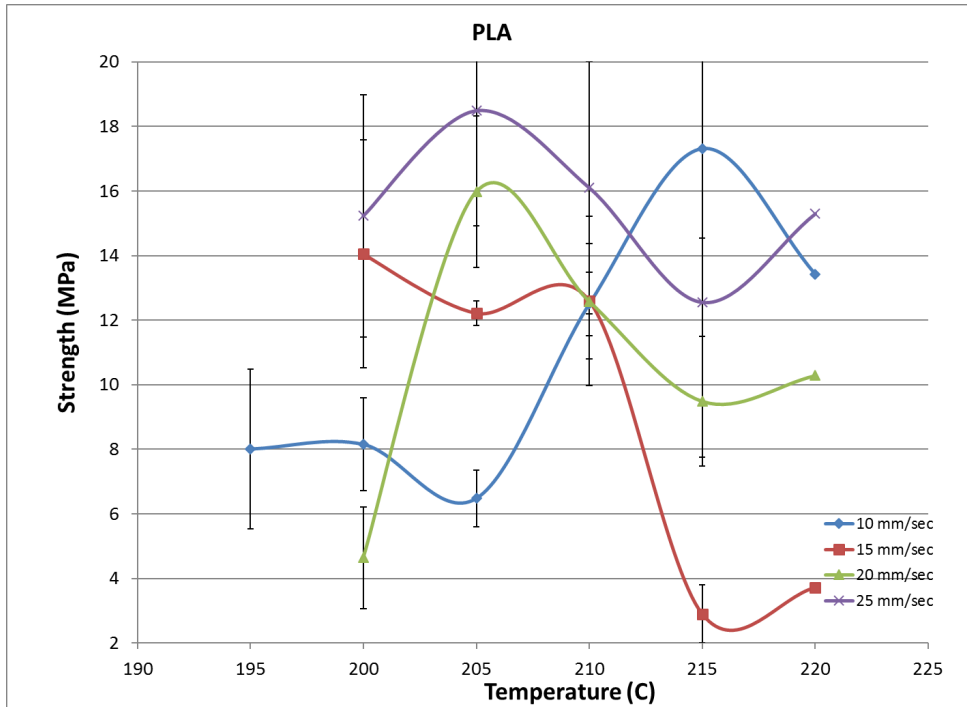
Figure 10 Strength as a function of temperature
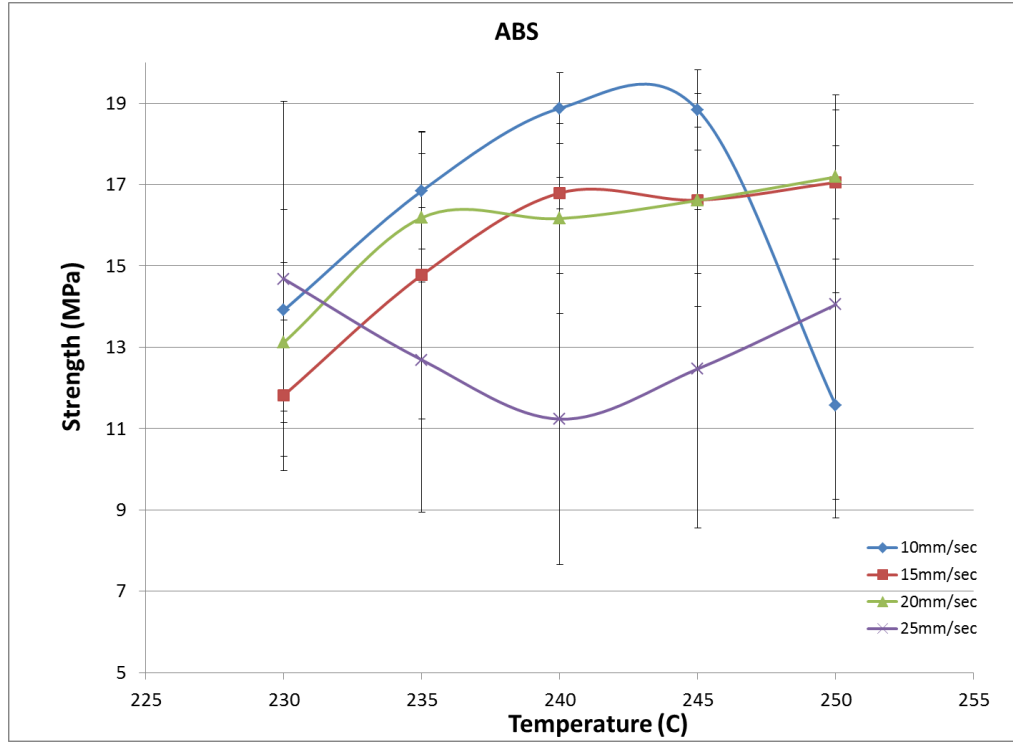


**Table 1 ABS Data**

| Vel | Temp | Average Strength | Std Dev S | Vel | Average Strength | Std Dev S | Vel | Average Strength | Std Dev S | Vel | Average Strength | Std Dev S |
|---|---|---|---|---|---|---|---|---|---|---|---|---|
| 10 | 230 | 13.9079 | 2.472 | 15 | 11.8188 | 1.850 | 20 | 13.1184 | 1.964 | 25 | 14.6803 | 4.358 |
| 10 | 235 | 16.8439 | 1.437 | 15 | 14.7755 | 3.535 | 20 | 16.1854 | 1.578 | 25 | 12.6898 | 3.747 |
| 10 | 240 | 18.8751 | 0.874 | 15 | 16.7929 | 0.386 | 20 | 16.1648 | 2.340 | 25 | 11.2343 | 3.576 |
| 10 | 245 | 18.8351 | 0.981 | 15 | 16.6175 | 2.621 | 20 | 16.6095 | 1.795 | 25 | 12.4692 | 3.913 |
| 10 | 250 | 11.5708 | 2.765 | 15 | 17.0519 | 0.899 | 20 | 17.1875 | 2.013 | 25 | 14.0481 | 4.785 |

**Table 2 PLA Data**

| Vel | Temp | Average Strength | Std Dev S | Vel | Average Strength | Std Dev S | Vel | Average Strength | Std Dev S | Vel | Average Strength | Std Dev S |
|---|---|---|---|---|---|---|---|---|---|---|---|---|
| 10 | 195 | 8.0048 | 3.127 | | | | | | | | | |
| 10 | 200 | 8.1479 | 1.323 | 15 | 14.0498 | 6.546 | 20 | 4.6425 | 2.591 | 25 | 15.2305 | |
| 10 | 205 | 6.4788 | 2.782 | 15 | 12.2175 | 3.308 | 20 | 15.9752 | 4.452 | 25 | 18.4952 | 8.342 |
| 10 | 210 | 12.5048 | 9.781 | 15 | 12.6036 | 0.283 | 20 | 12.5829 | | 25 | 16.1044 | 8.049 |
| 10 | 215 | 17.3110 | 6.406 | 15 | 2.8924 | 0.015 | 20 | 9.4872 | | 25 | 12.5485 | 5.611 |
| 10 | 220 | 13.4241 | 6.063 | 15 | 3.7128 | 0.717 | 20 | 10.2835 | 3.076 | 25 | 15.2972 | 3.686 |

**Table 3 Variability by Velocity**

| Vel | PLA Std Dev S | ABS Std Dev S |
|---|---|---|
| 10 | 4.914 | 1.706 |
| 15 | 2.174 | 1.858 |
| 20 | 3.373 | 1.938 |
| 25 | 6.422 | 4.076 |

**Table 4 Variability by Temperature**

| Temp | PLA Std Dev S | Temp | ABS Std Dev S |
|---|---|---|---|
| 195 | 3.127 | 230 | 2.661 |
| 200 | 3.487 | 235 | 2.574 |
| 205 | 4.721 | 240 | 1.794 |
| 210 | 6.038 | 245 | 2.328 |
| 215 | 4.011 | 250 | 2.615 |
| 220 | 3.386 | | |

## Acknowledgements

## References

1.  Wohlers Report 2015, 3D Prinding and Additive Manufacturing State of the Industry, Annual Worldwide Progress Report, Wohlers Associates, p.32-42

2.  Bickrest E.J., et al, "Material Selection" Chapter 2 *Tool and Manufacturing Engineers Handbook, Vol. 8 Plastic Part Manufacturing*, Society of Manufacturing Engineers, Dearborn, Michigan (1996)

3.  Sevidova E.K., Pupan L.I., and Tsyuryupa V.N., "Influence of Coatings on the Surface Strength of Rapid Prototyping Products", *Surface Engineering and Applied Electrochemistry,* Vol. 44 No. 5 2008.

4.  J. P. Kruth, M. C. Leu, T. Nakagawa, "Progress in Additive Manufacturing and Rapid Prototyping", Annals of the CIRP 47/2, 1998, 525-540.

5.  S. Crump, "Apparatus and method for creating three-dimensional objects". US patent 5,121,329 (1992).

6.  Grande J.A., "Blow Molders & Thermoformers Try Plastic Rapid Tooling", *Plastics Technology,* July 2008.

7.  Hadas Z., Zouhar J., Singule V. and Ondrusek C., "Design of Energy Harvesting Generator Base on Rapid Prototype Parts", *13th International Power Electronics and Motion Control Conference (EPE-PEMC 2008).*

8.  ThyssenKrupp, Polylactic acids (PLA), 5/27/2015
    https://www.thyssenkrupp.com/en/produkte/polylactide.html

9.  ABS Plastic.eu - The 3D Printing Hub, PLA Vs. ABS Plastic – The Pros and Cons, 5/27/2015,
    http://www.absplastic.eu/pla-vs-abs-plastic-pros-cons/

10. MakerBot – PLA and ABS Strength Data ASTM D256, D695, D638, D790, 6/4/2015,
    https://eu.makerbot.com/fileadmin/Inhalte/Support/Datenblatt/MakerBot_R__PLA_and_ABS_Strength_Data.pdf

# CHAPTER 4. EXPERIMENTAL DETERMINATION OF PLA WELD STRENGTH IN FUSED FILAMENT FABRICATION

Steven Devlin[a], Jonathan Jennings[a], David Grewell[b]

[a]College of Engineering, University of Missouri, Columbia, MO

[b]Department of Agricultural and Biosystems Engineering, Iowa State University, Ames, IA

## Abstract

Fused Filament Fabrication (FFF) systems are extrusion based technologies used to produce functional or near-functional parts from a variety of thermoplastic materials. For over 20 years Stratasys fused deposition modelers (FDM) dominated the extrusion market for additive manufacturing (AM). However, with the retirement of the original Scott Crump patent, a vibrant open-source development community spawned a new generation of personal fabrication machines and is exponentially driving interest in FFF technology and AM. Entrepreneurs and inventors around the globe are designing and fabricating new product designs without the limits of traditional manufacturing methods. However, as with all AM processes, variability in part strength continues to limit use in commercial markets. Development of accurate and repeatable methods for determining material strength in FFF produced parts is essential for mainstream manufacturing.

This paper documents progress made on a continuing study to experimentally quantify the weld strength of filament welds as a function of nozzle temperature and print head speed. Test data indicate that weld strength is generally inversely proportional to print head speed with an inflection point at 15 millimeters per second, however effects were minimal with the observed

range of strength changing only from 29.7 to 31.2 MPa. Weld strength was observed to be generally proportional to extrusion temperature, with an inflection point at 215°C. Analysis of previous experimental data and examination of tested samples provide favorable insights and opportunities for additional and continuing investigation.

## 1      Introduction

1.1      Developing Industry – Additive Manufacturing

1.1.1    A newly revived manufacturing technique aptly named "3D printing" is becoming a popular method of manufacturing and prototyping.  This additive manufacturing method has many benefits including a wide range of inexpensive readily available materials, the ability to produce complex geometries, reduce part redesign iteration times, simple computer aided design interface, and ease of use.

1.1.2    Almost thirty years ago the U.S. Patent and Trademark office issued to Charles Hull a patent (number 4575330) for an Apparatus for Production of Three-Dimensional Objects by Stereo Lithography. This development launched the rapid prototyping/rapid manufacturing industry. Rapid prototyping (RP) or rapid manufacturing (RM), sometimes referred to as solid freeform fabrication or additive manufacturing (AM), is a method of fabricating parts through additive manufacturing processes. This allows parts to be developed at very low volumes. It is ideal for prototyping, fit and function modelling, patterns for metal casting, technological pieces for functional purposes and other situations where parts are needed in small quantities (i.e. production-quality parts needed for small runs).  Because of this, it has the potential to significantly affect product development and manufacturing. Today there are seven primary technologies offered through numerous manufacturers worldwide: material extrusion, material

jetting, binder jetting, sheet lamination, vat photo polymerization, powder bed fusion, and directed energy deposition [1].

## 1.2    Fused Filament Fabrication for Functional Parts

1.2.1    As stated previously, rapid prototyping or additive manufacturing methods, are most frequently used for three applications: model-prototypes, patterns for production of casting molds, or as short-run functional parts.  In the latter case, properties of the material used in the AM process (physico-mechanical, chemical and corrosion factors) are of significant importance and determine the functional-operational characteristics of finished products.  When selecting a material, it is important to consider not only the part function, also the AM technology being used in fabrication.  With a growing selection of production grade thermoplastic materials, including nylon, polycarbonate (PC), ULTEM 9085, acrylonitrile butadiene styrene (ABS), and polylactic acid (PLA), fused filament fabricators offer engineers a functional pallet for part design. Monofilament materials are typically available in several standard colors with a diameter of $1.75 \pm 0.05$ mm [2]. However, it is important to note, a number of monofilament suppliers have entered the market in recent years, adding to material variability through poor quality control.

1.2.2    In the FFF process, building and support material is heated, to a molten state, in a liquefying unit, extruded through a circular die, and deposited on a translational platform to create material roads. Exterior contour roads define a two-dimensional cross section of the model, which is subsequently filled using a raster pattern. Disposable lattices are created to support overhanging features and the platform is lowered in the Z plane. The next cross sectional extrusion is fused to the previous layer with the process continuing until the part is completed

[3]. Afterwards, part support structures are removed with limited post-processing required. Parts with 0.1 mm high layers and a minimum wall thickness of 0.5 mm are possible using FFF.

1.2.3    Growing demand for FFF systems in the open-source development community has expanded use of polylactic acid (PLA) based filaments.  Produced from a renewable material (lactic acid), PLA offers a variety of applications while helping to conserve fossil resources [4]. Unsuitable for many durable goods applications, PLA filaments hold a significant market with artistic users because of its smoother surfaces, shinier appearance, and ease-of use [5]. However, with additional understanding of the mechanical properties associated with FFF parts made from PLA, additional short-term applications may be developed.

**1.3     Experimental Investigation**

1.3.1    In this experiment investigators seek to determine if nozzle temperature and print head speed effect the strength of FFF welds between deposited filaments.  Building on a set of screening experiments to establish extrusion temperatures, print head speeds and test procedures, an experiment was conducted following a full factorial experimental design. Single layer PLA coupons were produced with extrusion temperatures from 195°C to 225°C and print head speeds of 10, 15, 20, and 25mm/s. Five replicates of each treatment combination were machined and tested for break strength using standard tensile method. To reduce experiment complexity and maintain consistency one specific type of PLA researchers used throughout the entire trial. Figure 1. Displays the Makerbot Natural 1.75mm PLA.

**2       Materials and Methods**

2.1     Fabrication

2.1.1    Testing coupons were fabricated using a MakerBot Replicator 2X shown in Figure 2. The non-heated build plate was covered with a polyimide film to facilitate coupon removal. The same

machine, nozzle and build setup was used for all specimens to reduce variability. To achieve a raster fill perpendicular to the contour perimeter, samples were oriented at a 45° angle, with respect to the build plate, as MakerBot slicing software prints the first layer at a 45° angle, shown in Figure 3.

2.1.2    Typically, the first layer of a FFF build is smeared to help the part adhere to the build platform. This is problematic as it alters the thickness and profile of the bead weld shown in Figure 4. Alternative strategies such as, building the part in the Z plane or vertically on the build platform using support structures or a box design were considered, but would also make the build very difficult, as the one bead thick layer would cause the part to become unstable and topple during the build.

2.1.3    To reduce deformation associated with first layer smear, the distance between the nozzle tip and the platform was increased to 0.5mm producing a round bead. Figure 5 illustrates a rendition between smearing and not smearing on the build plate. However, the increased nozzle height did cause platform adhesion problems. To alleviate this problem, a polyimide heat resistive film was applied to the build plate. Surface roughness was increased by scratching the film with sandpaper or a medium duty scrubbing sponge. All prints were at a 0.5mm thickness which was measured with a caliper and held to a 0.02mm thickness deviation. Any parts outside of this deviation were discarded.

2.1.4    After producing the rectangular tensile testing coupons on the MakerBot they were machined to remove the outer shell and shaped in accordance with ASTM D638 type 3 standards. Figure 6 displays the standard ASTM Type 1 tensile test specimen, while Figure 7 displays the printed coupon and machined specimens used in all experiments. Specimens were

machined on a standard vertical mill using a circular milling cutter tool as seen in Figure 8.

Printed coupons were secured and protected using a jig fixture as shown in Figure 9.

2.2     Testing

2.2.1    To identify an initial test range a crude dead weight setup was created so that the proper

load cell (50 lbs.) could be chosen for the testing apparatus. Figure 10 shows the simplified

deadweight experimental setup. The deadweight testing was accomplished by first attaching the

tensile testing coupon to a military grade ammunition container and adding random metallic

items to the container until the coupon would fail.  After failure, the container and its contents

were weighed to gain the weight necessary to cause failure.  Three rectangular coupons of

printed PLA, with perimeter contours intact, were tested to gain an ultimate strength that would

never be surpassed while using the dog bone shaped specimens.  The three tests were only

partially successful as without the proper tensile shape the specimens would break at the

clamping area instead of in the center of the coupon.  The three samples broke at approximately

thirty pounds of dry hanging weight and it was noted that the factor of breaking is less than three

times the force when broken at the clamp area.  To improve the validity of the experiment two

additional tests were performed with the proper ASTM shape and both samples held 24.4 lbs. of

dry hanging weight before breaking.  This defined a fifty-pound load cell for testing.

2.2.2    Figure 11 shows the Soiltest U-590 table top tensile testing machine used to perform all

experiments. Sensors used in the load frame included an interface SML-50 fifty pound load cell

and a LVDT sensor, to measure specimen elongation, connected to a data acquisition system.

Specifications for the sensors can be found at the website posted in the appendix A 1-2.  The

LVDT voltage readings were first sent through a Schaevitz ATA-101 analog transducer amplifier

which is show in Figure 12. Specifications for the amplifier may be found at the website listed in

the appendix A3. The measured elongation values were too small for the system thus during later studies the measurements were not used. The data acquisition system included a voltage multiplier, data acquisition hub, and data recording program. Voltage output of the load cell was in the -30 to +30 millivolt range and required a signal amplifier that amplifies the signal by 166.667 to make the signal visible to the rest of the DAQ system. Figure 13 shows the Analog Devices 5B38 -30 to +30 millivolt input, 0-5 volt output signal amplifier. Documentation for this device can be found at the website listed in the appendix A4. As indicated in section 2.1.4, test specimens were machined using a proprietary jig to maintain proper cross sectional area, machined samples were measured using digital calipers and recorded by sample number. The crosshead speed of the loading member during all tests was 0.5 mm/min.

## 3    Data Analysis

### 3.1    Results

3.1.1    Test data were compiled for the treatment combinations and analyzed to characterize the relationship between breaking strength (MPa) and the levels of temperature and print head speed. Because there are 5 replications of each of the 28 temperature by print head speed combinations a full-factorial model with main effects for temperature and print head speed and a temperature by print head speed interaction effect was fit to the 140 breaking strength values.  The analysis of variance table is given in Table 1.

Table 1 Analysis of Variance of Breaking Strength (MPa)

| Source | df | Sum of Squares | Mean Square | F Ratio | P-value |
|--------|----|----------------|-------------|---------|---------|
| Temperature | 6 | 131.257 | 21.876 | 3.86 | 0.0015** |
| Speed | 3 | 40.689 | 13.563 | 2.39 | 0.0723 |
| Temperature*Speed | 18 | 136.542 | 7.586 | 1.34 | 0.1783 |
| Error | 112 | 634.946 | 5.669 | | |
| C. Total | 139 | 943.434 | | | |

* statistically significant at the $\alpha = 0.05$  ** statistically significant at the $\alpha = 0.01$

The only statistically significant term, at both the α = 0.05 and α = 0.01 levels, is Temperature.

An analysis of the residuals for this model fit revealed three (3) values that were 3 or more

standard deviations away from the mean and thus considered outliers.  By excluding these

outliers from the data and rerunning the full-factorial analysis on the 137 remaining breaking

strength values the analysis of variance table given in Table 2 is obtained.

Table 2 Analysis of Variance of Breaking Strength (MPa), 3 outliers removed

| Source | df | Sum of Squares | Mean Square | F Ratio | P-value |
|---|---|---|---|---|---|
| Temperature | 6 | 93.907 | 15.651 | 4.79 | 0.0002** |
| Speed | 3 | 28.159 | 9.386 | 2.87 | 0.0396* |
| Temperature*Speed | 18 | 138.981 | 7.721 | 2.36 | 0.0034** |
| Error | 109 | 356.016 | 3.266 | | |
| C. Total | 136 | 619.315 | | | |

* statistically significant at the α = 0.05  ** statistically significant at the α = 0.01

According to the analysis of the breaking strength data once the 3 outliers are removed,

Temperature is statistically significant at the α = 0.01 and Speed is statistically significant at the

α = 0.05 level.  Additionally, there is a statistically significant interaction at the α = 0.01 level

between Temperature and Speed.

3.1.2    Plotting the least squares mean strength values for the various temperatures, Figure 14,

reveals an increasing trend as temperature increases from 200°C to 215°C but then mean strength

decreases for the higher temperatures of 220°C and 225°C.  The highest mean breaking strength

of 31.9 MPa is obtained with a temperature of 215°C.

3.1.3    Plotting the least squares mean strength values for the various print head speeds, Figure

15, reveals an increasing trend as speed increases from 10 mm/s to 15 mm/s but then mean

strength decreases for the higher speeds of 20 mm/s and 25 mm/s.  The highest mean breaking

strength of 31.2 MPa is obtained with a print head speed of 15 mm/s.

3.1.4   The statistically significant interaction between temperature and print head speed indicates that the relationship between mean breaking strength and temperature is different for some print head speeds.  Figure 16 is an interaction plot of the mean breaking strengths for the 28 combinations of temperature and print head speed.  Print head speeds of 10 mm/s, 15 mm/s and 20 mm/s follow the general trend of increasing mean strength when temperature increases from 200°C to 215°C and lower mean strength values for the higher temperatures of 220°C and 225°C. However, for the 25 mm/s print head speed there appears to be a different relationship between mean breaking strength and temperature; decreasing mean strength as temperature increases from 195°C to 215°C and higher mean strength values for the higher temperatures of 220°C and 225°C.

## 4        Discussion

### 4.1      Temperature

4.1.1   As seen in Figure 14, the mean weld strength generally increases as temperature increases up to 215°C.  MakerBot PLA printed in the replicator 2x fails to print below the 195 °C temperature so no additional testing was possible in the low temperature range.  It was noted that PLA degraded at an extrusion temperature of 225°C and the extrusion nozzle clogged.  This allows a conclusion that 215°C is a better temperature to print with this specific filament and machine combination.

### 4.2      Speed

4.2.1   As seen in Figure 15, the weld strength is generally higher at 15 mm/s compared to the other print head speeds.  The MakerBot replicator 2x has a normal print head speed of 90 mm/s so more experimentation should be considered in the range from 25 mm/s to 100 mm/s.  While the graph and test of significance suggest that print head speed affects the mean breaking

strength, the effects is not that large given that the range of mean breaking strengths goes from 29.9 MPa to 31.2 MPa for the given print head speeds.

4.3     Interaction between Temperature and Speed

4.3.1   Given the statistically significant interaction between temperature and print head speed and the interaction plot in Figure 16, temperature appears to have a different effect on mean breaking strength for a print head speed of 25 mm/s compared to the other print head speeds.

4.4     Other Considerations

4.4.1   The statistical analysis presented above is based on the 137 breaking strength values after 3 outliers were removed.  The three values identified as outliers had breaking strengths much lower than would be expected given the other breaking strength values and the full-factorial analysis.  As there were only a few outliers we are assuming that these values are not true indications of the breaking strength but due to some anomaly in the experimental process.

4.4.2   Future studies looking at FFF weld strength should consider different methods for printing the test samples, including vertical orientation to eliminate filament spread induced by the platen.  It may also be advisable to reconsider the possibility of a direct test sample build to eliminate post processing stresses.  A sub-investigation to evaluate the impact of road-path loops versus machine cut edges may be needed.

4.4.3   Studies seeking to replicate the build in this experiment should consider using commercial grade FFF equipment.  Weld strength investigations of alternative rapid prototyping technologies, such as selective laser sintering, will also be needed for commercial market adoption.

**5      Conclusions**

5.1      Based on these experimental trials, it has been observed that changing extrusion head speed has some effect on the mean tensile strength of FFF parts.  Extrusion temperature settings demonstrate a larger effect on mean tensile strength than speed.  However, extrusion temperature has a different effect when the print head speed is 25 mm/s than it does for the other print head speeds examined in the experiment.  Final part strength may have been limited by the extrusion technology and further study is needed to evaluate the possibility of alternative heat sources being added to improve weld strength, such as those proposed by Grewell [6].

6      Recommended future tests

6.1      A number of opportunities continue to develop related to the operational methods being used to conduct the study and may also have an impact on production applications. As there was a separation of time between when samples were first produced and when they were tested, it could be implied that there is a relationship between part strength and time of part use. Additional research is required to determine the magnitude and driving factors associated with this variability, and may include handling damage, moisture absorption, and material degradation – specifically with biodegradable type materials (PLA). It would also be beneficial to investigate the impact of 'edge removal' on the research process, after two rounds of post processing experiments specimens, researchers suspect the resulting stresses introduced by machining may distort the model.

7        Figures
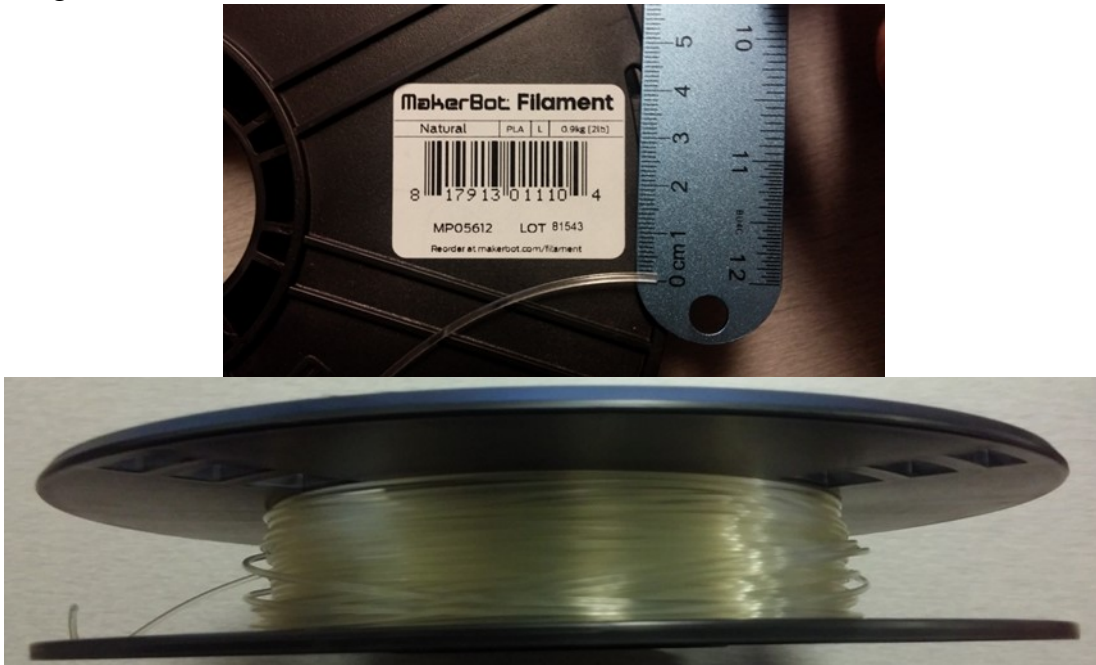


7.1      Figure 1 MakerBot Natural 1.75mm Filament
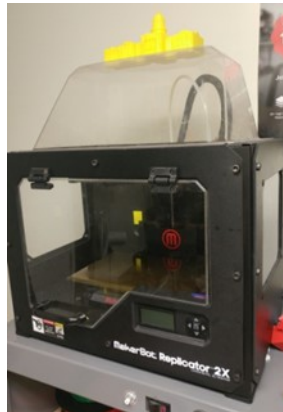


7.2      Figure 2 MakerBot Replicator 2X
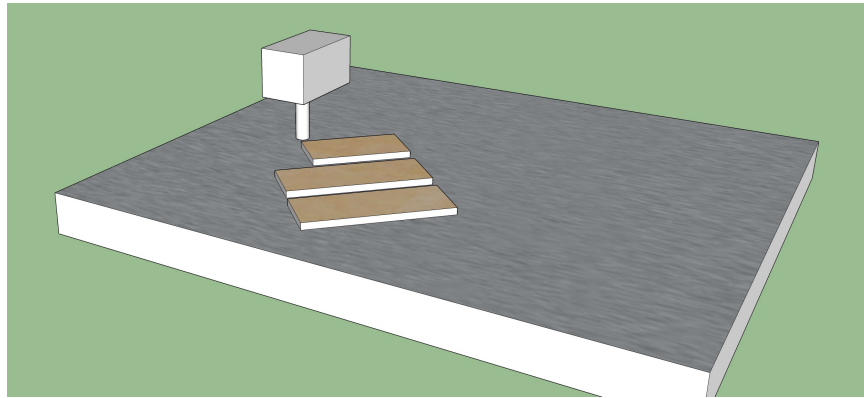
7.3     Figure 3 45° Build Orientation
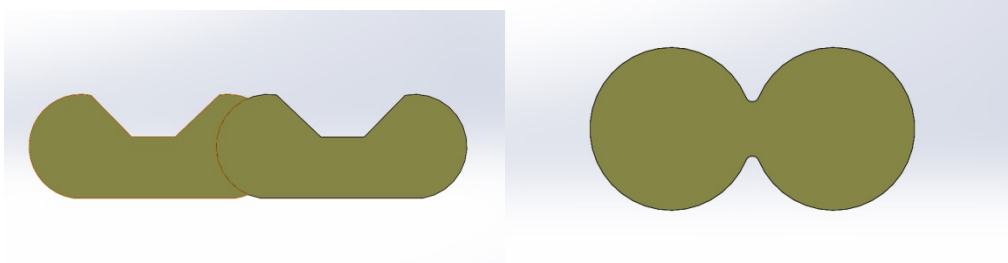


7.4     Figure 4 Extruded Road Rendition
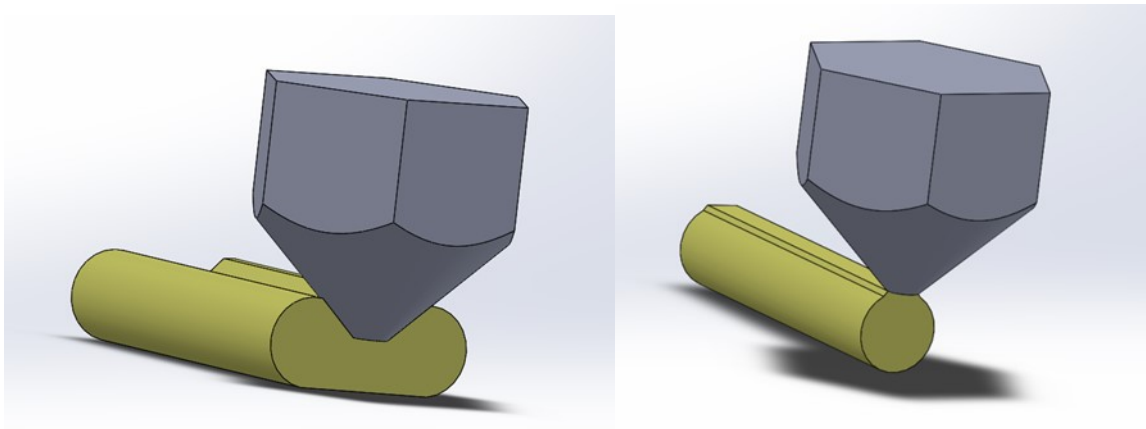


7.5     Figure 5 Smeared vs Tested Road Extrusion
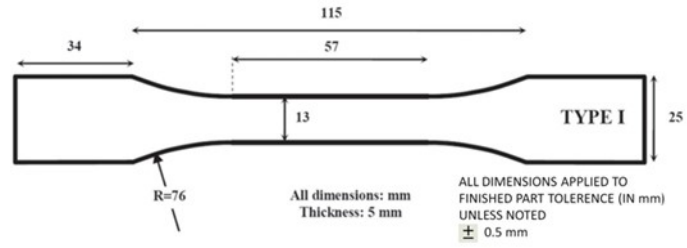
7.6     Figure 6 Dimensioned Type 1 ASTM Tensile Testing Coupon
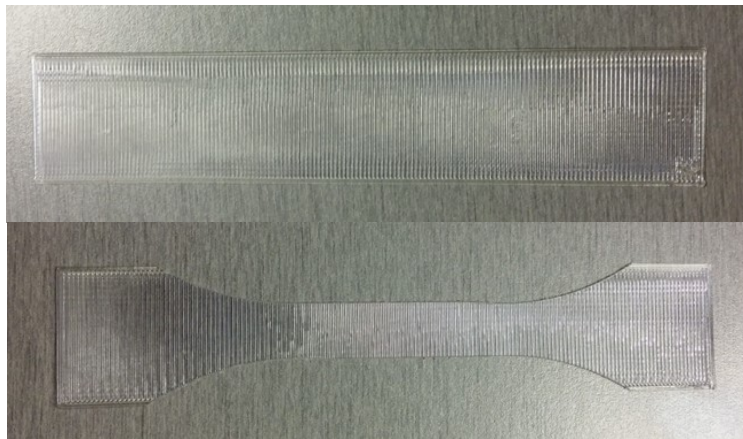


7.7     Figure 7 Printed & Cut Test Specimens



7.8     Figure 8 Circular Milling Cutter

7.9     Figure 9 Coupon Jig



7.10    Figure 10 Deadweight Testing
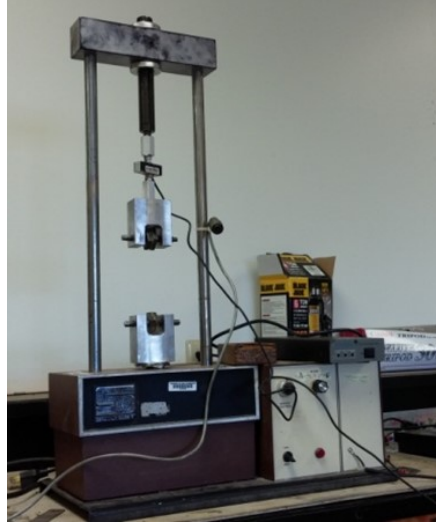
7.11    Figure 11 Soiltest U-590
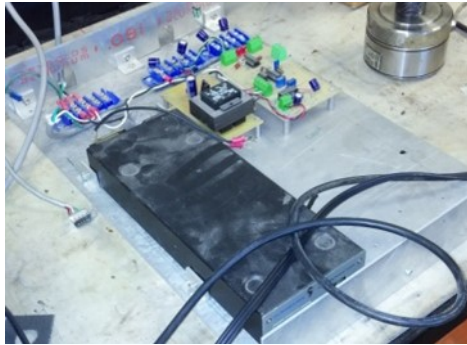


7.12    Figure 12 Schaevitz AT-101 Analog Transducer Amplifier
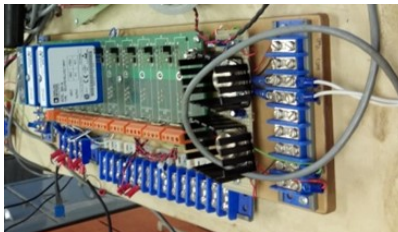


7.13    Figure 13 Analog Device 5B38 Signal Amplifier
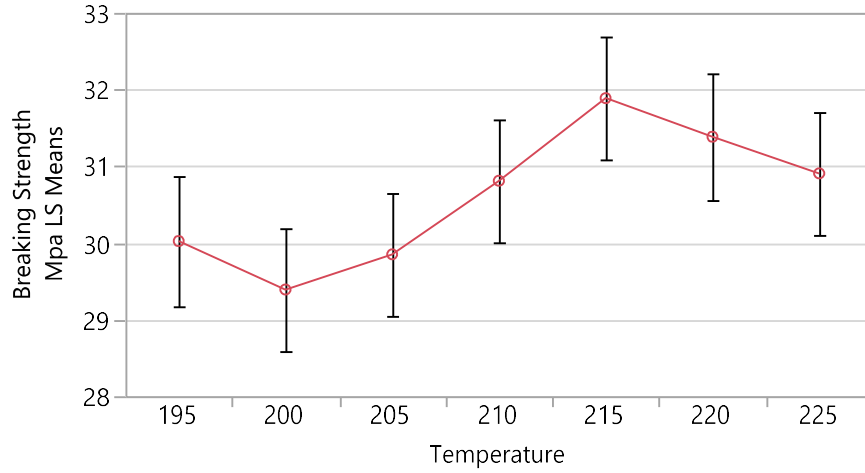
7.14    Figure 14 Mean Breaking Strength (MPa) versus Temperature (°C)
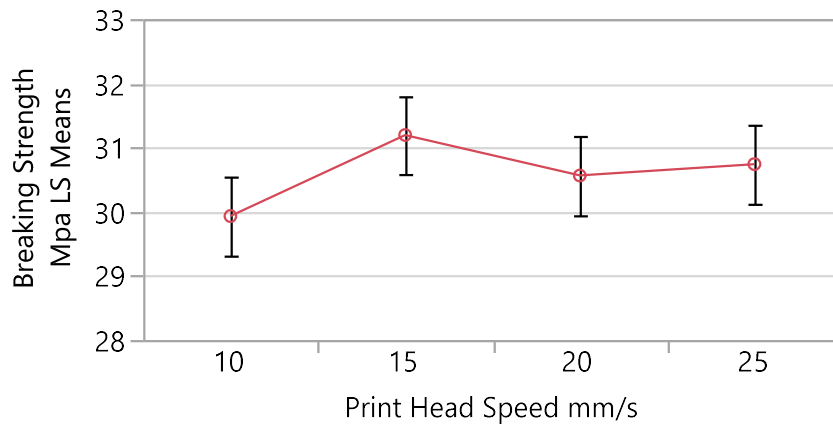


7.15    Figure 15 Mean Breaking Strength (MPa) versus Print Head Speed (mm/s)
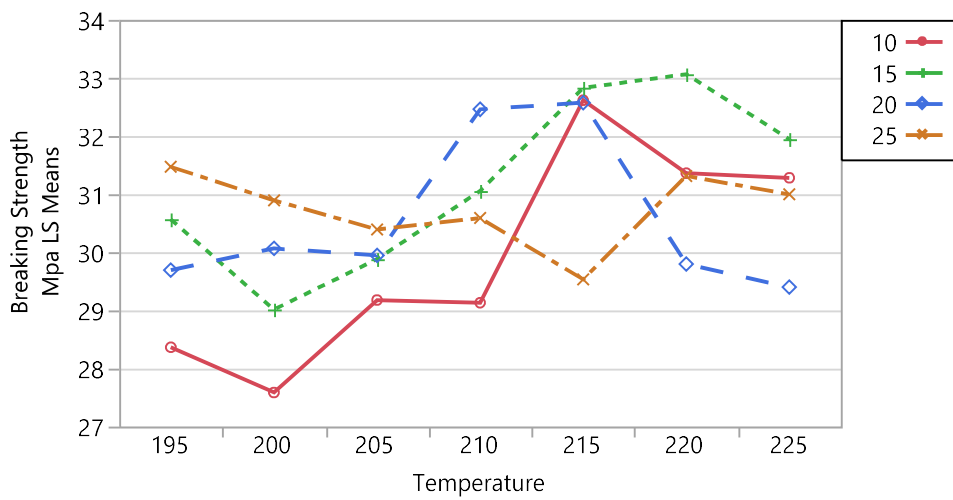


7.16    Figure 16 Interaction Plot of Mean Breaking Strength

8 References

1. Wohler, T., et al. (2015). Wohlers Report 2015, 3D printing and additive manufacturing state of the industry. Annual Worldwide Progress Report, Wohlers Associates, p.32-42.

2. Wendel, B., D., Rietzel, F., Kühnlein, R., Feulner, G., Hülder, & E., Schmachtenberg, (2008). Additive processing of polymers. Macromolecular Materials and Engineering, 293, S. 799-809.

3. Crump, S., (1992). Apparatus and method for creating three-dimensional objects. U.S. Patent # 5,121,329.

4. Hadas Z., J., Zouhar, V., Singule, & C., Ondrusek, (2008). Design of energy harvesting generator base on rapid prototype parts. 13th International Power Electronics and Motion Control Conference (EPE-PEMC 2008).

5. ABS Plastic.eu - The 3D Printing Hub, PLA Vs. ABS Plastic – The Pros and Cons, 5/27/2015, http://www.absplastic.eu/pla-vs-abs-plastic-pros-cons/

6. Grewell, D., (2017). Closed loop 3D printing. U.S. Patent Application # 20170087767. http://appft.uspto.gov/netacgi/nph Parser?Sect1=PTO2&Sect2=HITOFF&p=1&u=%2Fnetahtml%2FPTO%2Fsearch

bool.html&r=1&f=G&l=50&co1=AND&d=PG01&s1=grewell.IN.&OS=IN/grewell&RS=IN/grewell

9 Appendix

A1 http://www.interfaceforce.com/index.php?SML-Mini-Low-Height-S-Type-Load-Cell&mod=product&show=33

A2 https://www.cdiweb.com/ProductDetail/02560569006--schaevitz/51822/

A3 http://simhardware.org/img/ATA-101_manual.pdf

A4 http://www.analog.com/media/en/technical-documentation/data-sheets/5B38.pdf

A5 http://www.ni.com/pdf/manuals/374591c.pdf

Raw Data

| Extrusion temperature °C | Print head speed mm/s | Breaking Force - MPa | Thickness In | Width In |
|---|---|---|---|---|
| 195 | 10 | 26.475 | 0.02 | 0.381 |
| 195 | 10 | 28.035 | 0.019 | 0.409 |
| 195 | 10 | 30.045 | 0.018 | 0.38 |
| 195 | 10 | 29.94 | 0.018 | 0.386 |
| 195 | 10 | 27.33 | 0.018 | 0.386 |
| 195 | 15 | 31.83 | 0.019 | 0.391 |
| 195 | 15 | 31.71 | 0.018 | 0.389 |
| 195 | 15 | 30.03 | 0.018 | 0.371 |
| 195 | 15 | 30.69 | 0.019 | 0.405 |
| 195 | 15 | 28.575 | 0.019 | 0.381 |
| 195 | 20 | 30.36 | 0.019 | 0.398 |
| 195 | 20 | 27.045 | 0.019 | 0.384 |
| 195 | 20 | 30.825 | 0.018 | 0.389 |
| 195 | 20 | 30.54 | 0.019 | 0.39 |
| 195 | 20 | 20.325 | 0.017 | 0.391 |
| 195 | 25 | 34.245 | 0.019 | 0.382 |
| 195 | 25 | 29.745 | 0.018 | 0.388 |
| 195 | 25 | 17.955 | 0.017 | 0.381 |
| 195 | 25 | 28.485 | 0.017 | 0.408 |
| 195 | 25 | 33.405 | 0.019 | 0.382 |
| 200 | 10 | 31.71 | 0.02 | 0.393 |
| 200 | 10 | 29.43 | 0.021 | 0.381 |
| 200 | 10 | 26.31 | 0.02 | 0.354 |
| 200 | 10 | 24.075 | 0.02 | 0.404 |
| 200 | 10 | 26.415 | 0.02 | 0.382 |
| 200 | 15 | 29.055 | 0.019 | 0.387 |
| 200 | 15 | 30.045 | 0.019 | 0.395 |
| 200 | 15 | 28.47 | 0.021 | 0.385 |
| 200 | 15 | 28.155 | 0.02 | 0.395 |
| 200 | 15 | 29.355 | 0.02 | 0.379 |
| 200 | 20 | 30.945 | 0.019 | 0.406 |
| 200 | 20 | 29.265 | 0.02 | 0.404 |
| 200 | 20 | 29.85 | 0.019 | 0.397 |
| 200 | 20 | 29.115 | 0.019 | 0.414 |
| 200 | 20 | 31.155 | 0.019 | 0.409 |
| 200 | 25 | 32.145 | 0.018 | 0.407 |
| 200 | 25 | 29.07 | 0.018 | 0.416 |
| 200 | 25 | 30.825 | 0.018 | 0.4 |
| 200 | 25 | 30.465 | 0.018 | 0.413 |

| Extrusion temperature °C | Print head speed mm/s | Breaking Force MPa | Thickness In | Width In |
|---|---|---|---|---|
| 200 | 25 | 31.965 | 0.019 | 0.415 |
| 205 | 10 | 30.42 | 0.019 | 0.397 |
| 205 | 10 | 23.235 | 0.018 | 0.39 |
| 205 | 10 | 30.795 | 0.018 | 0.38 |
| 205 | 10 | 30.18 | 0.018 | 0.354 |
| 205 | 10 | 31.26 | 0.018 | 0.385 |
| 205 | 15 | 30.06 | 0.02 | 0.398 |
| 205 | 15 | 28.785 | 0.02 | 0.413 |
| 205 | 15 | 30.315 | 0.02 | 0.408 |
| 205 | 15 | 30.915 | 0.02 | 0.403 |
| 205 | 15 | 29.34 | 0.019 | 0.407 |
| 205 | 20 | 30.855 | 0.02 | 0.402 |
| 205 | 20 | 30.96 | 0.019 | 0.412 |
| 205 | 20 | 29.31 | 0.019 | 0.411 |
| 205 | 20 | 29.4 | 0.019 | 0.381 |
| 205 | 20 | 29.205 | 0.019 | 0.41 |
| 205 | 25 | 32.565 | 0.018 | 0.402 |
| 205 | 25 | 31.425 | 0.02 | 0.407 |
| 205 | 25 | 31.47 | 0.019 | 0.402 |
| 205 | 25 | 28.77 | 0.019 | 0.42 |
| 205 | 25 | 27.735 | 0.019 | 0.4 |
| 210 | 10 | 29.985 | 0.018 | 0.398 |
| 210 | 10 | 29.205 | 0.018 | 0.386 |
| 210 | 10 | 29.505 | 0.019 | 0.398 |
| 210 | 10 | 30.285 | 0.017 | 0.398 |
| 210 | 10 | 26.685 | 0.018 | 0.386 |
| 210 | 15 | 32.25 | 0.018 | 0.41 |
| 210 | 15 | 32.355 | 0.018 | 0.398 |
| 210 | 15 | 29.655 | 0.019 | 0.396 |
| 210 | 15 | 32.31 | 0.018 | 0.404 |
| 210 | 15 | 28.71 | 0.019 | 0.4 |
| 210 | 20 | 31.8 | 0.017 | 0.403 |
| 210 | 20 | 32.445 | 0.018 | 0.406 |
| 210 | 20 | 32.4 | 0.018 | 0.408 |
| 210 | 20 | 31.965 | 0.418 | 0.401 |
| 210 | 20 | 33.69 | 0.019 | 0.551 |
| 210 | 25 | 32.19 | 0.018 | 0.39 |
| 210 | 25 | 25.785 | 0.018 | 0.373 |
| 210 | 25 | 29.535 | 0.018 | 0.407 |
| 210 | 25 | 31.425 | 0.019 | 0.411 |

| Extrusion temperature °C | Print head speed mm/s | Breaking Force - MPa | Thickness -In | Width - In |
|---|---|---|---|---|
| 210 | 25 | 34.005 | 0.018 | 0.417 |
| 215 | 10 | 32.355 | 0.019 | 0.397 |
| 215 | 10 | 33.03 | 0.017 | 0.41 |
| 215 | 10 | 32.385 | 0.018 | 0.4 |
| 215 | 10 | 32.055 | 0.018 | 0.406 |
| 215 | 10 | 33.255 | 0.018 | 0.408 |
| 215 | 15 | 33.57 | 0.018 | 0.4 |
| 215 | 15 | 32.205 | 0.019 | 0.401 |
| 215 | 15 | 32.01 | 0.018 | 0.395 |
| 215 | 15 | 32.7 | 0.019 | 0.398 |
| 215 | 15 | 33.66 | 0.018 | 0.387 |
| 215 | 20 | 33.69 | 0.019 | 0.406 |
| 215 | 20 | 30.795 | 0.019 | 0.385 |
| 215 | 20 | 32.355 | 0.019 | 0.409 |
| 215 | 20 | 32.88 | 0.018 | 0.393 |
| 215 | 20 | 33.15 | 0.018 | 0.401 |
| 215 | 25 | 29.91 | 0.02 | 0.397 |
| 215 | 25 | 25.5 | 0.018 | 0.396 |
| 215 | 25 | 31.35 | 0.019 | 0.404 |
| 215 | 25 | 29.655 | 0.018 | 0.391 |
| 215 | 25 | 31.26 | 0.019 | 0.397 |
| 220 | 10 | 29.925 | 0.018 | 0.399 |
| 220 | 10 | 30.54 | 0.019 | 0.393 |
| 220 | 10 | 31.89 | 0.019 | 0.394 |
| 220 | 10 | 33.09 | 0.018 | 0.398 |
| 220 | 10 | 22.515 | 0.018 | 0.391 |
| 220 | 15 | 33.48 | 0.018 | 0.392 |
| 220 | 15 | 32.595 | 0.018 | 0.393 |
| 220 | 15 | 33.615 | 0.018 | 0.401 |
| 220 | 15 | 33.375 | 0.019 | 0.397 |
| 220 | 15 | 32.25 | 0.019 | 0.386 |
| 220 | 20 | 26.94 | 0.02 | 0.398 |
| 220 | 20 | 31.65 | 0.021 | 0.397 |
| 220 | 20 | 29.73 | 0.019 | 0.374 |
| 220 | 20 | 29.01 | 0.02 | 0.384 |
| 220 | 20 | 31.665 | 0.019 | 0.384 |
| 220 | 25 | 30.06 | 0.019 | 0.392 |
| 220 | 25 | 32.025 | 0.018 | 0.388 |
| 220 | 25 | 32.475 | 0.019 | 0.387 |
| 220 | 25 | 31.53 | 0.019 | 0.379 |
| 220 | 25 | 30.48 | 0.02 | 0.394 |

| Extrusion temperature °C | Print head speed mm/s | Breaking Force - MPa | Thickness -In | Width - In |
|---|---|---|---|---|
| 225 | 10 | 33.3 | 0.018 | 0.39 |
| 225 | 10 | 31.335 | 0.02 | 0.398 |
| 225 | 10 | 28.965 | 0.019 | 0.398 |
| 225 | 10 | 28.98 | 0.02 | 0.405 |
| 225 | 10 | 33.825 | 0.019 | 0.399 |
| 225 | 15 | 30.165 | 0.02 | 0.395 |
| 225 | 15 | 33.795 | 0.019 | 0.382 |
| 225 | 15 | 34.38 | 0.019 | 0.4 |
| 225 | 15 | 31.74 | 0.021 | 0.402 |
| 225 | 15 | 29.655 | 0.02 | 0.393 |
| 225 | 20 | 31.245 | 0.018 | 0.39 |
| 225 | 20 | 30.15 | 0.019 | 0.404 |
| 225 | 20 | 29.94 | 0.019 | 0.4 |
| 225 | 20 | 24.705 | 0.02 | 0.405 |
| 225 | 20 | 30.96 | 0.019 | 0.402 |
| 225 | 25 | 30.72 | 0.02 | 0.392 |
| 225 | 25 | 31.455 | 0.02 | 0.386 |
| 225 | 25 | 32.31 | 0.018 | 0.387 |
| 225 | 25 | 30 | 0.02 | 0.387 |
| 225 | 25 | 30.495 | 0.02 | 0.39 |

# CHAPTER 5. EXPERIMENTAL AND NUMERICAL EVALUATION OF 3D PRINTING FILAMENT GEOMETRY

A manuscript to be submitted for presentation at the Annual Technical (ANTEC) conference of

the Society of Plastics Engineers (SPE)

Steven L. Devlin[a(1)], Alaa E. Elsisi[a], David Grewell[b]

[a]College of Engineering, University of Missouri, Columbia, MO

[b]Department of Agricultural and Biosystems Engineering, Iowa State University, Ames, IA

[(1)]Corresponding author, devlinsl@missouri.edu

## Abstract

Rapid Prototyping (RP) or Rapid Manufacturing (RM), sometimes referred to as Solid Freeform Fabrication (SFF) or Additive Manufacturing (AM), is a method of fabricating parts directly from three-dimensional computer aided design models, typically using a layering approach. This allows complex parts to be developed typically at low volumes and low production rates. In this research, an experimental study and numerical modeling were performed in order to investigate the effect of nozzle temperature and print head speed on the strength between filaments as well as the geometry of deposited material.

An extrusion-based 3D printing system, with the capacity to vary print speeds and temperatures, was used to fabricate the samples made from polylactic acid. Cross-sectioning and microscopic evaluation was performed to find the effect of the speed and the temperature on the geometry of part sample cross-sections. It was found that the experimental error was generally proportional to the print speed of the extrusion printing, and was mainly the result of varying total cross-sectional area. In addition it was found the strength between the deposited filaments

was generally proportional to print temperature. Non-Linear finite element based numerical modeling was performed to predict the strength of the samples. The geometry produced from sample cross sections and typical PLA material properties were used to create the model. The finite element model was able to predict the size of filament geometry in the tested samples at different speeds and temperatures.

## Introduction

A newly revived manufacturing technique aptly named "3D printing" is becoming a popular method of manufacturing and prototyping. This additive manufacturing method has many benefits including being able to use a wide range of inexpensive readily available materials, the ability to produce complex geometries, reduce design iteration times, simple computer-aided design interface, and ease of use. One of the main drawbacks of this method is that the machine builds parts in layers, which create non-uniform part lines that are effectively shear planes, that can result in high stress concentration points and unless fully bonded can serve as failure points along the layered filaments.

Fused filament fabrication (FFF) has become one of the most important tools in custom part fabrication [1]. Although there are numerous advantages to this technique including:

- Ease of use

- Flexibility, and

- Cost as compared to other AM technologies as well as with traditional manufacturing methods

However, improving the strength, reliability, and repeatability of printed parts to the same quality of traditionally manufactured parts, remains a challenge [2]. One of the most common

printing materials used by FFF printers is the semi-crystalline thermoplastic polymer poly-lactic acid (PLA) [3], which is a biobased plastic.

In the FFF process, the feedstock material is a wire or monofilament often packaged in a cartridge, which is entered to the printing head where the ABS, PLA or other material is plasticized and is pressed through a nozzle to the build platform. The nozzle moves to produce a profile of the part. After one layer is fully "printed", the platform translates down and the next layer is built on top of the previous layer until the entire model is fully built. The key to ensuring the strength of the final printed part is successful inter-diffusion and re-entanglement of the polymer across the extruded filaments and layer-layer interfaces. In general, polymer-polymer joint strength is proportional to temperature and heating time at the interface or faying surface until the bulk material strength is reached [4-7]. In this paper it is assumed that weld strength is equal to the based material strength as the focus of this study was on the effect of filament-filament geometry.

Several molecular mechanisms are proposed to explain this interaction. Brown [8], Schnell [6], and others have suggested models built on De Gennes reputation function for polymer healing, where interpenetration depth is limited by the radius of gyration and determines the final joint strength [6,8-9]. Other studies identify the formation of surface bridges as being the key factor in breaking strength [10]. However, both methodologies are driven by the concept of polymer chain entanglements forming across the faying surface [11]. A number of interpenetration distance and entanglement formation studies adopt a simple proportionality relationship [10,12-14], while others propose a minimum interpenetration distance is necessary for an entanglement to form [8,15].

In fused filament fabrication polymer joining is fundamentally a thermally-dependent diffusion process [16], and inter-diffusion is limited as the extruded material rapidly cools towards its glass transition temperature where diffusion is inhibited [17]. Yang and Pitchmani proposed an inter-diffusion model for polymers under non-isothermal conditions by allowing for a varying temperature dependence [7]. Because variable thermal histories, predicted interfacial strength differs from predicted healing under static conditions. Other studies suggest, polymer microstructure alignment, resulting from high shear rates at the extrusion nozzle, may affect the diffusive behavior at the filament or layer line and cause de-bonding [18]. McIlroy and Olmsted, recently studied this deformation using a molecularly-aware model for a non-crystalline polymer melts, suggesting "interdiffusion" in FFF, "does not necessarily occur from an equilibrium state" [19].

In this paper, an experimental study, microscopic analysis, and finite element modeling were performed in order to investigate the effect of nozzle temperature and print head speed on the strength between the Ingeo PLA 4043D filaments. An extrusion-based 3D printer (Prusa i3) was used to print one layer samples at different combinations of speeds and temperature. It was found that increasing extrusion temperature and printing head speed leads to increases in strength and size of filament-filament geometry and that temperature has the most significant effect. The finite element model was able to predict the breaking strength and confirms that lower extrusion temperatures demonstrate sharper edges between filaments increasing stress concentrations and leading to failure at lower loads.

## Experimental Work

A total of 140 samples were manufactured by using Prusa i3 FFF machine. PLA 4043D is a biopolymer, with a plasticizing temperature range of 145–160 °C and a glass transition (Tg) of 55 – 60 °C. The density is 1.24 g/cm3, and bulk tensile strength is about 110 MPa. The objective of this study was to quantify the bonded filament strength of Ingeo 1.75mm 4043D PLA filaments and to determine the effect of the nozzle temperature or print head speed on the strength between the deposited filaments.  Single layer coupons were produced and tensile tested with temperatures varying the extrusion head by 5 degrees from 195° C to 225°C and print head speeds varying by 5mm/s from 10mm/s to 25mm/s. To keep the samples as uniform as possible the same machine, nozzle and machine setup was used.

"Dogbone" specimens were printed for mechanical testing to investigate mechanical properties. The dimensions for the PLA dog-bone specimens followed the testing Standard ASTM D638 (see Figure 1 and Table 1).
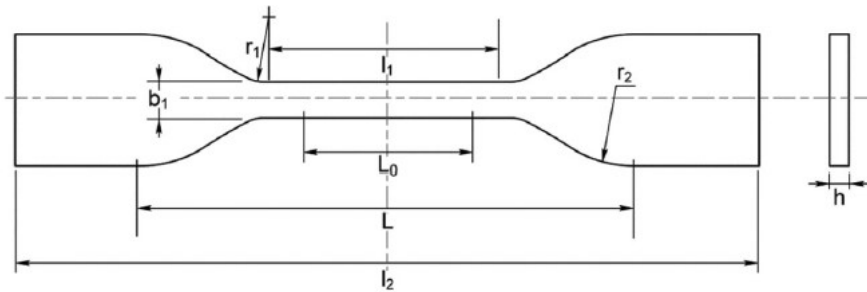


Figure 1: Sketch for the dog-bone specimen.

Table 1 Dimensions for PLA dog-bone specimen (corresponding to Fig. 1)

| Dimension (mm) | Value |
|---|---|
| Overall length, minimum (I2) | 75 |
| Length of narrow parallel-sided portion (I1) | 25 |
| Width of narrow parallel-sided portion (b1) | 4 |
| Small radius (r1) | 8 |
| Large radius (r2) | 12.5 |
| Initial distance between grips (L) | 50 |
| Gauge Length (Lo) | 20 |
| Thickness (h) | 0.4 mm |

Mechanical properties of the geometry between the PLA fibers were evaluated by uniaxial tensile testing on dog-bone samples at room temperature. An Admet machine (expert 2600, maximum load 10kN) was used for tensile testing. The crosshead speed of the loading member during all tests was 0.5 mm/min. Load-Displacement behavior was obtained to extract the maximum failure load. Five specimens were tested for each test condition, and the average value was used for drawing the different relationships. The cross sectional area were assumed to be constant of 0.4 mm x 4 mm. Table 2 summarizes the tested samples and the parameters that were selected.

Table 2: Different Parameters of the PLA Samples.

| Parameter | Values |
|---|---|
| Material | Ingeo Biopolymer 4043D |
| Thicknesses | 0.2, 0.4, 0.5 mm |
| Speeds | 10, 15, 20 and 25 mm/sec |
| Temperatures | 195, 200, 205, 210, 215, 220 and 225 ˚C |
| Geometry | ASTM D638 – 10 |

## Microscopic Analysis

In order to inspect the printed structure of the samples, a group of selected samples were cross-sectioned and microscopically examined. The objective was to characterize the effect of nozzle temperature and print head speed on the geometry of the filaments and bonded geometry between the filaments. The micrographs were performed for all treatment combinations using tested samples and some of the untested samples to show the effect of loading and plastic deformation, see Figure 2. By comparing printed part samples to machined samples from previous experiments, it was found that the use of any cutting tool, such as scalpel or rotary cutter, distort the cross-section of the samples, see Figure 3.
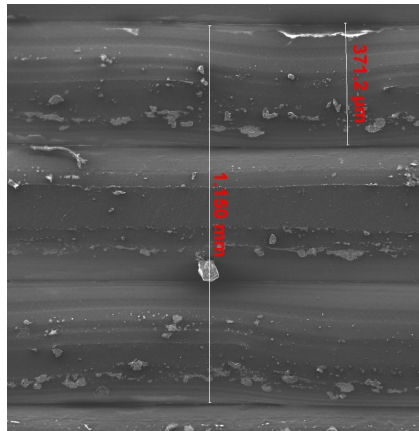


Figure 2: Electronic Microscope Picture Shows Fiber Alignment.
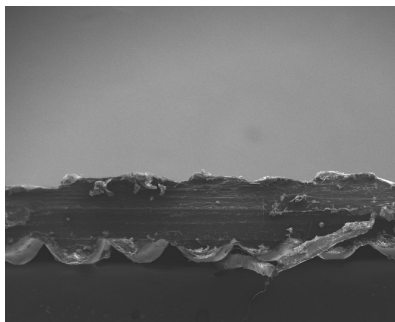


Figure 3: Cross-Section Deformation.

In order to avoid the distortion of the samples first, a piece of the printed PLA layer was mounted in a transparent epoxy media, see Figure 4. After the epoxy was hardened the mounted samples were ground in a direction perpendicular to the fibers.
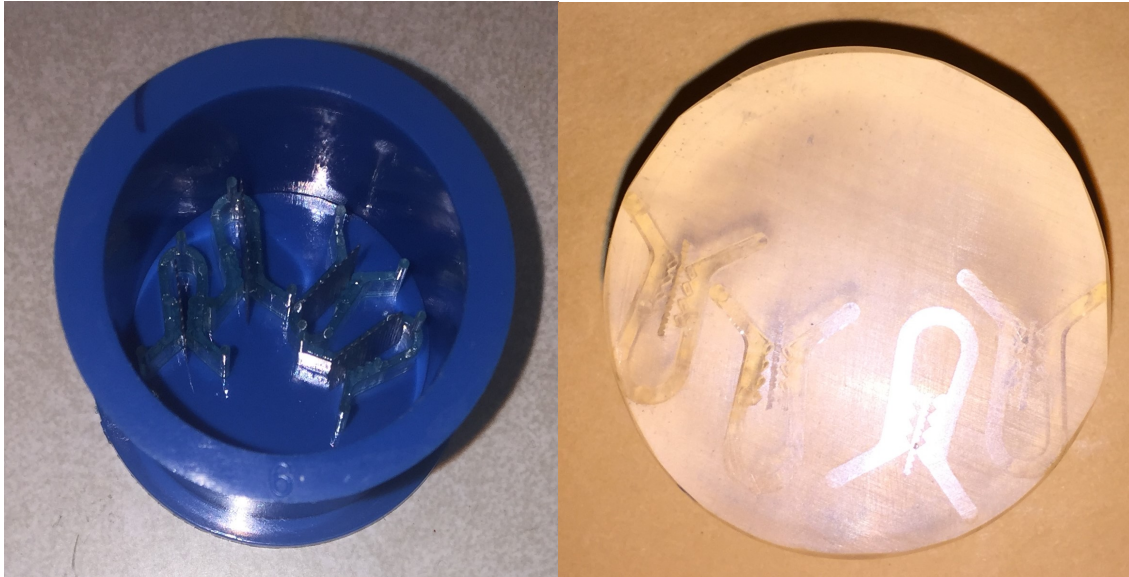


Figure 4: Mounting of the 3D Printed PLA Samples.

The hardened epoxy material which is stronger than the PLA constrained the cross-section edges and prevented deformation. Different sandpaper sizes were used beginning from the coarsest to the finest in order to produce the smoothest and clearest surface. The grinding process was continued until the effect of cutting tool disappeared completely.

An optical microscope with high-resolution digital camera was used to do the scanning of the cross-section. Microsoft Windows software, developed by the authors, was used to scale the pictures and produce CAD files. Figure 5 shows the micro-structure pictures with the borderline laid on it (for the case of the untested sample). While Figure 6 shows the pictures of the tested case. The basic section characteristics such as the area, maximum thickness, and minimum thickness were calculated for different speed and temperature treatments.
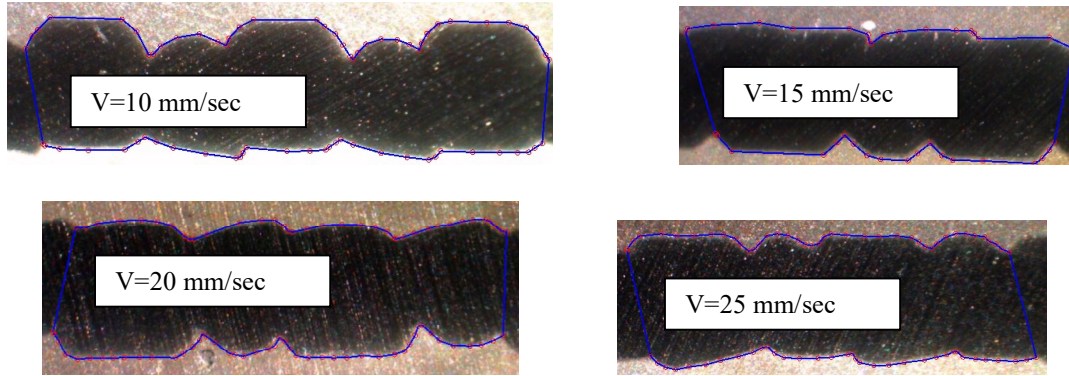
Figure 5: Micrographs of untested 3D Printed PLA Samples (T=210ºC).
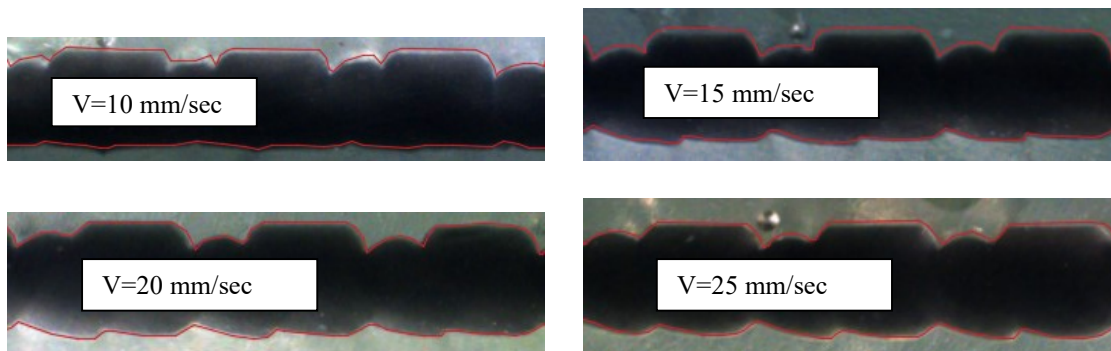


Figure 6: Micrographs of tested 3D Printed PLA Samples (T=210ºC).

The plastic deformation effects associated with tensile testing are displayed in Figure 7, with examples of tested and untested part samples. Figures 8 and 9, demonstrate the variable effects of print head velocity for high and low extrusion temperatures. Interestingly, at low temperatures, speed appears to have a greater effect on strength. This may be an effect of shear thinning taking place at higher printing velocities, alternatively it may be associated with the material feed rate control.
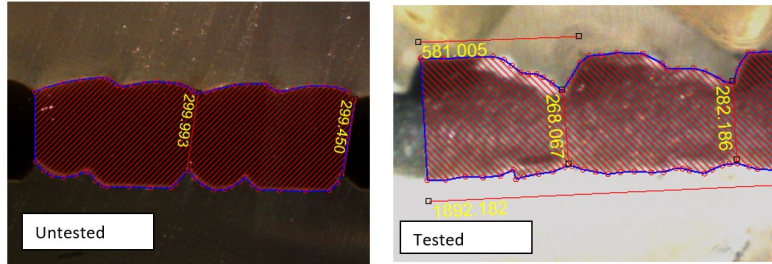
Figure 7: Plastic Deformation of Samples (195-25).
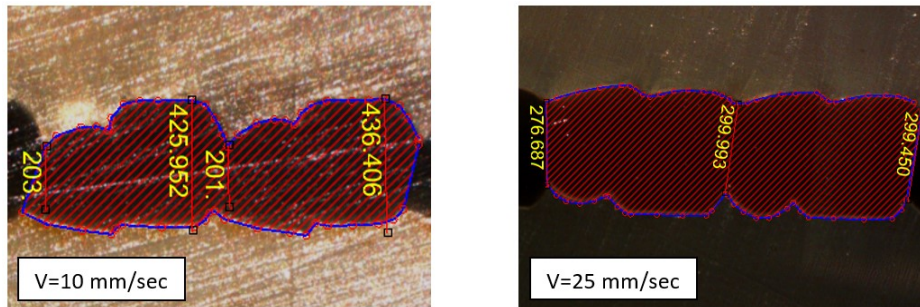


Figure 8: Effect of Printing Speed on Geometry Size at Low Temperature (T=195°C).
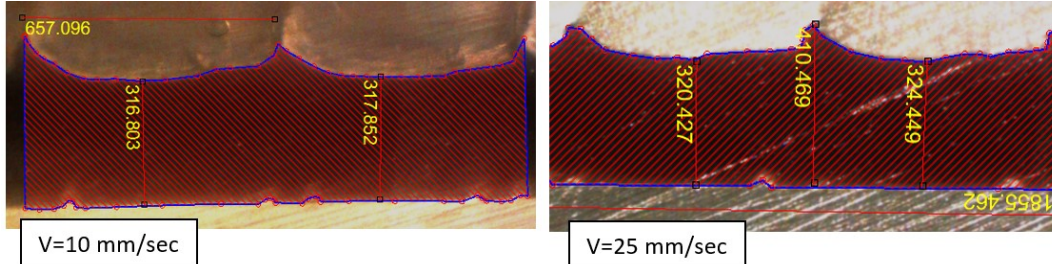


Figure 9: Effect of Printing Speed on Geometry Size at High Temperature (T=225°C).

## Numerical Modeling

In order to investigate the modes of failure of the 3D printing structure, find the locations of stress concentration and predict the failure loads a group of 3D FE models were developed. The non-linear finite element code ANSYS 18.0 [20], was used for simulating of the microstructure of the 3D printed plate. The geometry produced from the microscopic analysis in

the previous section was used to create the FE models. Each model consists of rectangle layer with a width of 1 mm and a length corresponding to at least 2 fibers. To allow for the complex geometries, the PLA plates were modeled by using ten nodes tetrahedral elements SOLID187. Figure 10 shows a sketch for the geometry, boundary conditions and loads. It is important to note that it was assumed the filaments were fully bonded and only geometric effects are considered.
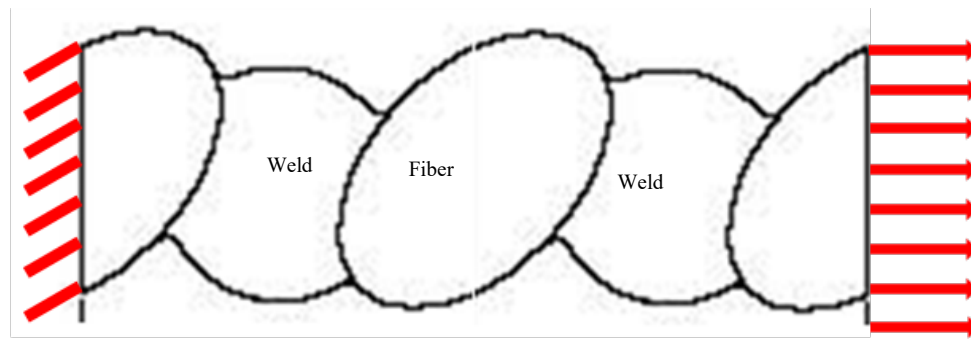


Figure 10: Schematic Diagram for The Microstructure and the Boundary Conditions.

The mechanical properties of the materials were taken from a technical report provided by the producer of the PLA material Biopolymer 4043D. Kinematic hardening plasticity model with Young's modulus of 2200 MPa, and Poisson's ratio of 0.36 and a yield stress (Fy) of 60 MPa was used. The tangent modulus of the second segment was taken 400 MPa. The boundary conditions are taken fixed supports at one end and the other end was restrained perpendicular to the loading direction. A pressure load was applied to the free end; the load was increased incrementally until the failure of the joints. In the elastic range, the stress concentration was monitored while in the plastic range the failure load and the plastic strain were calculated. Figure 11 shows the finite element mesh of the 3D model. In order to have accurate results a fine element with 10 μm edge length was used.
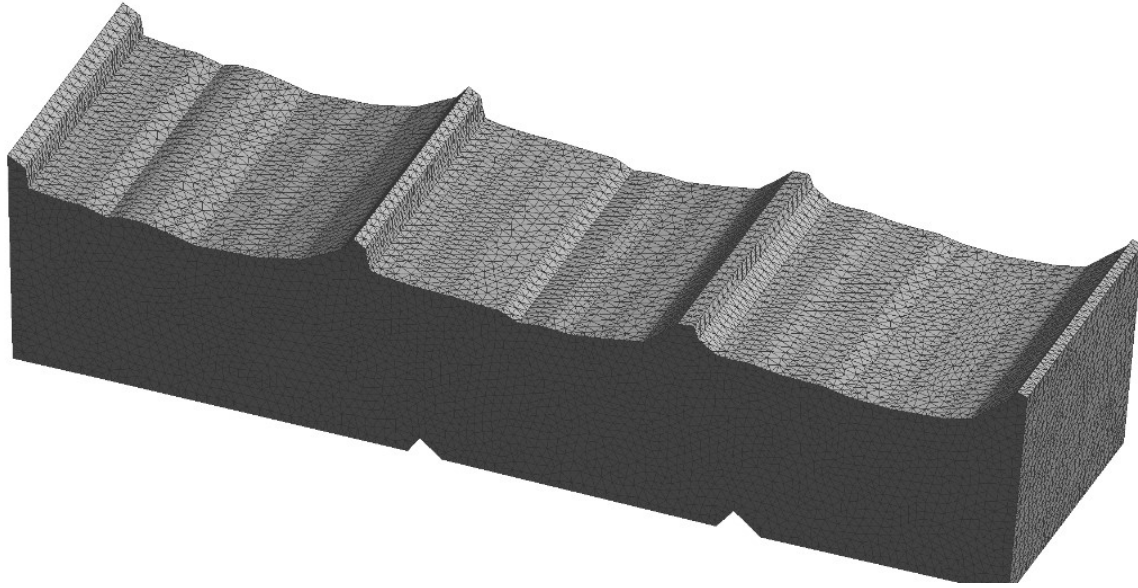
Figure 11: Finite Element Mesh of Real Structure of Case (V=25mm/sec, T=210°C).

**Results and Discussion**

In order to show the effect of different speeds, the relations between the temperature (T) and failure stress (σ) are seen in Figure 12. It can be observed that by increasing the temperature the theoretical strength increases. Again it is important to note, the interfaces between the filaments are assumed to be fully bonded (healed). It is seen that the predicted part strength is proportional to temperature. It is believed that at higher temperatures, the filaments flow more during and after extrusion reducing stress concentration points as well as promoting a wider bond area.
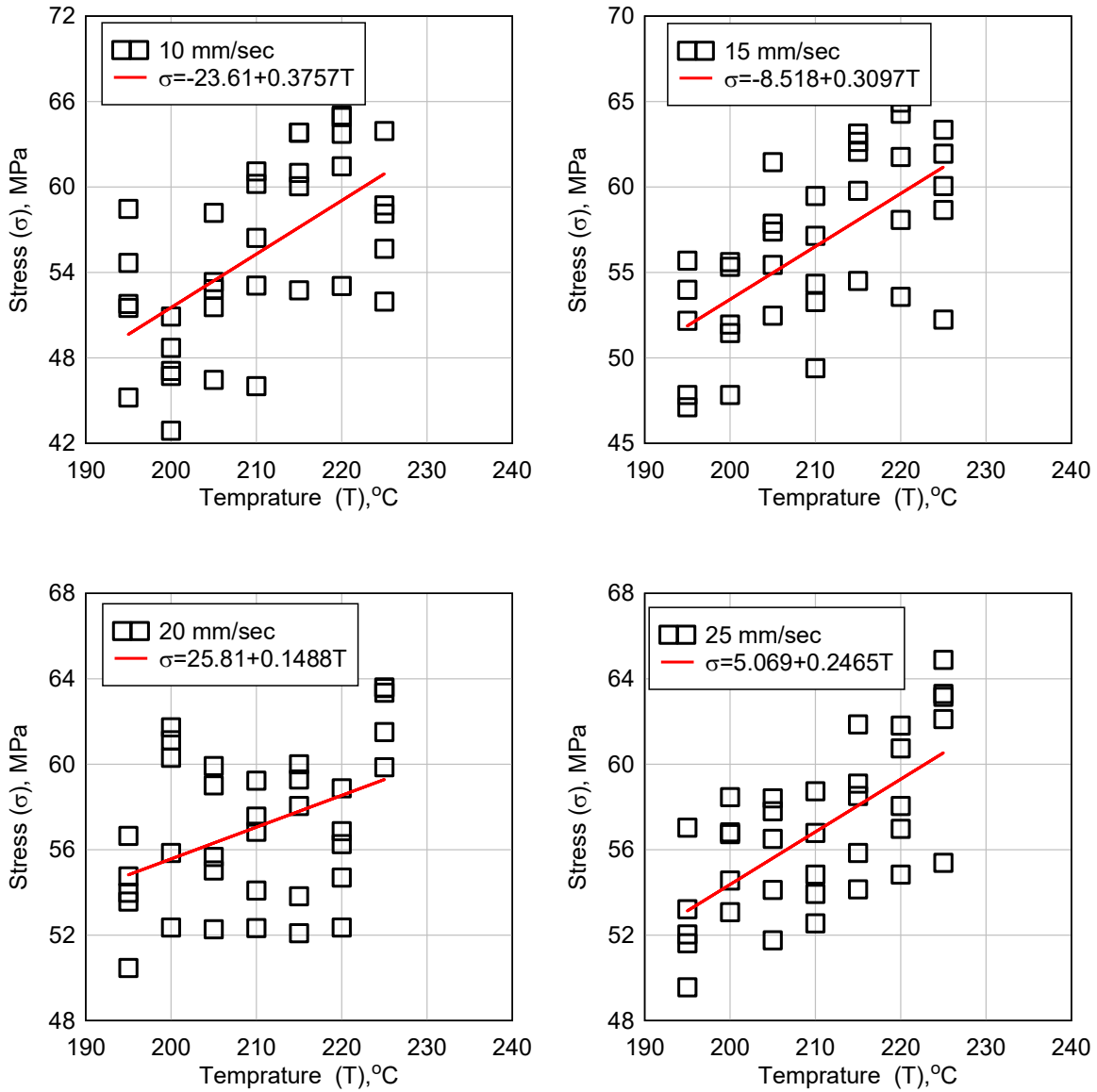
Figure 12: Effect of Temperature at Different Speeds

In order to show the effect of different speed, the relations between the speed and failure stress are seen in Figure 13 at different values of temperatures. It is seen that in general part strength is generally proportional to print speed. It is believed that at higher print speed the extruded material had higher levels of shear thinning, effectively reducing the effective viscosity.

This is in agreement with Figures 8 and 9, where higher cross sectional areas are seen at higher print speeds.
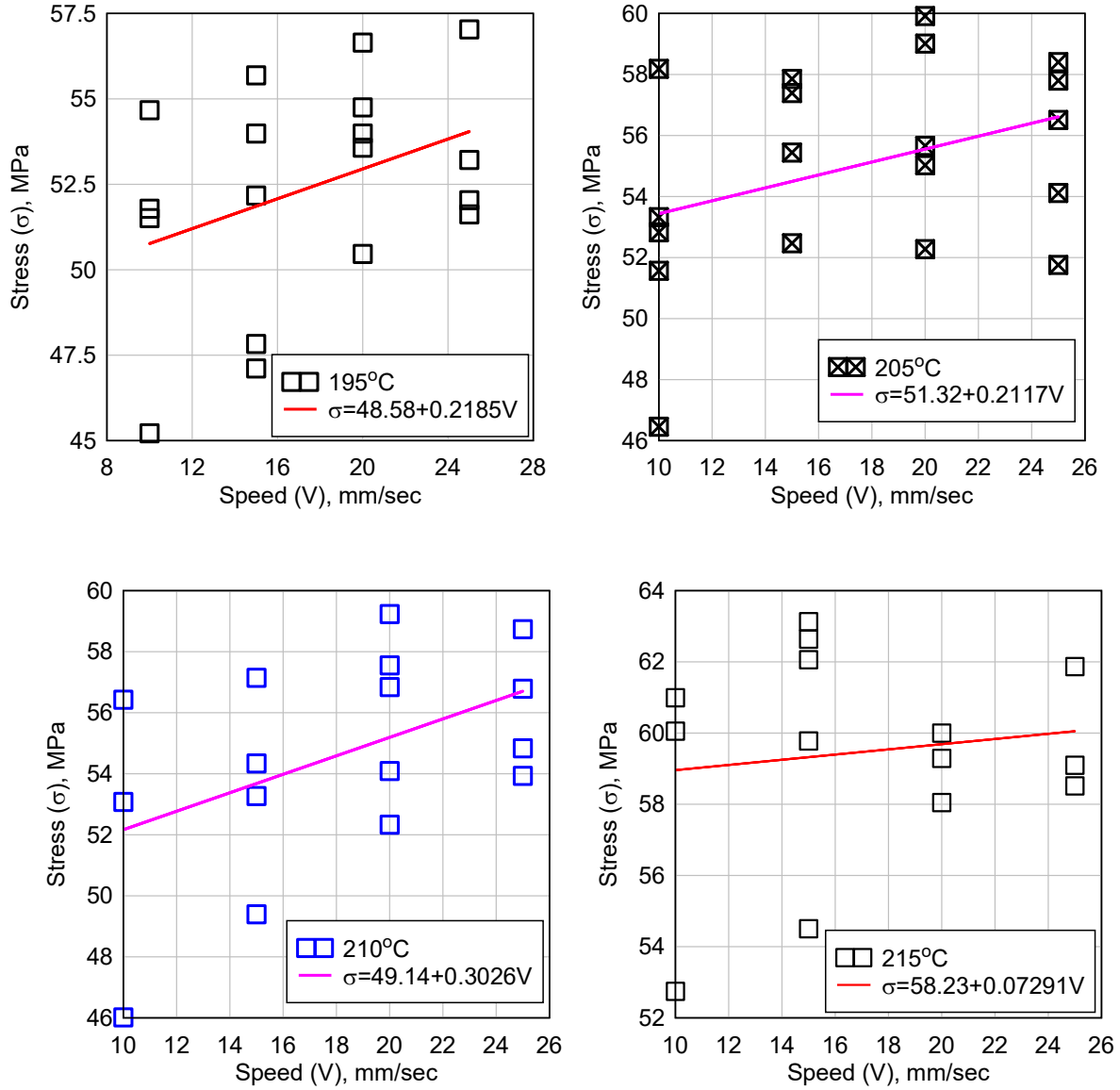


Figure 13: Effect of Speed at Different Temperatures.

Figure 14 shows the deformed shapes of the finite element model at maximum load of the case [T=195 ºC and V=10 mm/sec]. The average stress-strain curves of the models are shown in figure 15.  An approximate value for the strain was calculated by dividing the model

displacement by the model length. It can be found that the stress-strain relation is elastic until the

stress value of 17 MPa then the non-linear behavior starts and continues until failure.
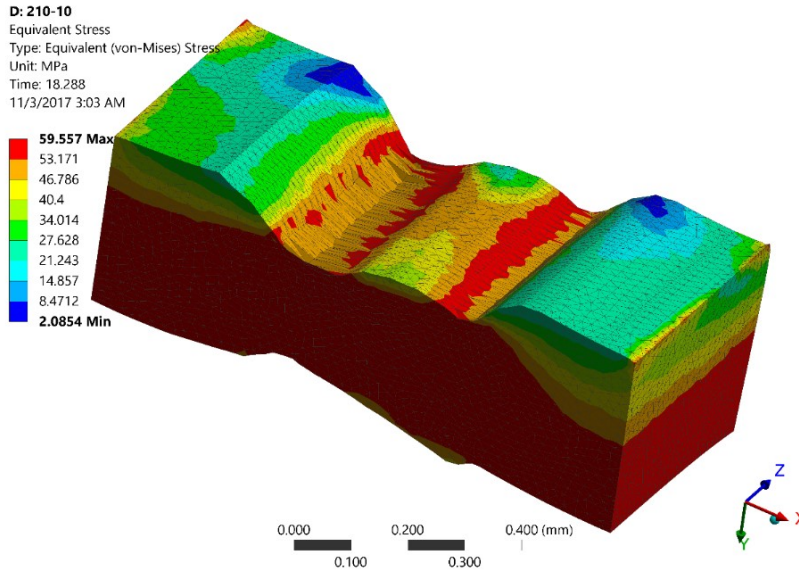


Figure 14: Deformed Shape of the Finite Element Model at Failure Load [ T=195 °C and V=10

mm/sec].
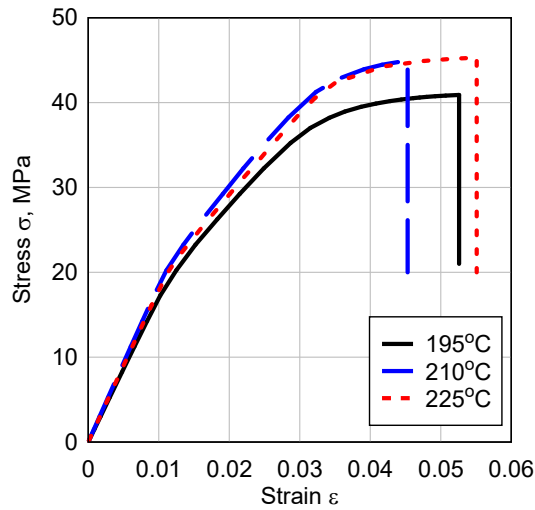


Figure 15: Stress-Strain Curves of Different Samples [ T=195 °C].

The stress concentration investigation is a very important step that can help to understand the causes of early failure. The irregularity of the cross-section prevents the samples from reaching the material failure stress and cause early failure. Figure 16 shows the elastic X direction stress distribution over the sample. It is observed that the corner locations (Geometry Boundaries) have a high-stress concentration. The value of the stress concentration factor ($K_c = \sigma_{applied}/\sigma_X$) is equal to 2.5, which can cause an early yielding at less than half the design loads. It is recommended to use a design factor of safety more than 2.5 for parts manufactured at low printing temperatures.
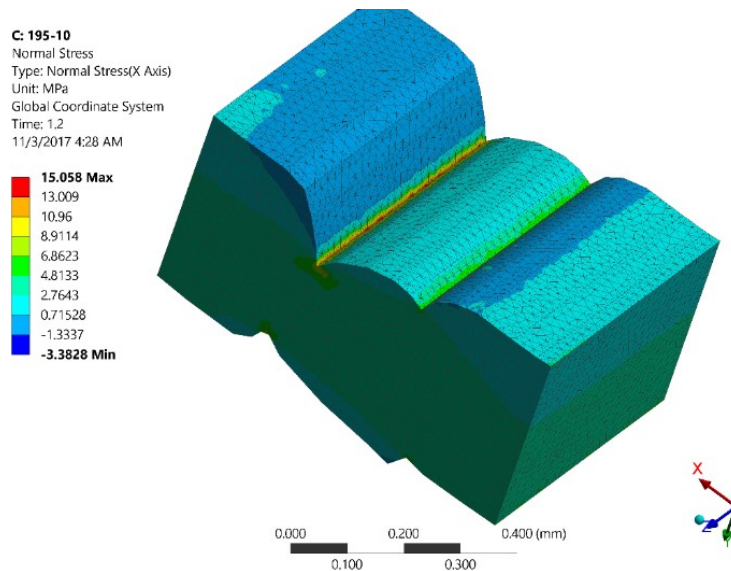


Figure 16: Elastic Normal Stress Distribution [ T=195 and V=10 mm/sec].

The values of $K_c$ for all the models are found in Figure 17a, it can be observed that by increasing the temperature the stress concentration value $K_c$ decreases. Figure 17b shows that load value at which the plastic strain begins to form. By increasing the temperature, the first plastic strain load increases, Figure 18 shows the distribution of plastic strain.
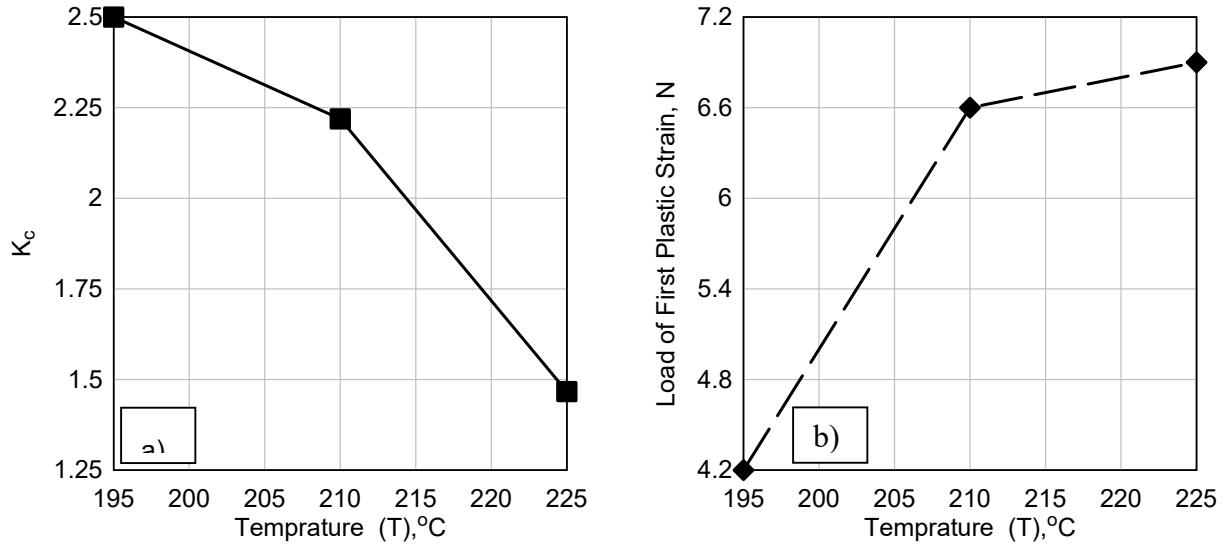
Figure 17: Damage Initiation Parameters a) Stress Concentration Value ($K_c$) and b) Plastic Strain Threshold.
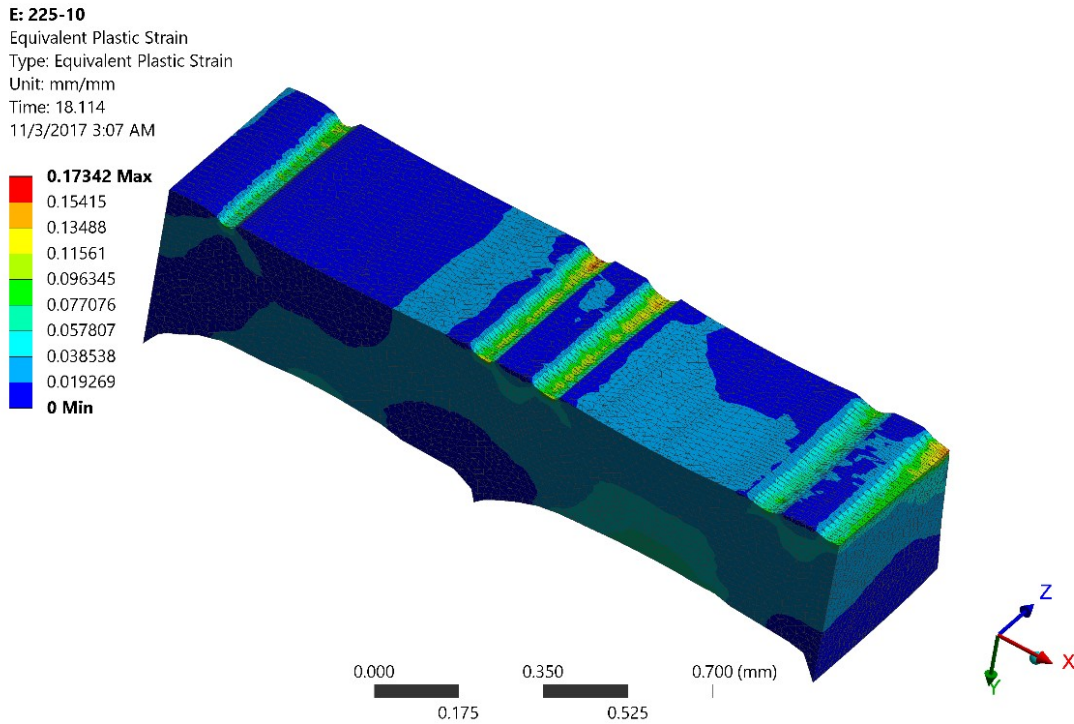


Figure 18: Equivalent Plastic Strain near the Failure.

## Conclusions

Final strength of parts fabricated using additive manufacturing methods are dependent upon the bonds between individual building blocks used to create the part. In fused filament fabrication, extruded beads of thermoplastic material are the basic building blocks and the welds between beads provide an estimate of final part strength. Extrusion temperatures, building environment, and thermal histories all play a factor in the bond between extruded beads. However, extruded bead geometry also plays a significant part in defining bead-to-bead bonds. Additional research is needed to develop extrusion build strategies that will reduce variability in extruded bead geometry and limit stress concentrations.

In this paper, an experimental study to investigate the effect of nozzle temperature and print head speed on the predicted strength of parts printed with Ingeo PLA 4043D filaments using an extrusion-based 3D printer (Prusa i3) system was performed. Microscopic analysis of tested and untested specimens were conducted in order to define the geometry of the printed filaments and to investigate the effect of printing parameters on the filament size and geometry. Increasing the temperature and the speed leads to an increase in part strength and size of the filament bond geometry and the temperature has the most significant effect. Finite element analysis of the printed bead geometry was performed to investigate the location of stress concentration and maximum plastic strain. It was observed that part strength was predicted to be generally proportional to print speed and temperature. It was also observed that increased print speed and temperature both promote wider and smoother geometries that reduce stress concentration points. The stress concentration exceeded 2.5 in some cases and it led to severe plastic strain in these locations.

**References**

1. Chua, C. K., Leong, K. F., & Lim, C. S. (2010). Rapid Prototyping: Principles and Applications. *Building*, 512. https://doi.org/978-981-277-898-7

2. N. Turner, B., Strong, R., & A. Gold, S. (2014). A review of melt extrusion additive manufacturing processes: I. Process design and modeling. *Rapid Prototyping Journal*, *20*(3), 192–204. https://doi.org/10.1108/RPJ-01-2013-0012

3. Drummer, D., Cifuentes-Cuéllar, S., & Rietzel, D. (2012). Suitability of PLA/TCP for fused deposition modeling. *Rapid Prototyping Journal*, *18*(6), 500–507. https://doi.org/10.1108/13552541211272045

4. Jud, K., Kausch, H. H., & Williams, J. G. (1981). Fracture mechanics studies of crack healing and welding of polymers. *Journal of Materials Science*, *16*(1), 204–210. https://doi.org/10.1007/BF00552073

5. Kline, D. B., & Wool, R. P. (1988). Polymer welding relations investigated by a lap shear joint method. *Polymer Engineering & Science*, *28*(1), 52–57. https://doi.org/10.1002/pen.760280109

6. Schnell, R., Stamm, M., & Creton, C. (1999). Mechanical properties of homopolymer interfaces: transition from simple pullout to crazing with increasing interfacial width. *Macromolecules*, *32*(10), 3420–3425. https://doi.org/10.1021/ma980860o

7. Yang, F., & Pitchumani, R. (2002). Healing of thermoplastic polymers at an interface under nonisothermal conditions. *Macromolecules*, *35*(8), 3213–3224. https://doi.org/10.1021/ma010858o

8. Brown, H. R. (2001). Relation between the width of an interface between two polymers and its toughness. *Macromolecules*, *34*(11), 3720–3724. https://doi.org/10.1021/ma991821v

9. De Gennes, P. G. (1981). The Formation of Polymer/Polymer Junctions. In J. M. B. T.-T. S. Georges (Ed.), *Microscopic Aspects of Adhesion and Lubrication* (Vol. 7, pp. 355–367). Elsevier. https://doi.org/https://doi.org/10.1016/S0167-8922(08)70894-0

10. Prager, S., & Tirrell, M. (1981). The healing process at polymer–polymer interfaces. *The Journal of Chemical Physics*, *75*(10), 5194–5198. https://doi.org/10.1063/1.441871

11. Ge, T., Pierce, F., Perahia, D., Grest, G. S., & Robbins, M. O. (2013). Molecular Dynamics Simulations of Polymer Welding: Strength from Interfacial Entanglements. *Phys. Rev. Lett.*, *110*(9), 98301. https://doi.org/10.1103/PhysRevLett.110.098301

12. Benkoski, J. J., Fredrickson, G. H., & Kramer, E. J. (2002). Model for the fracture energy of glassy polymer-polymer interfaces. *Journal of Polymer Science, Part B: Polymer Physics*, *40*(20), 2377–2386. https://doi.org/10.1002/polb.10288

13. Peppas, N. A. (1997). Polymer interfaces: Structure and strength. *Journal of Controlled Release*. https://doi.org/10.1016/S0168-3659(97)90025-0

14. Wool, R. P., & O'Connor, K. M. (1981). A theory of crack healing in polymers. *Journal of Applied Physics*, *52*(10), 5953–5963. https://doi.org/10.1063/1.328526

15. Adolf, D., Tirrell, M., & Prager, S. (1985). Molecular weight dependence of healing and brittle fracture in amorphous polymers above the entanglement molecular weight.

*Journal of Polymer Science: Polymer Physics Edition*, *23*(2), 413–427.
https://doi.org/10.1002/pol.1985.180230214

16. Sun, Q., Rizvi, G. M., Bellehumeur, C. T., & Gu, P. (2008). Effect of processing conditions on the bonding quality of FDM polymer filaments. *Rapid Prototyping Journal*, *14*(2), 72–80. https://doi.org/10.1108/13552540810862028

17. Seppala, J. E., & Migler, K. D. (2016). Infrared thermography of welding zones produced by polymer extrusion additive manufacturing. *Additive Manufacturing*, *12*, 71–76. https://doi.org/10.1016/j.addma.2016.06.007

18. Croccolo, D., De Agostinis, M., & Olmi, G. (2013). Experimental characterization and analytical modelling of the mechanical behaviour of fused deposition processed parts made of ABS-M30. *Computational Materials Science*, *79*, 506–518. https://doi.org/10.1016/j.commatsci.2013.06.041

19. McIlroy, C., & Olmsted, P. D. (2017). Deformation of an amorphous polymer during the fused-filament-fabrication method for additive manufacturing. *Journal of Rheology*, *61*(2), 379–397. https://doi.org/10.1122/1.4976839

20. Inc., A. (2012). *ANSYS Release 14.5 Documentation*.

# CHAPTER 6. A CLOSED FORM SOLUTION FOR PREDICTING FINAL PART STRENGTH OF FUSED DEPOSITION MODELING

Steven L. Devlin[a](1), David Grewell[b]

[a]College of Engineering, University of Missouri, Columbia, MO

[b]Department of Agricultural and Biosystems Engineering, Iowa State University, Ames, IA

(1)Corresponding author, devlinsl@missouri.edu

## Abstract

This article reviews the development of a molecular healing model coupling squeeze flow and intermolecular diffusion to predict final part strength of thermoplastic parts created using fused filament fabrication (FFF). Additive manufacturing (AM) is an innovative group of technology processes with the potential to help companies design products that meet specific customer requirements.  In this research, an experimental study and numerical modeling were developed and utilized to drive and validate a closed form heat transfer solution for FFF processes. Parts were printed from polylactic acid (PLA) at various temperatures and print speeds and tested for tensile strength.  These strengths were then used to validate the model. It was found that the coupled model was in good agreement with experimental values for a wide range of extrusion temperatures and higher head speeds.

**Introduction**

The ASTM International Committee F42 on Additive Manufacturing (AM) Technologies defines AM as the "process of joining materials to make objects from three-dimensional (3D) model data, usually layer by layer, as opposed to subtractive manufacturing methodologies" [1].

Fused Filament Fabrication (FFF) systems are extrusion-based technologies used to produce functional or near functional parts from a wide variety of plastic materials. First patented by S. Scott Crump and commercialized by Stratasys, Ltd in the early 1990s, this technology, like many additive manufacturing systems, offers significant opportunities for the design and production of complex part structures that are difficult if not impossible to produce using traditional manufacturing methods. However, part quality often limits use in final product commercial markets.

A number of studies have explored methods to improve the characteristics of FFF technology and the processes that influence them. Surface quality, dimensional accuracy and finished part strength directly relate to customer satisfaction, but are the result of highly complex interactions. Boschetto and Bottini classify some weaknesses of FFF, as either computer and/or mechanical aspects of the fabrication process: with "the former related to approximation involved in surface tessellation and virtual model slicing; the latter regarding positioning error and filament solidification problems" [2]. Surface quality, which subsequently affects dimensional accuracy of FFF parts, is highly dependent upon the tool paths used to deposit extruded material.

Parts fabricated using FFF typically have two separate tool paths within a sliced layer: a parallel path along the boundary of the layer typically referred to as the contour, and a series of

directionally parallel paths in the interior area of the layer called the fill. In standard build operations, the former can be altered to improve surface quality of the model and the latter is used to ensure a fast fabrication [3]. However, when attempting to build for part strength, operators often adjust road widths in an attempt to maximize interior fill rates.

Another area of additive manufacturing research focuses on surface quality, specifically as it results from the translation of curved surfaces and the stair-stepping effect of layer-by-layer fabrication. As with traditional manufacturing methods, greater detail and specialized approaches are needed to closely approximate complex curves. Adaptive slicing is a technique used in additive manufacturing to address this need, varying layer thickness in different sections to limit stair-step effects in critical areas [4]. This is especially relevant to the current research, as layer bond strength has been shown to vary with layer thickness. Therefore, having an accurate method for predicting part strength that can be adjusted for layer thickness is essential.

The FFF process has been described as being analogous to welding, where two pieces of a similar material are joined using a pool of molten (plasticized) material to heat and diffuse into the base creating a permanent bond as strong as or stronger than the base [5]. In thermoplastics, welding occurs when two polymer surfaces are brought together in a plasticized state allowing them to conform to each other and begin the intermolecular diffusion and polymer chain entanglement necessary for fusion bonding [6]. The degree of healing or welding being dependent on a number of factors including temperature, base material properties, time and interfacial pressure [7]. As in casting and molding processes, with FFF material temperatures above the polymer glass transition (Tg), the multi-stage healing process can occur, including surface rearrangement, surface approach, wetting, diffusion, and randomization [8].

## Interfacial Healing and Squeeze Flow

To understand the process of interfacial healing it is useful to separate the complex process into two fundamental mechanisms, squeeze flow and molecular diffusion. When two polymer faying surfaces are joined, a number of peaks and valleys must be displaced to allow the surfaces to come in full contact. During the welding process these peaks soften and deform to fill the gaps between surfaces [6]. As part of this research, the asperity deformation is initially modeled as an idealized squeeze flow of many small identical cylinders of molten material placed between two rigid plates separated by some distance 2h as described by Grewell [6] and seen in Figure 1.
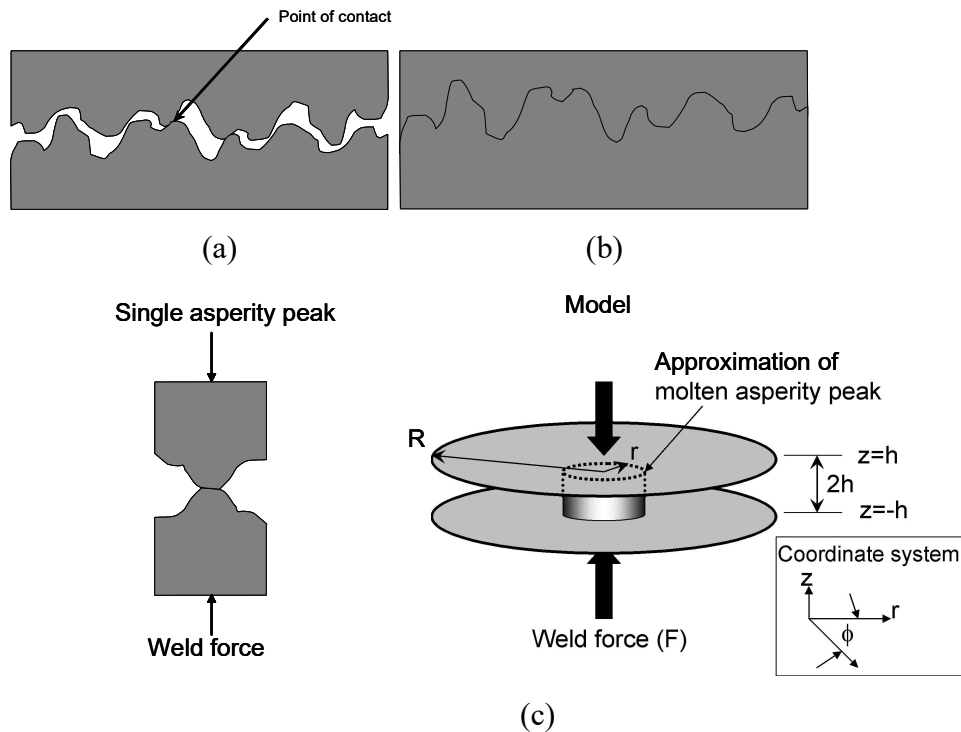


Figure 2. Cartoon of polymer interface with asperity peaks, (a) before welding (b) after welding and (c) idealized model

To further simplify the model, a single asperity peak is modeled, where the original height and radius are defined as $h_0$ and $r_0$, respectively and the final radius is defined as $r_{od}$. Assuming a Newtonian fluid with a viscosity ($\mu$) and other standard assumptions, Bird, et al., developed a similar model for a case where the volume between the gap is fully filled [9]. Independent of the gap being fully filled, they showed that the pressure (p) is defined as a function of time (t). By integrating that function over the asperity peak model, and by conversion of mass it is possible to define the time varying radius as a square root of $r_0{}^2 h_0/h$ and be substituted into the integration of the pressure function. With further integration relative to time we find the nondimensional asperity height defined in equation 1, which can be used to predict the closing of two faying surfaces as a function of time.

$$\frac{h_0}{h(t)} = \left( \frac{16\pi F h_0{}^2}{3\mu r_0{}^4} t - 1 \right)^{\frac{1}{4}} \quad \text{Eq. 1}$$

Interfacial healing occurs as the faying surfaces come into intimate contact. It is important to note, healing originates wherever connection occurs, even before the squeeze flow has deformed the asperity peaks and filled the surface gap. Therefore, squeeze flow and healing occur simultaneously [6]. Healing of the interfaces occurs through diffusion of polymer chains across the interface and entanglement with other polymer chains. Figure 2. displays the chain diffusion at various times and degrees of healing. Ideally, at complete healing, polymer chains from each side migrate across the interface so that it essentially becomes indistinguishable from the bulk material, in this case the degree of healing or degree of welding (DW), is 1 when the interface is fully healed.
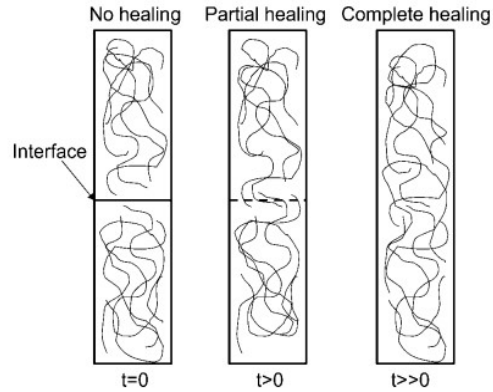
Figure 2. Molecular diffusion and interfacial healing [6]

Using reptation theory, the diffusion of polymer chains can be modeled as a function of molecular structure, molecular weight, chemical structure, and time and temperature [10]. Other factors, such as pressure, can also affect this process. In this model, each polymer chain is considered to be contained in an imaginary tube of length L. The tube is constrained by neighboring polymer chains and thus, the ends of the polymer chains have more freedom of movement compared to the bulk of the chain. The distance that a polymer chain moves outside the original tube is referred to as the diffusion distance $<l>^2$, and can be related to time as shown in Figure 3. In this case, the diffusion distance is noted as "$<l>$" is the mean square distance.



$$<l>^2 = 2D_c t$$
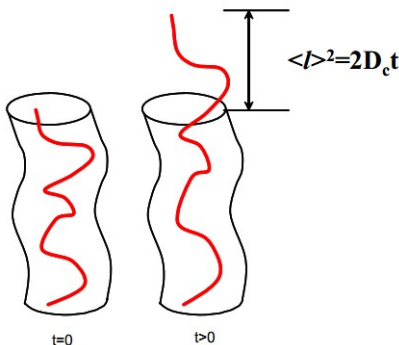
Figure 3. Single molecule motion [6]

It is possible to relate the mean diffusion distance squared ($<l>^2$) of any one chain near the interface to the distance that chain propagates across the interface (X) as shown in equation 2.

$$X \approx \sqrt{<l>^2}$$

Eq. 2

By using Einstein's diffusion equation and Eq. 1, where D is the diffusion coefficient, it is possible to show that healing time is related to time by a power of ¼, as shown in equation 3.

$$<l>^2 = 2Dt \Rightarrow l = \sqrt{2Dt} \Rightarrow X = (2Dt)^{\frac{1}{4}}$$
$$\therefore$$
$$X \sim t^{\frac{1}{4}}$$

Eq. 3

In addition, Jud, et al., proposed that the diffusion coefficient is an Arrhenius function of temperature ($T$) and it can be expressed as shown in equation 4 [11].

$$D(T) = D_0 e^{\left[\frac{-E_a}{RT}\right]}$$

Eq. 4

where $D_0$ is the diffusion constant, $E_a$ is the activation energy and k is the Boltzmann constant ($1.3807 \times 10^{-23}$ J/K). While many investigators have assumed that activation energy is temperature-independent, there is data in the open literature that suggest differently. For example, Loos and Dara, studied the healing of polysulphone and assumed an activation energy to be temperature-independent [12]. Grewell and Benatar, were able to estimate the activation energy by evaluating the relationship between plotted natural logs of the slopes of the various weld strength temperatures, as functions of the reciprocal of the temperatures, see Figure 4. [6] In this figure, the solid line is the slope assumed by Loos. While this estimate is reasonable,

Grewell and Benatar proposed a better fit is one that has a slope that is temperature-dependent (dashed line).
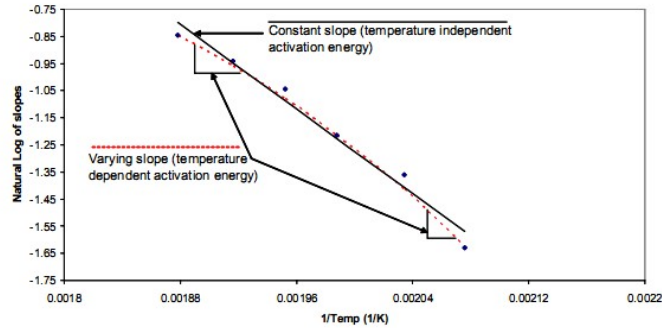


Figure 4. Plot of natural log of slopes as a function of inverse temperature [6]

Using a temperature-dependent model proposed by Grewell and Benatar provided more accurate predictions of interfacial healing [6]. Such a deviation from the classical model of a temperature independent activation energy, may be justified because their model lumps diffusion and squeeze together.

Because most industrial processes produce temperature histories that are time-dependent, then each duration at a given temperature contributes incrementally to healing until the interface is fully healed. For a continuously varying temperature it is possible to divide a given temperature history into finite time intervals ($\Delta t$) [6]. Thus it is possible that the degree of welding (DW), which combines squeeze flow and healing, can be defined as:

$$DW(T,t)_h = \sum_{t=0}^{t=t'} K_0 \cdot e^{-\frac{E_a}{kT}} \cdot \Delta t^{1/4}$$

Eq. 5

Which is graphically depicted in Figure 5.
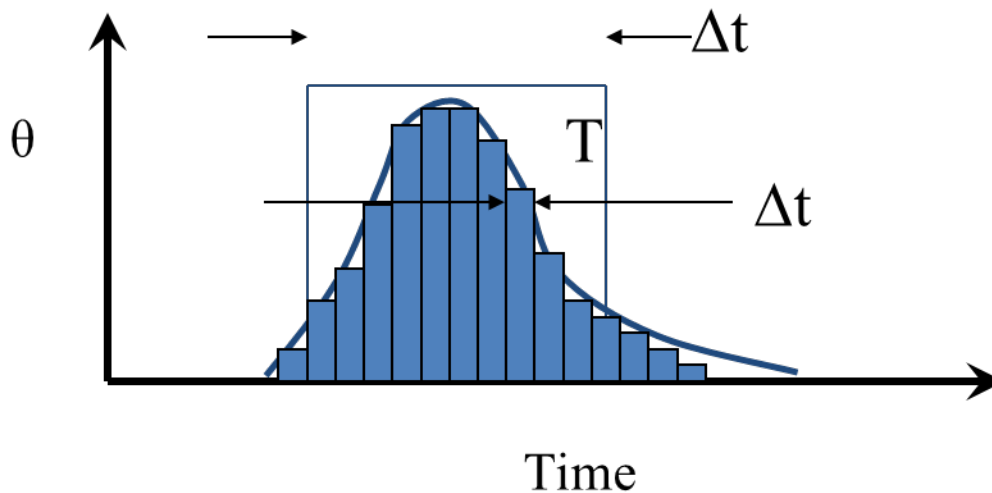
Figure 5. Graphical illustration of adhesion with varying temperature history

**Energy Flow Model**

In order to predict the temperature in the extruded filament, a model based on 1$^{st}$ order principles

was used. The variables include:

$\rho$   Material density of the filament
$\lambda$   Thermal conductivity of the filament material
C   Heat capacity of the filament material
H   Heat loss coefficient through convection between the filament and the surrounding air
$\theta_d$   Temperature of the die
$\theta_{air}$ Temperature of the air surrounding the filament
V   The speed of the filament extrusion

The assumption of the model were:

- Constant material properties
- Homogeneous material
- No phase change
- Constant velocity
- Heat loss only through convection
- Assume constant coefficient of heat loss
- Assume rod is uniform temperature in r-direction ( $\frac{\partial \theta}{\partial r} = 0$)
- No internal heat loss/generation (Q=0)
- Steady state condition($\frac{\partial \theta}{\partial t} = 0$)
- Fully developed system

The model is seen in Figure 6, where $q_r{}^h$ is the heat flux for the convection heat transfer (to the air) in the r-direction, $q_x{}^{cv}$ is the heat flux of the convection heat transfer (material movement) in the x-direction. The origin of the two dimensional coordinate system (x, r) are at the opening of the die and in the center of the die. A small volume with a dimension in the x-direction of $d_x$ is considered. Thus the heat flux entering the are detonated as $q_x$ and the heat fluxes at exiting the element are at $d_{x+dx}$ .
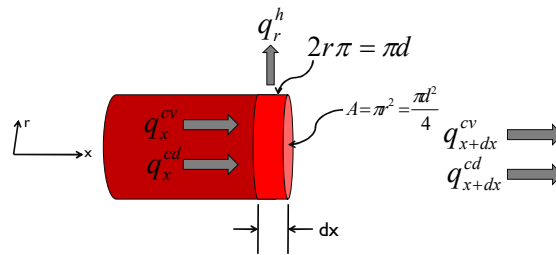


Figure 6. General model for filament extrusion

In order to simplify the model by reducing the number of independent parameters, a coordinate system fixed at the opening is defined and the system is assumed to be fully developed. This allows the time derivates to be set to zero. The circumferential surface area of the element (A) is $\pi d^2$ and the cross-sectional surface area of the element is $\frac{\pi d^2}{4}$. By using traditional assumptions and boundary conditions it is possible to derive a solution of the governing equations in the form seen in Eq. 5, that allows the temperature of an extruded filament to be modeled as a function of x.

$$\theta'(x) = \theta_d \exp\left( \frac{\dfrac{V}{\kappa} - \sqrt{\left(\dfrac{V}{\kappa}\right)^2 + 4\left(\dfrac{4h}{d\lambda}\right)}}{2} \right) x$$

Eq. 5

This solution can then be simplified into a time domain or absolute temperature by further substituting in the constitutive relations.

**Experimental Procedures – Fused Filament Extrusion**

Based on pre-experimental evaluation (screening experiments), it was decided single layer test specimens (Figure 5) would be fabricated and used for testing. Extruded filaments were oriented perpendicular to the axis of force to isolate bond strength. Possible parameter ranges were identified for both extrusion temperature (PLA @ 195° - 225° C) and printer head-speed (10 – 25 MM/Sec) using a PLA thermoplastic material. A full factorial experimental design was developed for 28 treatment combinations. The experimental fabrication runs were randomized and replicated five times for each velocity-temperature combination. Four PLA experiments were completed, two fabricated on a MakerBot 2X printer (2016 Exp. 1&2), and two on a Prusa i3 printer (2017 Exp. 3&4) as seen in figure 6.
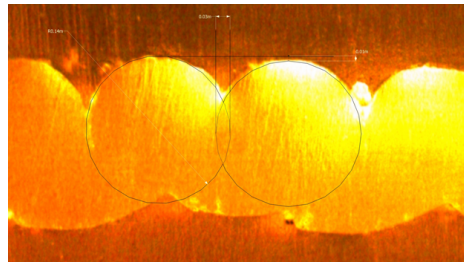


Figure 5. Single Layer PLA Test Specimen
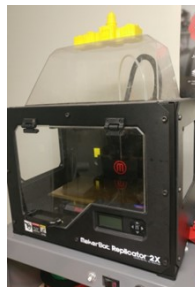


Figure 6. MakerBot 2X

Experiments 1, 2, and 3 were printed using a 0.40 mm layer height, and run 4 was printed using a 0.2 mm layer height. Samples fabricated on MakerBot 2X, were printed using a 0.4 mm extruder nozzle and a 10% overlap setting. It is important to note the MakerBot build platform was not heated and polyimide film applied to the build plate was used to facilitate easy part removal. Samples fabricated on the Prusa i3 printer also used a 0.4 mm extruder nozzle, however, the overlap setting was increased to 20% and the heated build platform was set to 60˚ C. In addition, samples produced on the MakerBot were subsequently machined into ASTM equivalent specimens (dog bones) using a proprietary jig fixture and rotary cutting tool. Samples produced using the Prusa i3 were printed directly into the ASTM equivalent shape.

Specimens were tested for ultimate breaking strength and elongation using an Admet machine (expert 2600, maximum load 10kN). The crosshead speed of the loading member during all tests was 0.5 mm/min. Load-Displacement behavior was obtained to extract the maximum failure load. Elongation values were insignificant and were not recorded.

Model

To predict the part strength, MathCad 14 was used. The temperature fields were predicted based on the steady state solution ($\frac{\partial \theta}{\partial t} = 0$) and redefined into a time domain. The model variables were defined as:

- $\rho$   Material density of the filament
- $\lambda$   Thermal conductivity of the filament material
- C   Heat capacity of the filament material
- H   Heat loss coefficient through convection between the filament and the surrounding air
- $\theta_d$   Temperature of the die
- $\theta_{air}$   Temperature of the air surrounding the filament
- V   The speed of the filament extrusion

The temperature as afunction of time was then incremented in 50 millisecond ($\Delta t$) intervals and again MathCad 14 was used to complete the summation of the discrete degree of welding. This was completed for all of the experimental printing temperatures and speeds. In all cases the degree of welding was truncated to a strength of 1, because it was assumed achieving base material strength is the highest achievable strength. In addition, the dimensionless degree of welding was multiplied by the highest experimental strength (62.5 MPa) to result in absolute strength (MPa).

## Results and Discussion

Frequency histograms and descriptive statistics were calculated for each experimental run, Least-Squares Regressions and series scatter charts (Figure 7) were developed for both changes in speed within individual temperatures, as well as for changes in temperature within head speeds to determine if the data would accurately represent the predicted values. Based on evaluation of the summary statistics, least-squares regressions, and preliminary results of the predictive thermal model it is postulated, changes in extrusion head velocity play a minimal role in the healing process. However, further investigation will be needed to accurately provide an answer, recent literature indicates head speeds of up to 150 mm/sec are possible with some machines.
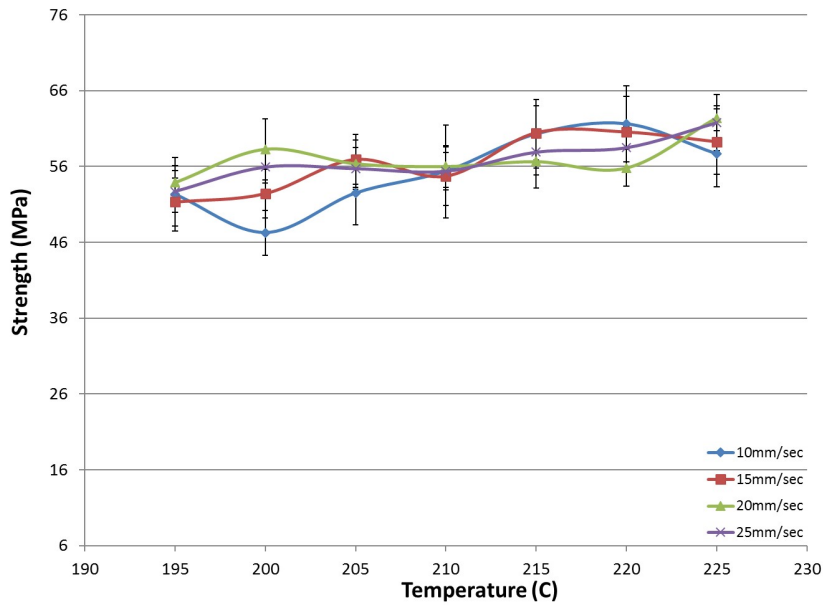
Figure 7. 2017 PLA Strength by Temperature (PLA 0.4 mm (2017))

Single factor ANOVA were created to further understand the influence of extrusion

temperature on the healing process for PLA experimental data.

Table 1. Single-Factor ANOVA

| ANOVA Single Factor 2017 PLA 10 mm/sec | | | | | | |
|---|---|---|---|---|---|---|
| *Source of Variation* | *SS* | *df* | *MS* | *F* | *P-value* | *F crit* |
| Between Groups | 760.3326 | 6 | 126.72 | 5.82 | 0.00 | 2.45 |
| Within Groups | 610.0702 | 28 | 21.79 | | | |
| | | | | | | |
| Total | 1370.403 | 34 | | | | |
| ANOVA Single Factor 2017 PLA 15 mm/sec | | | | | | |
| *Source of Variation* | *SS* | *df* | *MS* | *F* | *P-value* | *F crit* |
| Between Groups | 427.2508 | 6 | 71.208 | 4.810 | 0.002 | 2.445 |
| Within Groups | 414.493 | 28 | 14.803 | | | |
| | | | | | | |
| Total | 841.7438 | 34 | | | | |
| ANOVA Single Factor 2017 PLA  20 mm/sec | | | | | | |
| *Source of Variation* | *SS* | *df* | *MS* | *F* | *P-value* | *F crit* |
| Between Groups | 215.6081 | 6 | 35.935 | 4.223 | 0.004 | 2.445 |
| Within Groups | 238.2565 | 28 | 8.509 | | | |
| | | | | | | |
| Total | 453.8646 | 34 | | | | |
| ANOVA Single Factor 2017 PLA 25 mm/sec | | | | | | |
| *Source of Variation* | *SS* | *df* | *MS* | *F* | *P-value* | *F crit* |
| Between Groups | 247.747 | 6 | 41.291 | 5.137 | 0.001 | 2.445 |
| Within Groups | 225.0641 | 28 | 8.038 | | | |
| | | | | | | |
| Total | 472.8111 | 34 | | | | |

## Model validation

Utilizing the general model for filament extrusion and temperature histories, the degree

of weld was calculated for each of the PLA runs and plotted against the experimental data. In

figure 8 the experimental data is plotted as filled points with error bars and the predicted values

are plotted as a line graph (Figure 8). It is seen that the model is in good agreement with the

experimental values for a wide range of extrusion temperatures and higher head speeds. As

previously discussed, issues with 10 mm/sec velocity experiments may be a result of the head

speed test range being limited, recent literature indicates significantly higher velocities are

standard for newer FFF machines. However, in general it is unlikely that increased speed will

have any significant effect on weld strength given the relatively small cross-section of the

extruded filament. Comparing the cooling rates as a function of time, as seen in Figure 9, an

order of magnitude change in speed has little effect.
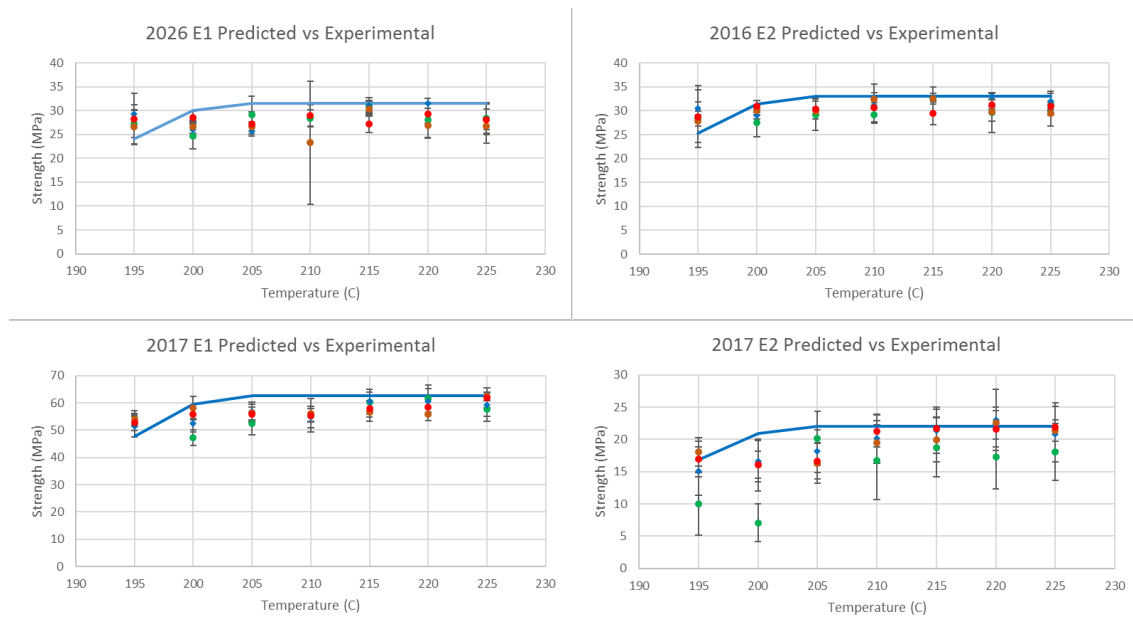


Figure 8. PLA Predicted Weld Strength vs Experimental
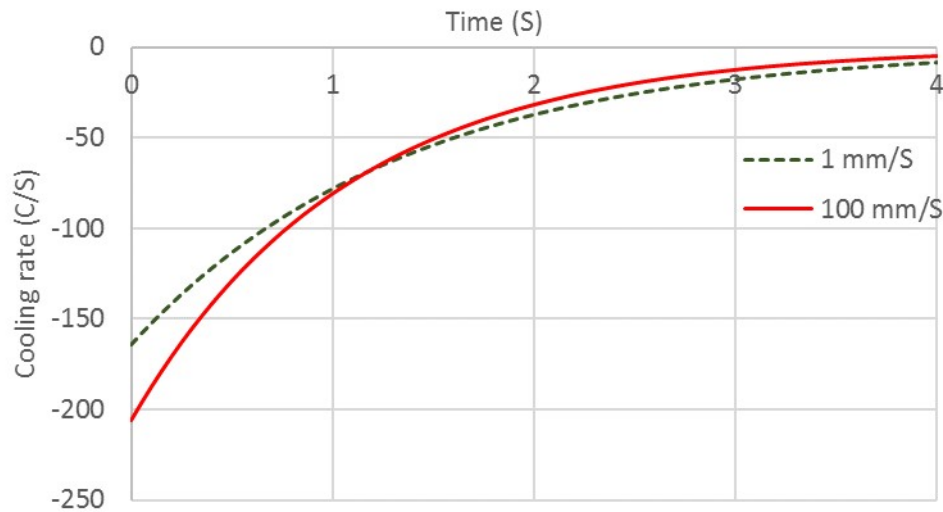
Figure 9. Cooling Rate vs Time

**Conclusions**

Additive manufacturing provides a number of opportunities to improve engineering design and increase customer satisfaction. Understanding strength of materials is a critical factor influencing adoption of a developing manufacturing technology. In fused filament fabrication, the bond or weld between beads of extruded thermoplastic material represent the basic elements of final part strength.

In this article, it was shown that the degree of welding between two faying surfaces produced by fused filament fabrication is best modeled with a combined squeeze flow and intermolecular diffusion model. This model can be utilized for a wide range of extrusion temperatures and print head speeds. The model can predict the degree of healing based on temperature histories. While additional research will be needed to fine-tune and expand the predictive model, comparison with available experimental data indicate favorable results, with predicted values slightly higher than tested parts for all but the lowest print head velocities.

Of the factors evaluated in this study, extrusion temperature appears to have the most significant effect on final degree of weld, with experimental and predicted values leveling off between 215 and 225 ℃. Over all, increasing print head velocity does not appear to have a significant effect on weld strength given the relatively small cross-section of the extruded filament. However, at lower extrusion temperatures there does appear to be some relationship between faster speeds and improved weld strength. This may be a result of increased shear thinning at lower temperatures.

## References

1. ASTM and ISO unveil plans to create global AM standards. (2017). Metal Powder Report, 72(1), 63-64.

2. Boschetto, A. & L. Bottini, (2014). Accuracy prediction in fused deposition modeling. International Journal of Advanced Manufacturing Technology, (2014) 73:913-928, DOI 10.1007/s00170-014-5886-4.

3. Jin, Y.A., Y. He, & J. Fu, (2013). An adaptive tool path generation for fused deposition modeling. Advanced Materials Research Vol. 819, pp 7-12, Trans Tech Publications, Switzerland, DOI 10.4028/www.scientific.net/AMR.819.7.

4. Ziemian, C.W. & P.M. Crawn, (2001). Computer aided decision support for fused deposition modeling. Rapid Prototyping Journal, 7(3), 138-147. Retrieved from http://search.proquest.com/docview/214011430?accountid=14576.

5. Amberg, G., & M. Do-Quang, (2007). Thermocapillary convection and phase change in welding. International Journal of Numerical Methods for Heat & Fluid Flow, Vol. 18 No. 3/4, pp. 378-386, DOI: 10:1108/09615530810853637.

6. Grewell D., & A. Benatar, (2008). "Semi-empirical, squeeze flow and intermolecular diffusion model. I. Determination of model parameters. Polymer Engineering and Science, Vol. 48, Issue 5, pp 860-867.

7. Wool, R.P., (1995). Polymer interfaces: structure and strength. Hanser, Munich, Germany, ISBN 1569901333.

8. Vogel, J., M. Kessler, S. Sundararajan, & D. Grewell, (2012). Activation energy for diffusion and welding of PLA films. Polymer Engineering and Science, Vol. 52 (8), pp. 1693-1700, DOI: http://dx.doi.org/10.1002/pen.23120.

9. Bird R., R. Armstrong, & O. Hassager, (1987). Dynamics of polymer liquids. 2nd ed., Wiley, New York, Vol. 1, 20.

10. DeGennes P.G., (1971). Reptation of a polymer chain in the presence of fixed obstacles. Journal of Chemical Physics, Vol. 55, Issue 2, pp. 572. DOI: http://dx.doi.org/10.1063/1.1675789.

11. Jud, K., H.H. Kausch, & J.G. Williams, (1981). Fracture mechanics studies of crack healing and welding of polymers. Journal of Materials Science, Vol. 16, Issue 1, pp. 204-210.

12. Loos, A.C. & P.H. Dara, (1985). Thermoplastic matrix composites processing model. Interim Report 57, NASE Cooperative Agreement NAG-1-343, Document ID 19860012148.

# CHAPTER 7. GENERAL REVIEW OF CONCLUSIONS AND RECOMENDATIONS

## General Review of Conclusions

The overriding goal of this study was to evaluate the application of a combined squeeze flow and intermolecular diffusion model to predict thermoplastic weld strength in FFF part samples as a function of the extrusion temperature and print-head velocity. Broadly, the research questions guiding this project included:

1. What is the acceptable range of extrusion head temperatures available for producing parts in ABS and PLA using fused deposition modeling?

2. What are the acceptable limits of extrusion head velocity available for producing parts in ABS and PLA using fused deposition modeling?

3. What combinations of speed and temperature can be used to increase final part strength?

4. What is the effect on part strength of extruded road geometry?

5. Is it possible to predict FDM part strength using a closed form mathematical formula for different additive manufacturing materials?

This research presented three primary areas of investigation. Development and documentation of a sample fabrication and testing method for weld strength, as seen in chapters three and four. Investigation and numerical modeling of the extruded bead geometry documented in chapter five. Finally, development and analysis of a predictive model for part strength based on squeeze flow and intermolecular healing as presented in chapter six.

Based on the experimental trials, it is possible to fabricate, post process, and test fused filament fabrication specimens for tensile strength. Using a single layer specimen, investigators were able to isolate part strength related to bonds between extruded filaments for a range of temperature and head speed combinations. The resulting data set provided a suitable benchmark

for comparison with predictive models for FFF part strength. However, it should be noted a number of tested samples failed to perform, suggesting there are other factors effecting the part strength.

Extrusion temperatures, building environment, and thermal histories all play a factor in the bond between extruded beads. However, extruded bead geometry also plays a significant part in defining bead-to-bead bonds. Microscopic analysis of tested and untested specimens suggest printing parameters have a significant effect on the filament size, geometry and bead-to-bead bond. It was found that by increasing the speed of the extrusion printing, the area of the cross-section and the maximum thickness decreased, while the welding minimum thickness increased at higher speeds, although actual weld strength appeared to plateau for speeds above 15 mm/sec. Increasing temperature was found to increase the welding minimum thickness. In most cases, test results show that by increasing temperature, the welding strength increased and is generally proportional. It was also observed that increased print speed and temperature both promote wider and smoother geometries that reduce stress concentration points. Non-Linear finite element based numerical modeling confirmed the location of stress concentrations and maximum plastic strain observed in the microscopic analysis. The stress concentration exceeded 2.5 in some cases and it led to severe plastic strain in these locations.

It was shown that the degree of welding between two faying surfaces produced by fused filament fabrication is best modeled with a combined squeeze flow and intermolecular diffusion model. This model can be utilized for a wide range of extrusion temperatures and print head speeds. The model can predict the degree of healing based on temperature histories. While additional research will be needed to fine-tune and expand the predictive model, comparison

with available experimental data indicate favorable results, with predicted values slightly higher than tested parts for all but the lowest print head velocities.

## Recommendations

Based on the results of this research a number of areas are suggested for potential improvement in the experimental method and include:

- Utilization of a more accurate load-cell
- Reduce cross head speed
- Increase print-head speed range
- Develop approximation to sphere geometry ratio
- Utilize sacrificial sample frames for printed dog-bone samples
- Create sample sets with units for untested microscopic analysis
- Conduct multiple slice microtome series analysis of part failure surface
- Implement more ridged sample control measures
    - Directional orientation (top, bottom, left, right)
    - Filament identification

In addition, the following future research questions are included to further improve the understanding of additive manufacturing part strength:

- What effect would alternating raster and spiral deposition paths have on part characteristics?
- What is the effect of machining on part strength?
- What is the effect of monofilament diameter variation on FFF feed rates?
- What is the level of consistency for monofilament diameters within spool/cartridge, between batches, between suppliers, … materials (ABS, PLA, …)?
- What feed control mechanisms exist or could be developed to mitigate monofilament diameter variation?
- What feed controls are needed to allow for increased print head speed?
- What are the effects of shear thinning on extruded bead geometry and bond strength?

o   What are the effects of acceleration and deceleration on bead geometry and weld strength?

o   What change in pressure between faying surfaces occurs as a function of layer thickness?

o   What are the effects of restricted extrusion bead on bead geometry and weld strength?

o   What is the effect of print direction on bead geometry?

o   What is the effect of secondary heat sources (heated bed, IR laser, ultrasonic)?

o   Explore use of fiber-optic microscope with high-speed camera to better understand extrusion process and bead geometry behavior during process?

## APPENDIX A

## RAW DATA CHARTS

**ABS 2015 Raw Data**

| mm/s | C | | | MPa | | | |
|---|---|---|---|---|---|---|---|
| | | **Trial 1** | **Trial 2** | **Trial 3** | **Trial 4** | **Trial 5** | **Trial 6** |
| **Velocity** | **Temp** | | | | | | |
| 10 | 230 | 13.78 | 17.22 | 14.69 | 14.96 | 9.78 | 13.01 |
| 15 | 230 | 11.99 | 14.17 | 8.80 | 10.74 | 12.44 | 12.78 |
| 20 | 230 | 12.96 | 10.61 | 14.81 | 11.39 | 13.16 | 15.79 |
| 25 | 230 | 17.24 | 11.00 | 9.79 | 20.33 | 15.04 | 0.00 |
| 10 | 235 | 16.35 | 17.87 | 14.98 | 15.60 | 18.73 | 17.52 |
| 15 | 235 | 13.50 | 15.62 | 8.35 | 15.60 | 17.88 | 17.70 |
| 20 | 235 | 16.93 | 17.11 | 17.89 | 13.44 | 15.41 | 16.33 |
| 25 | 235 | 14.70 | 10.11 | 6.52 | 12.91 | 16.29 | 15.61 |
| 10 | 240 | 18.55 | 19.66 | 18.48 | 17.80 | 19.88 | 0.00 |
| 15 | 240 | 17.33 | 16.95 | 16.29 | 16.73 | 16.66 | 0.00 |
| 20 | 240 | 18.69 | 14.41 | 14.87 | 13.09 | 18.33 | 17.61 |
| 25 | 240 | 13.00 | 8.20 | 8.94 | 9.34 | 16.71 | 0.00 |
| 10 | 245 | 19.60 | 18.11 | 18.75 | 20.02 | 17.69 | 0.00 |
| 15 | 245 | 18.66 | 20.39 | 13.84 | 14.55 | 17.45 | 14.81 |
| 20 | 245 | 14.66 | 16.19 | 14.68 | 18.64 | 16.82 | 18.66 |
| 25 | 245 | 10.60 | 11.83 | 6.38 | 17.33 | 15.90 | 12.78 |
| 10 | 250 | 8.38 | 8.73 | 13.71 | 13.25 | 13.78 | 0.00 |
| 15 | 250 | 15.95 | 17.76 | 15.95 | 17.80 | 17.80 | 17.04 |
| 20 | 250 | 17.20 | 15.30 | 15.37 | 16.15 | 20.29 | 18.82 |
| 25 | 250 | 10.69 | 13.32 | 20.02 | 8.49 | 12.05 | 19.71 |

**PLA 2015 Raw Data**

| mm/s | C | | | MPa | | |
|---|---|---|---|---|---|---|
| | | **Trial 1** | **Trial 2** | **Trial 3** | **Trial 4** | **Trial 5** |
| **Velocity** | **Temp** | | | | | |
| 10 | 195 | 6.3 | 8.4 | 10.4 | 3.6 | 11.3 |
| 15 | 195 | | | | | |
| 20 | 195 | | | | | |
| 25 | 195 | | | | | |
| 10 | 200 | 8.5 | 6.7 | 9.8 | 7.6 | |
| 15 | 200 | 9.2 | 13.8 | 9.9 | 23.4 | |
| 20 | 200 | | | | | |
| 25 | 200 | 15.2 | | | | |
| 10 | 205 | 9.7 | 5.2 | 4.6 | | |
| 15 | 205 | 14.1 | 14.1 | 8.4 | | |
| 20 | 205 | 16.7 | 20.0 | 11.2 | | |

| | | | | | |
|---|---|---|---|---|---|
| 25 | 205 | 23.9 | 22.5 | 21.6 | 6.1 |
| 10 | 210 | 8.3 | 5.6 | 23.7 | |
| 15 | 210 | 12.4 | 12.8 | | |
| 20 | 210 | 12.6 | | | |
| 25 | 210 | 8.4 | 9.9 | 23.4 | 22.7 |
| 10 | 215 | 26.7 | 14.9 | 15.3 | 12.3 |
| 15 | 215 | 2.9 | 2.9 | | |
| 20 | 215 | 9.5 | | | |
| 25 | 215 | 17.7 | 8.3 | 17.1 | 7.1 |

**PLA 2016 Exp.1**

| mm/s | C | | | MPa | | |
|---|---|---|---|---|---|---|
| | | **Trial** | **Trial** | **Trial** | **Trial** | **Trial** |
| **Velocity** | **Temp** | **1** | **2** | **3** | **4** | **5** |
| 10 | 195 | 23.96 | 24.87 | 30.29 | 29.71 | 27.12 |
| 15 | 195 | 29.54 | 31.22 | 31.00 | 27.50 | 27.22 |
| 20 | 195 | 27.68 | 25.56 | 30.35 | 28.42 | 21.08 |
| 25 | 195 | 32.53 | 29.36 | 19.11 | 28.32 | 31.73 |
| 10 | 200 | 27.82 | 25.36 | 25.62 | 20.54 | 23.84 |
| 15 | 200 | 27.24 | 27.60 | 24.28 | 24.57 | 26.70 |
| 20 | 200 | 27.66 | 24.97 | 27.28 | 25.52 | 27.64 |
| 25 | 200 | 30.25 | 26.77 | 29.52 | 28.26 | 27.95 |
| 10 | 205 | 27.81 | 22.82 | 31.04 | 32.66 | 31.10 |
| 15 | 205 | 26.04 | 24.03 | 25.61 | 26.45 | 26.16 |
| 20 | 205 | 26.46 | 27.27 | 25.88 | 28.00 | 25.85 |
| 25 | 205 | 31.03 | 26.62 | 28.41 | 24.86 | 25.16 |
| 10 | 210 | 28.86 | 28.98 | 26.90 | 30.86 | 26.48 |
| 15 | 210 | 30.13 | 31.14 | 27.17 | 30.63 | 26.05 |
| 20 | 210 | 32.00 | 30.61 | 30.42 | 1.31 | 22.19 |
| 25 | 210 | 31.62 | 26.48 | 27.80 | 27.75 | 31.24 |
| 10 | 215 | 29.57 | 32.67 | 31.01 | 30.24 | 31.22 |
| 15 | 215 | 32.15 | 29.14 | 31.04 | 29.81 | 33.32 |
| 20 | 215 | 30.11 | 29.03 | 28.71 | 32.05 | 31.67 |
| 25 | 215 | 25.97 | 24.67 | 28.16 | 29.05 | 28.57 |
| 10 | 220 | 28.73 | 28.20 | 29.37 | 31.85 | 22.06 |
| 15 | 220 | 32.71 | 31.77 | 32.11 | 30.51 | 30.32 |
| 20 | 220 | 23.33 | 26.17 | 28.85 | 26.04 | 29.92 |
| 25 | 220 | 27.83 | 31.62 | 30.45 | 30.19 | 26.67 |
| 10 | 225 | 32.71 | 27.14 | 26.41 | 24.67 | 30.76 |
| 15 | 225 | 26.33 | 32.10 | 31.19 | 25.92 | 26.01 |
| 20 | 225 | 30.69 | 27.08 | 27.16 | 21.03 | 27.95 |
| 25 | 225 | 27.02 | 28.09 | 31.98 | 26.72 | 26.96 |

**PLA 2016 Exp.2**

| mm/s | C | | | MPa | | |
|---|---|---|---|---|---|---|
| Velocity | Temp | Trial 1 | Trial 2 | Trial 3 | Trial 4 | Trial 5 |
| 10 | 195 | 26.475 | 28.035 | 30.045 | 29.94 | 27.33 |
| 15 | 195 | 31.83 | 31.71 | 30.03 | 30.69 | 28.575 |
| 20 | 195 | 30.36 | 27.045 | 30.825 | 30.54 | 20.325 |
| 25 | 195 | 34.245 | 29.745 | 17.955 | 28.485 | 33.405 |
| 10 | 200 | 31.71 | 29.43 | 26.31 | 24.075 | 26.415 |
| 15 | 200 | 29.055 | 30.045 | 28.47 | 28.155 | 29.355 |
| 20 | 200 | 30.945 | 29.265 | 29.85 | 29.115 | 31.155 |
| 25 | 200 | 32.145 | 29.07 | 30.825 | 30.465 | 31.965 |
| 10 | 205 | 30.42 | 23.235 | 30.795 | 30.18 | 31.26 |
| 15 | 205 | 30.06 | 28.785 | 30.315 | 30.915 | 29.34 |
| 20 | 205 | 30.855 | 30.96 | 29.31 | 29.4 | 29.205 |
| 25 | 205 | 32.565 | 31.425 | 31.47 | 28.77 | 27.735 |
| 10 | 210 | 29.985 | 29.205 | 29.505 | 30.285 | 26.685 |
| 15 | 210 | 32.25 | 32.355 | 29.655 | 32.31 | 28.71 |
| 20 | 210 | 31.8 | 32.445 | 32.4 | 31.965 | 33.69 |
| 25 | 210 | 32.19 | 25.785 | 29.535 | 31.425 | 34.005 |
| 10 | 215 | 32.355 | 33.03 | 32.385 | 32.055 | 33.255 |
| 15 | 215 | 33.57 | 32.205 | 32.01 | 32.7 | 33.66 |
| 20 | 215 | 33.69 | 30.795 | 32.355 | 32.88 | 33.15 |
| 25 | 215 | 29.91 | 25.5 | 31.35 | 29.655 | 31.26 |
| 10 | 220 | 29.925 | 30.54 | 31.89 | 33.09 | 22.515 |
| 15 | 220 | 33.48 | 32.595 | 33.615 | 33.375 | 32.25 |
| 20 | 220 | 26.94 | 31.65 | 29.73 | 29.01 | 31.665 |
| 25 | 220 | 30.06 | 32.025 | 32.475 | 31.53 | 30.48 |
| 10 | 225 | 33.3 | 31.335 | 28.965 | 28.98 | 33.825 |
| 15 | 225 | 30.165 | 33.795 | 34.38 | 31.74 | 29.655 |
| 20 | 225 | 31.245 | 30.15 | 29.94 | 24.705 | 30.96 |
| 25 | 225 | 30.72 | 31.455 | 32.31 | 30 | 30.495 |

**PLA 2017 Exp.1**

| | | Trial | Trial | Trial | Trial | Trial |
|---|---|---|---|---|---|---|
| Velocity | Temp | 1 | 2 | 3 | 4 | 5 |
| mm/s | C | | | MPa | | |
| 10 | 195 | 16.55 | 7.69 | 19.82 | 6.16 | 0.00 |
| 15 | 195 | 22.99 | 5.61 | 22.61 | 2.74 | 21.56 |
| 20 | 195 | 20.35 | 6.07 | 22.48 | 20.97 | 20.48 |
| 25 | 195 | 19.54 | 21.63 | 5.78 | 18.48 | 19.56 |
| 10 | 200 | 7.43 | 5.12 | 19.65 | 3.12 | 0.00 |
| 15 | 200 | 18.20 | 17.73 | 18.40 | 21.63 | 7.18 |
| 20 | 200 | 21.25 | 19.10 | 5.43 | 15.58 | 18.82 |
| 25 | 200 | 21.14 | 6.88 | 16.73 | 19.67 | 15.91 |

| | | | | | |
|---|---|---|---|---|---|
| 10 | 205 | 20.84 | 21.04 | 20.46 | 21.47 | 17.17 |
| 15 | 205 | 17.49 | 16.24 | 14.42 | 21.52 | 21.34 |
| 20 | 205 | 20.15 | 21.04 | 17.87 | 3.63 | 19.01 |
| 25 | 205 | 18.86 | 19.34 | 18.57 | 20.72 | 5.47 |
| 10 | 210 | 20.22 | 14.79 | 12.77 | 20.86 | 15.32 |
| 15 | 210 | 21.87 | 21.82 | 19.38 | 20.31 | 17.23 |
| 20 | 210 | 21.12 | 21.78 | 13.40 | 19.84 | 21.36 |
| 25 | 210 | 21.52 | 22.46 | 23.50 | 17.06 | 22.04 |
| 10 | 215 | 17.93 | 19.21 | 20.22 | 16.35 | 20.13 |
| 15 | 215 | 19.28 | 19.69 | 23.00 | 21.93 | 23.19 |
| 20 | 215 | 22.77 | 20.64 | 21.74 | 11.47 | 23.30 |
| 25 | 215 | 21.91 | 23.43 | 22.17 | 19.06 | 22.13 |
| 10 | 220 | 21.95 | 18.90 | 4.57 | 20.59 | 20.66 |
| 15 | 220 | 22.35 | 24.20 | 23.98 | 20.70 | 24.02 |
| 20 | 220 | 21.91 | 21.21 | 23.80 | 21.65 | 24.09 |
| 25 | 220 | 21.49 | 22.35 | 22.17 | 21.45 | 20.73 |
| 10 | 225 | 22.59 | 10.68 | 20.53 | 15.43 | 21.08 |
| 15 | 225 | 24.00 | 18.77 | 22.84 | 16.79 | 21.58 |
| 20 | 225 | 22.97 | 20.33 | 20.84 | 20.95 | 21.89 |
| 25 | 225 | 22.26 | 21.67 | 20.44 | 22.39 | 23.01 |

**PLA 2017 Exp.1 0.4mm Layer**

| Velocity mm/s | Temp C | Trial 1 | Trial 2 | Trial 3 MPa | Trial 4 | Trial 5 |
|---|---|---|---|---|---|---|
| 10 | 195 | 54.67 | 51.79 | 58.46 | 45.22 | 51.51 |
| 15 | 195 | 55.69 | 47.11 | 53.99 | 47.83 | 52.17 |
| 20 | 195 | 53.57 | 54.75 | 56.65 | 50.46 | 53.99 |
| 25 | 195 | 53.21 | 52.03 | 57.03 | 49.56 | 51.62 |
| 10 | 200 | 48.70 | 47.08 | 42.89 | 50.90 | 46.73 |
| 15 | 200 | 55.33 | 51.95 | 55.61 | 47.83 | 51.46 |
| 20 | 200 | 61.73 | 60.30 | 61.12 | 55.85 | 52.36 |
| 25 | 200 | 56.73 | 56.81 | 58.46 | 53.08 | 54.56 |
| 10 | 205 | 53.32 | 52.83 | 58.18 | 46.46 | 51.57 |
| 15 | 205 | 57.85 | 55.44 | 61.45 | 52.47 | 57.39 |
| 20 | 205 | 59.01 | 55.03 | 59.92 | 52.28 | 55.66 |
| 25 | 205 | 58.41 | 56.51 | 57.80 | 54.12 | 51.76 |
| 10 | 210 | 60.22 | 56.43 | 61.09 | 46.02 | 53.08 |
| 15 | 210 | 57.14 | 54.34 | 59.47 | 49.39 | 53.27 |
| 20 | 210 | 57.55 | 56.84 | 59.23 | 52.33 | 54.09 |
| 25 | 210 | 56.79 | 53.93 | 58.74 | 52.55 | 54.83 |
| 10 | 215 | 60.99 | 63.82 | 63.82 | 52.74 | 60.05 |
| 15 | 215 | 62.64 | 62.06 | 63.13 | 54.50 | 59.78 |
| 20 | 215 | 60.00 | 58.05 | 59.29 | 52.09 | 53.82 |

| 25 | 215 | 59.09 | 58.52 | 61.87 | 54.14 | 55.85 |
| 10 | 220 | 64.91 | 65.02 | 63.74 | 53.05 | 61.45 |
| 15 | 220 | 61.76 | 64.29 | 64.94 | 53.57 | 58.07 |
| 20 | 220 | 58.87 | 56.26 | 56.87 | 52.36 | 54.70 |
| 25 | 220 | 60.74 | 56.98 | 61.81 | 54.83 | 58.05 |
| 10 | 225 | 58.71 | 55.66 | 58.13 | 51.95 | 63.93 |
| 15 | 225 | 61.95 | 60.05 | 63.35 | 52.24 | 58.65 |
| 20 | 225 | 61.51 | 63.35 | 63.60 | 63.57 | 59.86 |
| 25 | 225 | 55.39 | 64.89 | 63.16 | 62.11 | 63.29 |

# APPENDIX B

## DESCRIPTIVE STATISTICS

### PLA

| 2016 Exp 1 | Vel | Temp | Average Strength | Std Dev S | Vel | Average Strength | Std Dev S | Vel | Average Strength | Std Dev S | Vel | Average Strength | Std Dev S |
|---|---|---|---|---|---|---|---|---|---|---|---|---|---|
| | 10 | 195 | 27.19 | 2.818 | 15 | 29.30 | 1.888 | 20 | 26.62 | 3.538 | 25 | 28.21 | 5.366 |
| | 10 | 200 | 24.64 | 2.692 | 15 | 26.08 | 1.547 | 20 | 26.62 | 1.274 | 25 | 28.55 | 1.366 |
| | 10 | 205 | 29.08 | 3.922 | 15 | 25.66 | 0.959 | 20 | 26.69 | 0.932 | 25 | 27.21 | 2.555 |
| | 10 | 210 | 28.42 | 1.770 | 15 | 29.02 | 2.268 | 20 | 23.31 | 12.888 | 25 | 28.97 | 2.303 |
| | 10 | 215 | 30.94 | 1.166 | 15 | 31.09 | 1.695 | 20 | 30.31 | 1.509 | 25 | 27.28 | 1.879 |
| | 10 | 220 | 28.04 | 3.625 | 15 | 31.48 | 1.037 | 20 | 26.86 | 2.593 | 25 | 29.35 | 2.035 |
| | 10 | 225 | 28.34 | 3.301 | 15 | 28.31 | 3.066 | 20 | 26.78 | 3.533 | 25 | 28.15 | 2.203 |

### PLA

| 2016 Exp 2 | Vel | Temp | Average Strength | Std Dev S | Vel | Average Strength | Std Dev S | Vel | Average Strength | Std Dev S | Vel | Average Strength | Std Dev S |
|---|---|---|---|---|---|---|---|---|---|---|---|---|---|
| | 10 | 195 | 28.37 | 1.586 | 15 | 30.57 | 1.339 | 20 | 27.82 | 4.463 | 25 | 28.77 | 6.509 |
| | 10 | 200 | 27.59 | 2.989 | 15 | 29.02 | 0.744 | 20 | 30.07 | 0.942 | 25 | 30.89 | 1.248 |
| | 10 | 205 | 29.18 | 3.347 | 15 | 29.88 | 0.834 | 20 | 29.95 | 0.881 | 25 | 30.39 | 2.040 |
| | 10 | 210 | 29.13 | 1.431 | 15 | 31.06 | 1.743 | 20 | 32.46 | 0.741 | 25 | 30.59 | 3.127 |
| | 10 | 215 | 32.62 | 0.504 | 15 | 32.83 | 0.761 | 20 | 32.57 | 1.105 | 25 | 29.54 | 2.383 |
| | 10 | 220 | 29.59 | 4.142 | 15 | 33.06 | 0.603 | 20 | 29.80 | 1.982 | 25 | 31.31 | 1.021 |
| | 10 | 225 | 31.28 | 2.303 | 15 | 31.95 | 2.110 | 20 | 29.40 | 2.680 | 25 | 31.00 | 0.902 |

### PLA

| 2017 Exp 1 | Vel | Temp | Average Strength | Std Dev S | Vel | Average Strength | Std Dev S | Vel | Average Strength | Std Dev S | Vel | Average Strength | Std Dev S |
|---|---|---|---|---|---|---|---|---|---|---|---|---|---|
| | 10 | 195 | 12.56 | 6.666 | 15 | 15.64 | 11.180 | 20 | 18.07 | 6.763 | 25 | 17.00 | 6.375 |
| | 10 | 200 | 8.83 | 7.424 | 15 | 16.63 | 5.500 | 20 | 16.03 | 6.266 | 25 | 16.07 | 5.558 |
| | 10 | 205 | 20.19 | 1.731 | 15 | 18.20 | 3.143 | 20 | 16.34 | 7.206 | 25 | 16.59 | 6.270 |
| | 10 | 210 | 16.79 | 3.558 | 15 | 20.12 | 1.929 | 20 | 19.50 | 3.484 | 25 | 21.32 | 2.489 |
| | 10 | 215 | 18.77 | 1.635 | 15 | 21.42 | 1.834 | 20 | 19.98 | 4.865 | 25 | 21.74 | 1.614 |
| | 10 | 220 | 17.33 | 7.217 | 15 | 23.05 | 1.510 | 20 | 22.53 | 1.319 | 25 | 21.64 | 0.649 |
| | 10 | 225 | 18.06 | 4.927 | 15 | 20.79 | 2.967 | 20 | 21.39 | 1.044 | 25 | 21.95 | 0.973 |

### PLA

| 2017 Exp 2 | Vel | Temp | Average Strength | Std Dev S | Vel | Average Strength | Std Dev S | Vel | Average Strength | Std Dev S | Vel | Average Strength | Std Dev S |
|---|---|---|---|---|---|---|---|---|---|---|---|---|---|
| | 10 | 195 | 52.33 | 4.864 | 15 | 51.33 | 3.164 | 20 | 53.88 | 2.247 | 25 | 52.69 | 2.762 |
| | 10 | 200 | 47.26 | 2.950 | 15 | 52.43 | 3.196 | 20 | 58.27 | 4.032 | 25 | 55.93 | 2.113 |
| | 10 | 205 | 52.47 | 4.198 | 15 | 56.92 | 3.303 | 20 | 56.38 | 3.107 | 25 | 55.72 | 2.758 |
| | 10 | 210 | 55.37 | 6.127 | 15 | 54.72 | 3.844 | 20 | 56.01 | 2.769 | 25 | 55.37 | 2.431 |
| | 10 | 215 | 60.29 | 4.538 | 15 | 60.42 | 3.549 | 20 | 56.65 | 3.497 | 25 | 57.89 | 2.994 |
| | 10 | 220 | 61.64 | 5.010 | 15 | 60.53 | 4.731 | 20 | 55.81 | 2.443 | 25 | 58.48 | 2.826 |
| | 10 | 225 | 57.68 | 4.393 | 15 | 59.25 | 4.307 | 20 | 62.38 | 1.654 | 25 | 61.77 | 3.703 |

### ABS

| 2015 Exp 1 | Vel | Temp | Average Strength | Std Dev S | Vel | Average Strength | Std Dev S | Vel | Average Strength | Std Dev S | Vel | Average Strength | Std Dev S |
|---|---|---|---|---|---|---|---|---|---|---|---|---|---|
| | 10 | 230 | 13.9079 | 2.47181 | 15 | 11.8188 | 1.84992 | 20 | 13.1184 | 1.96444 | 25 | 14.6803 | 4.35788 |
| | 10 | 235 | 16.8439 | 1.4371 | 15 | 14.7755 | 3.53541 | 20 | 16.1854 | 1.57808 | 25 | 12.6898 | 3.74724 |
| | 10 | 240 | 18.8751 | 0.87427 | 15 | 16.7929 | 0.38619 | 20 | 16.1648 | 2.34048 | 25 | 11.2343 | 3.57612 |
| | 10 | 245 | 18.8351 | 0.98092 | 15 | 16.6175 | 2.62148 | 20 | 16.6095 | 1.79529 | 25 | 12.4692 | 3.9125 |
| | 10 | 250 | 11.5708 | 2.76524 | 15 | 17.0519 | 0.89863 | 20 | 17.1875 | 2.01309 | 25 | 14.0481 | 4.78454 |

# APPENDIX C

# PLA SINGLE FACTOR ANOVA

**2016 E1**

Anova: Single Factor 10MM/S

SUMMARY

| Groups | Count | Sum | Average | Variance |
|---|---|---|---|---|
| Column 1 | 5 | 135.946 | 27.19 | 7.94 |
| Column 2 | 5 | 123.180 | 24.64 | 7.25 |
| Column 3 | 5 | 145.425 | 29.08 | 15.38 |
| Column 4 | 5 | 142.083 | 28.42 | 3.13 |
| Column 5 | 5 | 154.723 | 30.94 | 1.36 |
| Column 6 | 5 | 140.202 | 28.04 | 13.14 |
| Column 7 | 5 | 141.688 | 28.34 | 10.90 |

ANOVA

| Source of Variation | SS | df | MS | F | P-value | F crit |
|---|---|---|---|---|---|---|
| Between Groups | 110.252 | 6.000 | 18.38 | 2.18 | 0.08 | 2.45 |
| Within Groups | 236.402 | 28.000 | 8.44 | | | |
| | | | | | | |
| Total | 346.654 | 34.000 | | | | |

**2016 E1**

Anova: Single Factor 15MM/S

SUMMARY

| Groups | Count | Sum | Average | Variance |
|---|---|---|---|---|
| Column 1 | 5 | 146.485 | 29.30 | 3.56 |
| Column 2 | 5 | 130.399 | 26.08 | 2.39 |
| Column 3 | 5 | 128.284 | 25.66 | 0.92 |
| Column 4 | 5 | 145.123 | 29.02 | 5.14 |
| Column 5 | 5 | 155.462 | 31.09 | 2.87 |
| Column 6 | 5 | 157.419 | 31.48 | 1.08 |
| Column 7 | 5 | 141.556 | 28.31 | 9.40 |

ANOVA

| Source of Variation | SS | df | MS | F | P-value | F crit |
|---|---|---|---|---|---|---|
| Between Groups | 151.060 | 6.000 | 25.177 | 6.948 | 0.000 | 2.445 |
| Within Groups | 101.465 | 28.000 | 3.624 | | | |
| | | | | | | |
| Total | 252.525 | 34.000 | | | | |

**2016 E1**

Anova: Single Factor 20MM/S

SUMMARY

| Groups | Count | Sum | Average | Variance |
|---|---|---|---|---|
| Column 1 | 5.000 | 133.091 | 26.62 | 12.52 |
| Column 2 | 5.000 | 133.078 | 26.62 | 1.62 |
| Column 3 | 5.000 | 133.458 | 26.69 | 0.87 |
| Column 4 | 5.000 | 116.534 | 23.31 | 166.11 |
| Column 5 | 5.000 | 151.557 | 30.31 | 2.28 |
| Column 6 | 5.000 | 134.323 | 26.86 | 6.72 |
| Column 7 | 5.000 | 133.907 | 26.78 | 12.49 |

ANOVA

| Source of Variation | SS | df | MS | F | P-value | F crit |
|---|---|---|---|---|---|---|
| Between Groups | 122.957 | 6 | 20.493 | 0.708 | 0.646 | 2.445 |
| Within Groups | 810.429 | 28 | 28.944 | | | |
| | | | | | | |
| Total | 933.386 | 34 | | | | |

**2016 E1**

Anova: Single Factor 25MM/S

SUMMARY

| Groups | Count | Sum | Average | Variance |
|---|---|---|---|---|
| Column 1 | 5.000 | 141.058 | 28.21 | 28.80 |
| Column 2 | 5.000 | 142.744 | 28.55 | 1.87 |
| Column 3 | 5.000 | 136.073 | 27.21 | 6.53 |
| Column 4 | 5.000 | 144.873 | 28.97 | 5.30 |
| Column 5 | 5.000 | 136.422 | 27.28 | 3.53 |
| Column 6 | 5.000 | 146.752 | 29.35 | 4.14 |
| Column 7 | 5.000 | 140.768 | 28.15 | 4.85 |

ANOVA

| Source of Variation | SS | df | MS | F | P-value | F crit |
|---|---|---|---|---|---|---|
| Between Groups | 19.201 | 6 | 3.200 | 0.407 | 0.868 | 2.445 |
| Within Groups | 220.064 | 28 | 7.859 | | | |
| | | | | | | |
| Total | 239.264 | 34 | | | | |

**2016 E2** — Anova: Single Factor 10MM/S

SUMMARY

| Groups | Count | Sum | Average | Variance |
|---|---|---|---|---|
| Column 1 | 5 | 141.825 | 28.37 | 2.51 |
| Column 2 | 5 | 137.940 | 27.59 | 8.93 |
| Column 3 | 5 | 145.890 | 29.18 | 11.20 |
| Column 4 | 5 | 145.665 | 29.13 | 2.05 |
| Column 5 | 5 | 163.080 | 32.62 | 0.25 |
| Column 6 | 5 | 147.960 | 29.59 | 17.15 |
| Column 7 | 5 | 156.405 | 31.28 | 5.30 |

ANOVA

| Source of Variation | SS | df | MS | F | P-value | F crit |
|---|---|---|---|---|---|---|
| Between Groups | 89.240 | 6.000 | 14.873 | 2.196 | 0.073 | 2.445 |
| Within Groups | 189.630 | 28.000 | 6.772 | | | |
| Total | 278.870 | 34.000 | | | | |

**2016 E2** — Anova: Single Factor 15MM/S

SUMMARY

| Groups | Count | Sum | Average | Variance |
|---|---|---|---|---|
| Column 1 | 5 | 152.835 | 30.57 | 1.79 |
| Column 2 | 5 | 145.080 | 29.02 | 0.55 |
| Column 3 | 5 | 149.415 | 29.88 | 0.70 |
| Column 4 | 5 | 155.280 | 31.06 | 3.04 |
| Column 5 | 5 | 164.145 | 32.83 | 0.58 |
| Column 6 | 5 | 165.315 | 33.06 | 0.36 |
| Column 7 | 5 | 159.735 | 31.95 | 4.45 |

ANOVA

| Source of Variation | SS | df | MS | F | P-value | F crit |
|---|---|---|---|---|---|---|
| Between Groups | 68.040 | 6.000 | 11.340 | 6.917 | 0.000 | 2.445 |
| Within Groups | 45.902 | 28.000 | 1.639 | | | |
| Total | 113.942 | 34.000 | | | | |

**2016 E2** — Anova: Single Factor 20MM/S

SUMMARY

| Groups | Count | Sum | Average | Variance |
|---|---|---|---|---|
| Column 1 | 5.000 | 139.095 | 27.82 | 19.91 |
| Column 2 | 5.000 | 150.330 | 30.07 | 0.89 |
| Column 3 | 5.000 | 149.730 | 29.95 | 0.78 |
| Column 4 | 5.000 | 162.300 | 32.46 | 0.55 |
| Column 5 | 5.000 | 162.870 | 32.57 | 1.22 |
| Column 6 | 5.000 | 148.995 | 29.80 | 3.93 |
| Column 7 | 5.000 | 147.000 | 29.40 | 7.18 |

ANOVA

| Source of Variation | SS | df | MS | F | P-value | F crit |
|---|---|---|---|---|---|---|
| Between Groups | 86.165 | 6 | 14.361 | 2.917 | 0.024 | 2.445 |
| Within Groups | 137.838 | 28 | 4.923 | | | |
| Total | 224.003 | 34 | | | | |

**2016 E2** — Anova: Single Factor 25MM/S

SUMMARY

| Groups | Count | Sum | Average | Variance |
|---|---|---|---|---|
| Column 1 | 5.000 | 143.835 | 28.77 | 42.36 |
| Column 2 | 5.000 | 154.470 | 30.89 | 1.56 |
| Column 3 | 5.000 | 151.965 | 30.39 | 4.16 |
| Column 4 | 5.000 | 152.940 | 30.59 | 9.78 |
| Column 5 | 5.000 | 147.675 | 29.54 | 5.68 |
| Column 6 | 5.000 | 156.570 | 31.31 | 1.04 |
| Column 7 | 5.000 | 154.980 | 31.00 | 0.81 |

ANOVA

| Source of Variation | SS | df | MS | F | P-value | F crit |
|---|---|---|---|---|---|---|
| Between Groups | 24.355 | 6 | 4.059 | 0.435 | 0.850 | 2.445 |
| Within Groups | 261.576 | 28 | 9.342 | | | |
| Total | 285.930 | 34 | | | | |

**2017 E1** — Anova: Single Factor 10MM/S

SUMMARY

| Groups | Count | Sum | Average | Variance |
|---|---|---|---|---|
| Column 1 | 5 | 50.2214 | 10.04 | 64.86 |
| Column 2 | 5 | 35.3219 | 7.06 | 56.93 |
| Column 3 | 5 | 100.9737 | 20.19 | 2.99 |
| Column 4 | 5 | 83.9575 | 16.79 | 12.66 |
| Column 5 | 5 | 93.8515 | 18.77 | 2.67 |
| Column 6 | 5 | 86.6740 | 17.33 | 52.09 |
| Column 7 | 5 | 90.3076 | 18.06 | 24.28 |

ANOVA

| Source of Variation | SS | df | MS | F | P-value | F crit |
|---|---|---|---|---|---|---|
| Between Groups | 726.239 | 6.0000 | 121.040 | 3.914 | 0.006 | 2.445 |
| Within Groups | 865.947 | 28.0000 | 30.927 | | | |
| Total | 1592.186 | 34.0000 | | | | |

**2017 E1** — Anova: Single Factor 15MM/S

SUMMARY

| Groups | Count | Sum | Average | Variance |
|---|---|---|---|---|
| Column 1 | 5 | 75.511 | 15.10 | 100.81 |
| Column 2 | 5 | 83.137 | 16.63 | 30.25 |
| Column 3 | 5 | 91.011 | 18.20 | 9.88 |
| Column 4 | 5 | 100.608 | 20.12 | 3.72 |
| Column 5 | 5 | 107.089 | 21.42 | 3.37 |
| Column 6 | 5 | 115.260 | 23.05 | 2.28 |
| Column 7 | 5 | 103.973 | 20.79 | 8.80 |

ANOVA

| Source of Variation | SS | df | MS | F | P-value | F crit |
|---|---|---|---|---|---|---|
| Between Groups | 237.167 | 6.000 | 39.528 | 1.739 | 0.149 | 2.445 |
| Within Groups | 636.411 | 28.000 | 22.729 | | | |
| Total | 873.579 | 34.000 | | | | |

**2017 E1** — Anova: Single Factor 20MM/S

SUMMARY

| Groups | Count | Sum | Average | Variance |
|---|---|---|---|---|
| Column 1 | 5.000 | 90.3558 | 18.07 | 45.74 |
| Column 2 | 5.000 | 80.1723 | 16.03 | 39.27 |
| Column 3 | 5.000 | 81.6960 | 16.34 | 51.92 |
| Column 4 | 5.000 | 97.5057 | 19.50 | 12.14 |
| Column 5 | 5.000 | 99.9120 | 19.98 | 23.67 |
| Column 6 | 5.000 | 112.6604 | 22.53 | 1.74 |
| Column 7 | 5.000 | 106.9722 | 21.39 | 1.09 |

ANOVA

| Source of Variation | SS | df | MS | F | P-value | F crit |
|---|---|---|---|---|---|---|
| Between Groups | 180.289 | 6 | 30.048 | 1.198 | 0.336 | 2.445 |
| Within Groups | 702.276 | 28 | 25.081 | | | |
| Total | 882.565 | 34 | | | | |

**2017 E1** — Anova: Single Factor 25MM/S

SUMMARY

| Groups | Count | Sum | Average | Variance |
|---|---|---|---|---|
| Column 1 | 5.000 | 84.992 | 17.00 | 40.64 |
| Column 2 | 5.000 | 80.331 | 16.07 | 30.89 |
| Column 3 | 5.000 | 82.965 | 16.59 | 39.31 |
| Column 4 | 5.000 | 106.579 | 21.32 | 6.19 |
| Column 5 | 5.000 | 108.703 | 21.74 | 2.60 |
| Column 6 | 5.000 | 108.193 | 21.64 | 0.42 |
| Column 7 | 5.000 | 109.771 | 21.95 | 0.95 |

ANOVA

| Source of Variation | SS | df | MS | F | P-value | F crit |
|---|---|---|---|---|---|---|
| Between Groups | 227.047 | 6 | 37.841 | 2.189 | 0.074 | 2.445 |
| Within Groups | 484.042 | 28 | 17.287 | | | |
| Total | 711.089 | 34 | | | | |

**2017 E2**
Anova: Single Factor 10MM/S

SUMMARY

| Groups | Count | Sum | Average | Variance |
|---|---|---|---|---|
| Column 1 | 5 | 261.642 | 52.33 | 23.66 |
| Column 2 | 5 | 236.311 | 47.26 | 8.70 |
| Column 3 | 5 | 262.359 | 52.47 | 17.62 |
| Column 4 | 5 | 276.831 | 55.37 | 37.54 |
| Column 5 | 5 | 301.425 | 60.29 | 20.59 |
| Column 6 | 5 | 308.175 | 61.64 | 25.10 |
| Column 7 | 5 | 288.380 | 57.68 | 19.30 |

ANOVA

| Source of Variation | SS | df | MS | F | P-value | F crit |
|---|---|---|---|---|---|---|
| Between Groups | 760.333 | 6.000 | 126.72 | 5.82 | 0.00 | 2.45 |
| Within Groups | 610.070 | 28.000 | 21.79 | | | |
| | | | | | | |
| Total | 1370.403 | 34.000 | | | | |

**2017 E2**
Anova: Single Factor 15MM/S

SUMMARY

| Groups | Count | Sum | Average | Variance |
|---|---|---|---|---|
| Column 1 | 5 | 256.788 | 51.36 | 14.20 |
| Column 2 | 5 | 262.173 | 52.43 | 10.21 |
| Column 3 | 5 | 284.609 | 56.92 | 10.91 |
| Column 4 | 5 | 273.619 | 54.72 | 14.77 |
| Column 5 | 5 | 302.108 | 60.42 | 12.59 |
| Column 6 | 5 | 302.632 | 60.53 | 22.38 |
| Column 7 | 5 | 296.247 | 59.25 | 18.55 |

ANOVA

| Source of Variation | SS | df | MS | F | P-value | F crit |
|---|---|---|---|---|---|---|
| Between Groups | 427.251 | 6.000 | 71.208 | 4.810 | 0.002 | 2.445 |
| Within Groups | 414.493 | 28.000 | 14.803 | | | |
| | | | | | | |
| Total | 841.744 | 34.000 | | | | |

**2017 E2**
Anova: Single Factor 20MM/S

SUMMARY

| Groups | Count | Sum | Average | Variance |
|---|---|---|---|---|
| Column 1 | 5.000 | 269.420 | 53.88 | 5.05 |
| Column 2 | 5.000 | 291.359 | 58.27 | 16.26 |
| Column 3 | 5.000 | 281.892 | 56.38 | 9.65 |
| Column 4 | 5.000 | 280.044 | 56.01 | 7.67 |
| Column 5 | 5.000 | 283.244 | 56.65 | 12.23 |
| Column 6 | 5.000 | 279.058 | 55.81 | 5.97 |
| Column 7 | 5.000 | 311.884 | 62.38 | 2.74 |

ANOVA

| Source of Variation | SS | df | MS | F | P-value | F crit |
|---|---|---|---|---|---|---|
| Between Groups | 215.608 | 6 | 35.935 | 4.223 | 0.004 | 2.445 |
| Within Groups | 238.257 | 28 | 8.509 | | | |
| | | | | | | |
| Total | 453.865 | 34 | | | | |

**2017 E2**
Anova: Single Factor 25MM/S

SUMMARY

| Groups | Count | Sum | Average | Variance |
|---|---|---|---|---|
| Column 1 | 5.000 | 263.463 | 52.69 | 7.63 |
| Column 2 | 5.000 | 279.638 | 55.93 | 4.46 |
| Column 3 | 5.000 | 278.590 | 55.72 | 7.60 |
| Column 4 | 5.000 | 276.838 | 55.37 | 5.91 |
| Column 5 | 5.000 | 289.470 | 57.89 | 8.96 |
| Column 6 | 5.000 | 292.414 | 58.48 | 7.99 |
| Column 7 | 5.000 | 308.837 | 61.77 | 13.71 |

ANOVA

| Source of Variation | SS | df | MS | F | P-value | F crit |
|---|---|---|---|---|---|---|
| Between Groups | 247.747 | 6 | 41.291 | 5.137 | 0.001 | 2.445 |
| Within Groups | 225.064 | 28 | 8.038 | | | |
| | | | | | | |
| Total | 472.811 | 34 | | | | |